2004

Photoconductivity and acoustic wave interaction with charge carriers in cadmium sulfide.

Wesley Arthur
University of Windsor

Follow this and additional works at: https://scholar.uwindsor.ca/etd

Recommended Citation

PHOTOCONDUCTIVITY AND ACOUSTIC WAVE INTERACTION WITH CHARGE CARRIERS IN CADMIUM SULFIDE

by

Wesley Arthur

A Thesis
Submitted to the Faculty of Graduate Studies and Research
Through the Department of Physics
In Partial Fulfillment of the Requirements for
The Degree of Master of Science at the
University of Windsor

WINDSOR, ONTARIO, CANADA

January 2004

© 2004 Wesley Arthur

National Library
of Canada

Bibliothèque nationale
du Canada

Acquisitions and
Bibliographic Services

Acquisisitons et
services bibliographiques

395 Wellington Street
Ottawa ON K1A 0N4
Canada

395, rue Wellington
Ottawa ON K1A 0N4
Canada

The author has granted a non-exclusive licence allowing the National Library of Canada to reproduce, loan, distribute or sell copies of this thesis in microform, paper or electronic formats.

L'auteur a accordé une licence non exclusive permettant à la Bibliothèque nationale du Canada de reproduire, prêter, distribuer ou vendre des copies de cette thèse sous la forme de microfiche/film, de reproduction sur papier ou sur format électronique.

The author retains ownership of the copyright in this thesis. Neither the thesis nor substantial extracts from it may be printed or otherwise reproduced without the author's permission.

L'auteur conserve la propriété du droit d'auteur qui protège cette thèse. Ni la thèse ni des extraits substantiels de celle-ci ne doivent être imprimés ou aturement reproduits sans son autorisation.

In compliance with the Canadian Privacy Act some supporting forms may have been removed from this dissertation.

Conformément à la loi canadienne sur la protection de la vie privée, quelques formulaires secondaires ont été enlevés de ce manuscrit.

While these forms may be included in the document page count, their removal does not represent any loss of content from the dissertation.

Bien que ces formulaires aient inclus dans la pagination, il n'y aura aucun contenu manquant.

Canadä

Abstract

The principle focus of this investigation is ultrasonic acoustic wave interaction with charge carriers in Cadmium Sulfide. In order to facilitate this study, however, effort is spent to better characterize the metastable crystal conductivities that were observed in preliminary research. Specifically, an experiment is carried out to determine the behaviour of thee instabilities over time periods of one hour. Upon analysing the results of this procedure, the effect of temperature on CdS conductivity is considered. In the portion of thesis paper regarding acoustics, preliminary endevours are made to observe some of the fundamental phenomenon associated with the acousto-electric effect. Wave attenuation and velocity dispersion are documented for specific frequencies of 4.1 MHz. Further, they are compared to theory. Having completed this, an investigation is undertaken which explores the amplitudes of the higher harmonics with respect to conductivity. In the first experiment, the amplitude of the 2nd harmonic is compared with the relative amplitudes of consecutive echoes. As well, the relationship between the relative amplitudes of the 2nd through 5th harmonic is explored. And finally, correlations are made between the data taken in the first and second procedures.

To my sailboat Dead Ahead,
without which this may not have been possible.

iv

Acknowledgements

I am deeply indebted to many people for their support not only through the writing of this thesis paper, but also throughout my entire Master's degree campaign. Naturally, I am sincerely thankful to Dr. Maev for his constant and continued support. His guidance both with respect to this thesis project and academic pursuit as a whole has been indispensable.

Further, the members of Dr. Maev's research group have provided both encouragement and assistance. Especially, I would like to thank Dr. Fedar Seviaryn, Dr. Ron Kumon and Brian O'Neill for their help with regards to theory and experiment. Surely their advice and guidance was central to my success. Also, I would be remiss if I did not mention two of my colleagues, Andrew Chertov and Jeff Sadler, who also provided support.

The role of Dr. Kedzierski, Dr. Aroca and Dr. Drake as my committee members was also greatly appreciated. The careful examination of this thesis paper, along with their constructive evaluation was beneficial, both with respect to this particular research project and beyond to future endeavours.

As well, I would like to thank Sarah Beneteau and Emily Schmidt for the many times they have come to my aid.

And finally, I would like to thank my parents Laverne and Anne Arthur. Throughout my life they have encouraged and, further, provided a model for, academic achievement. I will always be grateful for their loving support and inspiration.

Table of Contents

List of Tables

List of Figures

x

CHAPTER I

Preliminary Remarks

Media which couple the piezoelectric effect with the form of conductivity known as photoconductivity have been prevalent throughout academic literature over the past several decades. So celebrated are the relationships between these two phenomena, in fact, that at this point in development, it is difficult to find a reference text that does not at least introduce a preliminary discussion of their curious association. Although their concomitance is well documented today, the excitement surrounding the pairing of these two subject areas did not seem to fully come to a head until the middle of the twentieth century. It was at this time that the consequences of acoustic wave propagation within a piezoelectric photoconductor were first considered. The unexpected phenomena resulting from this interaction between acoustic, photoconductive and piezoelectric effects ignited an excited and frenzied interest within this area of research. Indeed, this initial excitement, although it exists in a somewhat muted form today, has continued over the years to influence the development of this field of physics.

1. Piezoelectricity

The phenomenon that eventually came to be known as piezoelectricity, first formally studied in the late 1800s, has been well-established over the past century and a half. It was, of course, Pierre and Jacques Currie who made the original observations of the piezoelectric effect. Much of the significant and substantial development, however, took place at the turn of the century. In 1910 Woldemar Voigt [1] completed his

1

influential manuscript that first began to lay the foundation for what is considered modern theory. The success of these works and the ease with which theory was translated into such piezoelectric devices such as the transducer had an indispensable impact on the continued interest in the development of piezoelectric technology. Through the middle of the nineteenth century Walter G. Cady's [3] prominent book, *Piezoelectricity*, as well as much work at Bell Laboratories by Warren P. Mason further expanded the field.

Today piezoelectricity is a well documented, understood and, further, a well respected area of physics. As a result of the interest associated with it there are numerous resources available for reference. For this reason little or no reference must be made to original articles pertaining to piezoelectricity as a distinct subject. The reader is referred to Ikeda [4] and Auld [5] for the mathematical framework of piezoelectricity. These two resources are utilized throughout modern literature concerning the piezoelectric effect.

2. Photoconductivity

Photoconduction, although first observed in the same period as piezoelectricity, has developed on a slightly different timeline and in a rather distinct manner. It was in 1873, seven years preceding the detection of the piezoelectric effect, that the first form of photoconductivity, *photoresistance*, was observed [52]. Now despite very little initial progress being made with respect to understanding this peculiar behaviour, the turn of the century brought with it a heightened interest. In fact, by the 1930s much of what is considered to be part of the modern field know as *photoconductivity* had already been encountered. Indeed, physicists of this era had already come across both the *photovoltaic*

2

and *photomagnetic* effects—each responsible for the voltage (and magnetic field in the latter case) generated within certain materials as consequence of increased illumination. As well, the light radiation phenomenon known as *luminescence* had also been discovered. The observation had also been made that that all of these phenomena had dependencies on the wavelength of light employed for excitation.

Over and above simple examination of these several curious phenomena, various theoretical interpretations had been put forth. The most consequential, perhaps, was the characterization of photoconductivity as a quantum effect; that is, it had been determined that the excitation of an electron was a direct consequence of the absorption of a single photon. In this way, by the early 1900s these first scientists had already set about laying a strong foundation for what is considered modern photoconduction theory.

Despite much initial interest in photoconductivity, however, little or no attempt had been made to amass the results of the previous few decades into a single resource. As a result, the collective body of research, to this point, had remained somewhat porous and scattered. It was the original manuscript *Lichtelektrische Erscheinungen* compiled by Gudden [6] which first made the attempt to document this development. This remained, at least for the next few decades, the only true reference within this area of research.

Around the 1950s the interest in photoconductivity swelled and, subsequently, both the quality and quantity of research done within this domain increased exponentially. The argument can be made that this was due in no small part to external experimental and technological advancements which improved crystal growth technique. As a consequence there was a considerably more abundant supply of photoconductive

3

crystals with which to work. Naturally, then, increased interest coupled with a now sufficient supply of experimental materials meant a substantial increase in academic literature upon the subject was sure to follow. This indeed was the case.

Despite the fact that there were merely a handful of published discourses on photoelectric phenomena in existence, this number, however, would bloom over the next few years. Although three such treatises were introduced in the 50s, the most notable document of this era—and still to this day a staple resource in the exploration and understanding of photoconductivity—was *Photoconductivity of Solids*, penned by one of the most renowned physicists to date within this field, Richard H. Bube [7]. Working for RCA Laboratories in New Jersey, Bube had completed the without a doubt the most comprehensive textbook on this subject matter. Surely the circulation of this helped this area of physics to emerge as one of the forefronts of physics.

In 1963, Albert Rose, a mentor to Bube at RCA, released his manuscript *Concepts in Photoconductivity and Allied Problems* [8]. Rather than rehash the concepts that Bube had only just introduced, Rose focused his treatise on the mechanism of excitation and recombination processes within a photoconductive medium. Indeed the nature of developments in photoconductive theory had already begun to shift. At this point the theoretical progress was aimed at resolving the slight difficulties that the current theories of that time had in describing the compound and varied experimental anomalies. Subject matter within this document is decidedly directed towards traps and centers— mechanisms thought to be responsible for most inconsistencies within photoconductive experimentation.

4

The next contribution of particular note within this field, *Photoconductivity and Related Phenomenon*, was edited by J. Mort and D. Pai [9] was not made until 1976. This was, as implied by the title, a survey of the field of photoconductivity, demonstrating the extent to which this phenomenon had expanded and mutated over the preceding years. Indeed, at this point in its development, photoconductive phenomenon was prevalent throughout numerous areas of research, both within the domain of pure experimental and applied. Surely by this time in their development, the use of photoelectronic devices as photo-conductive cells and photodiodes were prevalent throughout technology. The diversity and advancement of this relatively new field of physics was reflected within the pages of this significant collection of academic work.

Having expounded upon the first twenty-five years of modern photoconductive research, it is appropriate to make a few statements which characterize the discussion so far. Firstly, it is important to point out that, for the most part, the theories which were fleshed out in the aforementioned resources were able to correctly, or at least adequately interpret predict experimental outcome. And secondly, thus far nothing has been said that photoconductivity is necessarily an exclusive property of a semiconductor. In fact, this is not the case. From this section forward, however, as in this thesis we are explicitly concerned with CdS, it will be assumed that all photoconductive materials discussed are simultaneously semiconductors. With having been said we can once again resume the discussions of the development of photoconductivity in more recent times.

In the last few decades one of the major difficulties presented to photoelectronic physicists has been the inability of present theories of excitation and recombination mechanisms to explain what oftentimes appears as ambiguous experimental data.

5

Specifically related to this particular research project are examples such as: metastable levels of excitation shown through the measurement of Hall coefficients and longer than expected carrier relaxation periods [14], or, similar to the problem with which we are faced in Chapter II of this research project, the observation of a deliberate decrease in crystal conductivities over long periods of time [12]. In an attempt to respond to this constant, and most notably, consistent emergence of experimental data which defies conventional understanding, both Richard H. Bube and David Redfield have recently responded with responded with recent publications. In 1992 Bube wrote *Photoelectronic Properties of Semiconductors* [13] and just four years later contributed to Redfield's work entitled *Photoinduced Defects in Semiconductors* [14].

Philosophically speaking, it is interesting to note the distinct mutation in perspective that is evident upon comparison of Bube's first [8] contributions to the discussion of photoelectric theory with his second [13]. In fact, this comparison is rather descriptive in terms of evaluating the recent state of affairs in experimental analysis: the many recent innovations of modern photoelectronic devices have placed a much greater demand on semiconductor consistency and stability. For this reason, emphasis has moved from describing the idealized mechanism of photo-semiconductor physics to flushing out the potential mechanisms of defect and center configurations which might account for these observed anomalies. It is in this state of affairs that we are left today, constantly amending and improving present-day band theory in order to generate a more robust framework with which we can work. Though many of the mechanisms are well understood, full comprehension of the quantum interactions that are responsible for photoconductivity has yet to be fully realized.

6

3. Acoustoelectric Interactions

In the middle part of the twentieth century J. J. Kyame published a paper entitled *Wave Propagation in Piezoelectric Crystals* [15]. Within this article he exposed the pentafringent nature of piezoelectric media, presenting for the first time the coupling that exists between the acoustic and the electromagnetic modes of a propagating waveform. Five years later, in 1954, Kyame followed up his initial effort with a second paper demonstrating the theoretical implications of conductivity within the piezoelectric material. These relatively straightforward, yet vastly profound, contributions to the field of acoustics appear, at least in retrospect, to have initiated a veritable avalanche of investigations involving acoustics, piezoelectricity and photoconductivity. Although some of these studies are outside the scope of this thesis project, if nothing else they are closely related and for this reason it is of great benefit to elucidate them at this time. Indeed, due to the interdisciplinary nature of this research paper, even seemingly peripheral resources can provide enlightenment.

Right around the time of Kyame's two pieces of work regarding piezoelectric conductors, R.H. Parmeter first defined what is now considered a common acoustoelectric phenomenon. As he termed it, the *acoustoelectric effect* described the generation of an electric current by an acoustic wave traveling amongst conduction electrons [17]. Around this time, thanks to the contributions of many authors, wave propagation within metals was documented [18, 19]. These works seemed to champion Parmeter's treatise and the general philosophies embodied within his paper were well

7

received. Semiconductive materials, on the other hand, were just coming to the forefront of investigation. For this reason, in light of studies by Gabriel Weinrich [22] and Nobo Mikoshiba [23], it soon became clear that the single-electron model on which Parmeter based his theory contained certain fundamental flaws. However, by introducing electron bunching as one mechanism by which the acoustoelectric effect was still valid, Weinrich remedied its shortcomings. The acoustoelectric effect, then, was able to fully account for much of the phenomenon of interest regarding acoustic interactions with conduction electrons in semiconductors, as well as in metals.

As a further development, Mikoshiba demonstrated that the acoustoelectric examination is better served in three limiting regimes [23]:

$$\omega\tau \ll 1 \quad (\text{low}), \tag{1.1}$$

$$\omega\tau < 1 \quad (\text{medium}), \tag{1.2}$$

and

$$\omega\tau > 1 \quad (\text{high}). \tag{1.3}$$

where ω is the angular frequency of the acoustic wave and τ is the relaxation time of conduction electrons. These same limiting regions appear throughout the literature and, consequently, may be utilized to define the scope of this research project. In fact, as all experimentation within this thesis project takes place between 4 and 25 MHz, and $\tau \sim 10^{-12}$ [53], the mathematical simplifications which are associated with the low frequency region are valid for analysis. For this it seems appropriate to limit our attention exclusively to the material associated with this approximation.

With the preliminary theoretical foundation for acoustoelectric interactions firmly in place by the late fifties, several experimental papers came to the forefront within this

8

field [24-30]. Although it is not necessary to introduce the results of each study, three of these reports illustrate the fundamental findings of these papers which supported earlier theoretical work. Harmon Nine, in one of the first experiments of its kind, observed the dependence of photoconductivity and ultrasonic attenuation on both the level of illumination and the frequency of light used to stimulate a CdS crystal [25]. Also in strong support of theory, A. R. Hutson, J. H. McFee and D. L. White, were the first to determine that through the addition of an electric field, this ultrasonic attenuation could be reversed and the wave could indeed be amplified [28]. In fact, they experimentally demonstrated the prediction of White that, at as the velocity of the drift field began to exceed that of the acoustic field, ultrasonic amplification should be observed. And finally, in 1962, Wen-Chung Wang developed an experimental procedure to measure the acoutoelectric field as a function of crystal conductivity [30]. Together these experiments not only established the fundamental existence of the acoustoelectric effect, but also initiated a great deal of interest in the potential utility of such piezoelectric semiconductors as Cadmium Sulfide.

Although many authors and institutions contributed to the development of the particular theories which governed the acoustoelectric effect, it was without a doubt Bell Laboratories was at the forefront of this investigation. This was demonstrated through the vast quantity a papers published by the various researchers that worked under their banner. Indeed, they pushed this field throughout the sixties and well into the seventies. Two particular examples were the articles composed by D.L. White and A.R. Hutson in 1962 [31, 32]. Certainly these papers explicated and, in turn, consummated the linear theory of ultrasonic wave propagation in semiconductors. These comprehensive works

9

covered the theories of wave amplification, attenuation and dispersion. Nonlinearity, however, had not yet been addressed within this domain.

The observation of several peculiarities associated with the point at which the applied electric field within a semiconductor caused the drift velocity of electrons to overcome the velocity sound field stemmed several new experimental initiates. As an example, a non-Ohmic current-voltage characteristic of piezoelectric semiconductors was observed by R. Smith [33] and J. H. McFee [34] in 1962. It was found in that the current passing through such materials as CdS saturated for a characteristic level of voltage. This 'kink' in the V-I curve was determined to correspond to the the drift velocity of electrons overcoming the velocity of the sound field velocity [35]. Also associated with this characteristic level of voltage "an oscillatory behavior of electron currents flowing in CdS" was observed [36].

Several physicists engaged these difficulties with varied success [37-40]. Although the extent of these papers starts to transcend scope of this project, they are worth mentioning in that they helped spawn an interest in the acoustical nonlinearities of this field. In effort to determine the source of the anomalies occurrences listed above, several physicists developed an interest in the causes and consequences of higher harmonics [41-45]. The first major study on nonlinear theory of this type was initiated in 1964 by B. Tell of Bell Laboratories [43]. Though his results were rather meager due to technological limitations, along with laying the theoretical groundwork for harmonic generation, he successfully observed sizeable second harmonic amplitudes. A numerical treatise of nonlinear theory has also been attempted by Tien [44]. Also, it should be

mentioned that a substantial review of the field was compiled by V. Pustovoit in 1969 [11].

To this point, then, by the early 70s, the basic fundamental concepts that govern the propagation of acoustic fields within in piezoelectric semiconductors had been almost completely developed. Both linear and nonlinear theories had been introduced and their central subject matter had been validated. Unfortunately, however, technological limitations slowed experimental progress, particularly in the areas concerning harmonic generation. For this reason, both theoretical and experimental physicists shifted their focus towards more promising areas of development. The physics of closely related areas such as piezoelectric surface waves and acoustic waves in layered piezoelectric structures began to flourish at the expense of nonlinearity. Consequently, there are still many attractive experimental opportunities within this rewarding area of physics—particularly of a nonlinear nature.

4. Scope of Thesis

Due to the multitude of diverse fields which govern the nature of Cadmium Sulfide, even for academic purposes alone, its study can prove a fruitful endeavor. Indeed, as discussed at length in the previous sections, in order to begin a study of CdS, one must investigate several disciplines of physics. It is, in fact, the coupling of the various phenomena associated with each field that has intrigued physicists for nearly an entire century. As a thesis project, then, the intricacies of Cadmium Sulfide provide fertile ground for intellectual growth.

11

Unfortunately, due to the intricate nature of this special crystal, it can also prove difficult to comprehend. For many years physicists have toiled to understand the nature of the peculiarities surrounding both the mechanisms of electron excitation, and the wave curiosities that are associated with piezoelectric photo-semiconductors. Although much has been resolved, there are still many nuances that have yet to be fully scrutinized. Indeed, then, there are still many opportunities for scientific discovery within this field.

The primary objective of this thesis project, at least at the outset, is the investigation of acoustic wave propagation in a piezoelectric semiconductor, specifically Cadmium Sulfide. As outlined earlier, much work has been done to date in this area— particularly with respect to the attenuation of ultrasonic waves. There is, in fact, much theoretical and experimental evidence of this occurrence. Dispersion, on the other hand, has not yet been exhaustively documented. In fact, despite having robust theoretical models demonstrating significant velocity changes as a function of crystal conductivity, most experimental work seems to focus on the aspects of wave attenuation and amplification. Further, although harmonic generation is a fundamental aspect of many theoretical models, it can be difficult to find experimental studies which shed light on its relationship with illumination levels. Even rarer, it seems, are academic papers which deal with harmonics higher than the 2nd. Thus, there is still much of worth that can be accomplished in this area of research.

Also, as mentioned earlier, Cadmium Sulfide can prove a challenging crystal with which to work. In fact, there have been several studies published demonstrating the metastable conductivity levels of Cadmium Sulfide and other such crystals. The form

12

and behavior of these instabilities, however, seem dependent on individual crystal characteristics.

With this being stated, the objective of this thesis is twofold. Firstly, in Chapter IV an investigation is undertaken whose purpose is the exploration and subsequent discussion of metastable conductivity levels. The principle intention of this portion of research is to determine a method with which stable conductivity levels can be attained, not to develop an understanding of the mechanisms of crystal excitation,. Upon completing this analysis, the wave peculiarities that come as a result of the acoustoelectric effect are explored in Chapter VI, specifically in Cadmium Sulfide. It is in this Chapter that is found the work considered to be the primary focus of this research project. The experimental aspects of this chapter include both linear and nonlinear sections. In the linear portion of this research project both wave attenuation and dispersion are examined, while the second half of this chapter explores the generation of higher harmonics.

Upon obtaining experimental results, the proper discussions are undertaken. All findings from both Chapter IV and Chapter VI are properly scrutinized and, where appropriate, compared with theory. Principle literature is also utilized in attempt to validate experimental discoveries. Also, where possible, comparisons of a quantitative nature are made with appropriate theoretical models. Final discussions and conclusions regarding the success of this thesis project are undertaken and closing remarks are made in Chapter VII.

13

CHAPTER II

Photoconductivity and Photoelectrical Processes

If any progress is to be made in terms of experimentation within the field of photo-acoustics, it is necessary to have an appropriate understanding of the characteristics of photoconductive crystals such as Cadmium Sulfide. For this reason, before undertaking a complete discussion of the experimental methods and procedures involved in this research project, we first include a section devoted to the theory of electronic process and mechanisms of photoconductivity. A preliminary explanation of this phenomenon will be addressed subsequently. For a more complete discussion readers are further referred to Bube [7,13] or Rose [8].

1. Conductivity Processes in Crystals

Before undertaking a discussion of photoconductivity it is necessary to have a proper understanding of the field of conductivity as a whole. For this reason we begin this section with a quick review of the fundamentals of semiconductor crystals.

The quantum-mechanical interaction between neighboring atoms within a crystal cause the energy levels of an individual atom to split into what are called energy bands. Situated between these *allowed* bands are *forbidden* energy levels. In a semiconductor, the band structure (see Figure 2.1) is such that for $\Delta E > kT$ the outer, or *conduction band* is unoccupied (where ΔE is the energy gap between the valence and conduction band and kT is the thermal energy of an electron). In this way as the thermal energy of a material

14

increases to the point where $\Delta E < kT$, electrons may 'jump' from the fully occupied *valence band* to the conduction band where they may behave as *free electrons*.
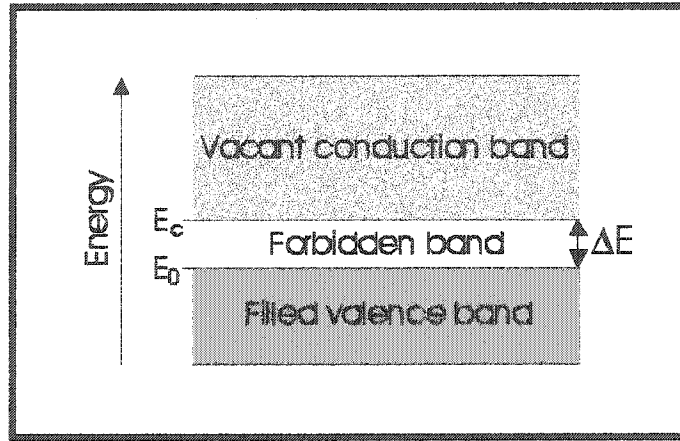
Figure 2.1. The band structure of a semiconductor.

When electrons are raised to the conduction band of a semiconductor, they leave behind vacant orbitals in the valence band. These vacancies are commonly referred to as holes and their equation of motion is that of a particle of charge opposite an electron. In other words, free holes in the valence band act in a manner similar to free electrons in the conduction band. Although their electric currents remain in the same direction under the application of an external electric field, their drift velocities are in opposite directions.

Now, although, an excited electron is considered to be free everywhere within the conduction band, it is known to have zero momentum at both the upper and lower edges. It is, in fact, only at the center of the band that the momentum is a maximum, approaching a value of a truly free electron. In order to compensate for this discrepancy, the electron is considered to be essentially free with an *effective mass* defined by

$$m^* = \hbar^2 \left(\frac{\partial^2 E}{\partial k^2} \right)^{-1} ,$$

(2.1)

15

where E is energy and k is the so-called propagation or wave vector. Interestingly enough, the band structure is such that at times this equation can give rise to negative effective masses.

With these basic principles in mind, let us now explore the mechanisms of electronic transitions within a semiconductor. As a specific example, consider optical transition of an electron from the valence band to the conduction band of a particular intrinsic semiconductor. The specifics of this individual transition are nicely summarized below.
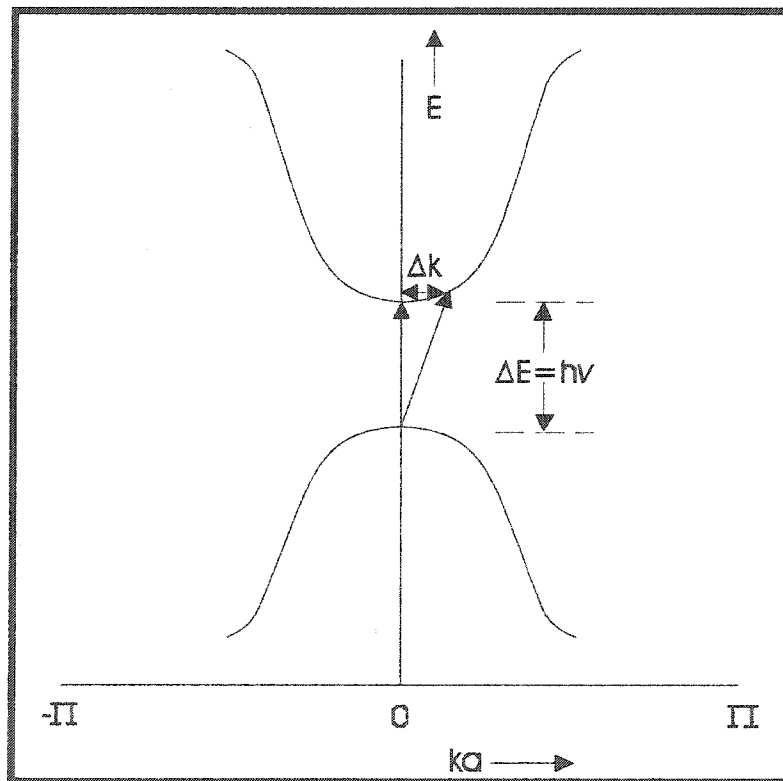
Figure. 2.2. A representation of electron excitation in one dimensional E vs. k space.

The momentum of such an electron, in the case of a single spatial dimension, is given by

$$p_e = \hbar k .$$ (2.2)

16

Likewise, the momentum associated with an absorbed photon can be expressed in terms of light frequency, v, the index of refraction, n, and the speed of light, c as

$$p_{ph} = \frac{2\pi \hbar v\, n}{c}.$$

(2.3)

Through the consideration of conservation of momentum and energy, it can be shown that for values for n and ΔE, the additional momentum provided by the photon (Δk) is negligible. For this reason it is often ignored with little loss in accuracy. Thus, we are left with only vertical transitions between allowed bands and Figure 2.2 is greatly simplified; it can be then represented by a diagram such as Figure 2.1.

Having established that we need really only consider energy transitions in cases involving only photonic excitation, we can further explore the nature of transitions in a more simplified manner. In this regard, the electronic transitions observed in common photoconductors are summarized in Figure 2.3. Transition 1, known as *intrinsic* or *direct absorption*, results, for each photon absorbed, there is both a corresponding free electron and a free hole. In a similar manner, Transition 2 produces a free hole in the valence band and an electron bound in the neighborhood of the imperfection and Transition 3 produces a free electron in the valence band and a bound hole. Individually, these transitions are characterized as excitations; together they constitute *extrinsic absorption* with an end result similar to that of Transition 1. Also illustrated in Figure 2.3, Transitions 4 and 5 are two photoconductor phenomena known as *trapping*. Transitions 6 and 7 signify capture and recombination whose end result is classified as *indirect recombination*. And finally, in a manner opposite Transition 1, Transition 8 represents what is known as *direct recombination*. The probability of this last transition is quite small with respect to the mechanism of Transitions 6 and 7 and is generally associated

17

with a radiative phenomenon such as the emission of photons with energy approximately equal to that of the band gap.
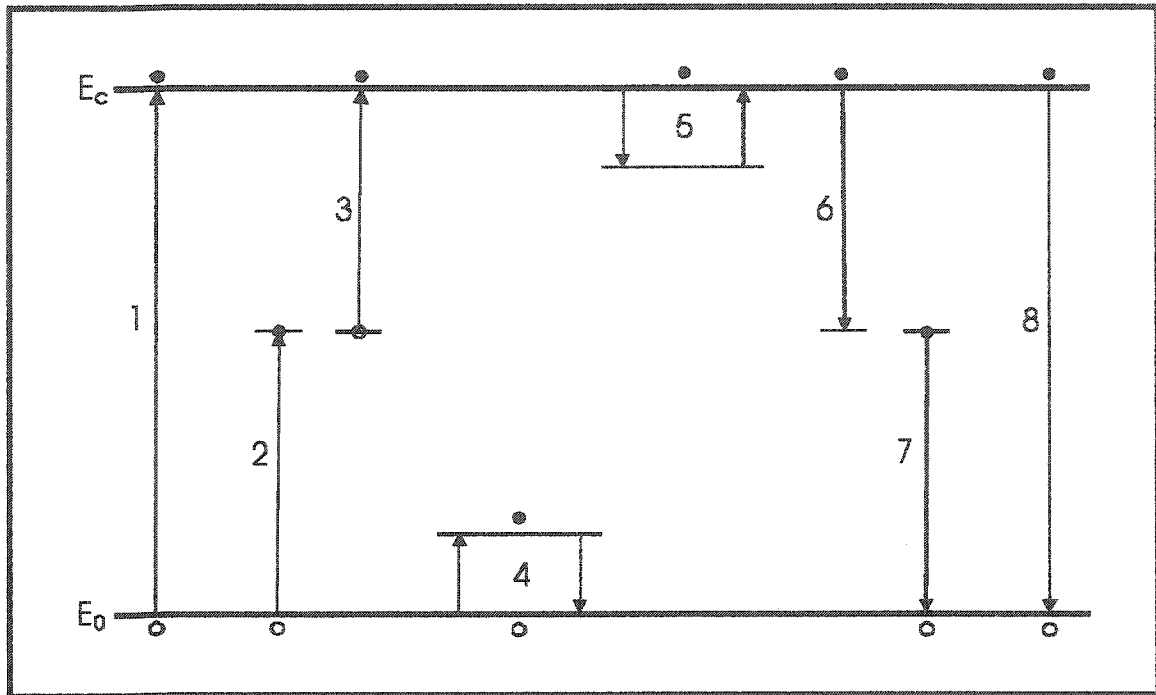
Figure. 2.3. Common transitions in photoconductors.

At this point we have introduced the preliminary concepts regarding the mechanisms of absorption, excitation and recombination without demarking the fundamental difference between traps and recombination centers. In order to properly undertake this analysis, however, it is imperative that we discuss the Fermi energy as it is often used to differentiate between types of impurities.

The Fermi distribution function is valuable in the analysis of conductivity levels or, more specifically, occupation levels in that it identifies the probability that a state with energy E will be occupied. It is written as

18

$$f(E) = \frac{1}{\exp[(E - E_F)/kT] + 1}.$$ (2.4)

The so-called *Fermi energy* (or *chemical potential*) is denoted by E_F. Simply put, the Fermi-level is the level where the occupation probability is 1/2. Using Equation (2.4), then, the number of occupied states is given by

$$n = \int_{Ec}^{\infty} f(E) N(E) dE$$ (2.5)

where integration begins at the bottom of the conduction band and $N(E)$ is known as the density of states. For a given material the value $N(E)dE$ can be calculated assuming the shape of the energy surfaces in k space are known. A similar expression can be found for the occupation of imperfection levels within an extrinsic semiconductor:

$$n_I = \frac{N_I}{\frac{1}{2}\exp[(E_{fn} - E_I)/kT] + 1}$$ (2.6)

Here N_I represents the density of imperfections, $E_{fn} = |E_c - E_F|$, and E_I is the energy difference between the bottom of the conduction band and the imperfection level.

With this being said, we can once again return to our discussion of impurities. As Figure 2.3 demonstrates, the absorption of a photon excites a free electron into the conduction band. The hole, corresponding to this electron, remains in the valence band. Once in the conduction band, however, this free electron will remain there until it is captured by on of these imperfections. These capturing centers are ultimately classified according to the propensity of the electron in this captured state to become thermally re-excited to a free state or to recombine with a carrier of the opposite sign. If the probability of re-excitation is greater, the imperfection is classified as a *trapping center*. Otherwise, it is referred to as a *recombination center*. The delineation of a center as

19

either a trapping or recombination center is not an intrinsic property of the center itself; however, its demarcation is a dependent on external kinetic conditions, i.e., on light levels and temperature.

Trapping centers and recombination centers are mathematically differentiated as follows: A center lying at an energy level E_I below the conduction band is said to be a trapping center if and only if

$$n_I p \upsilon S_p \ll n_I S_n \upsilon N_c \exp\left(-\frac{E_I}{kT}\right). \tag{2.7}$$

Otherwise, if

$$n_I p \upsilon S_p \gg n_I S_n \upsilon N_c \exp\left(-\frac{E_I}{kT}\right), \tag{2.8}$$

it is said to be a recombination center. Here n_I is said to be the density of centers occupied by an electron, p is the density of free holes, S_n is the capture cross section for a free electron by a center occupied by a hole, S_p is the capture cross section for a free hole by a center occupied by an electron, and N_c is the effective density of states in the conduction band, v is the thermal velocity of the carrier ($\sqrt{2kT/m}$).

Just as it is often convenient to locate the Fermi level for a given semiconductor, it is equally beneficial to denote what are called demarcation levels. By definition, a charge carrier at its respective demarcation level has equal probability of being ejected into the conduction band and being recombined into the valence band. These demarcation levels, along with the Fermi levels, as discussed earlier, are illustrated for a crystal such as CdS below in Figure 2.5.

20
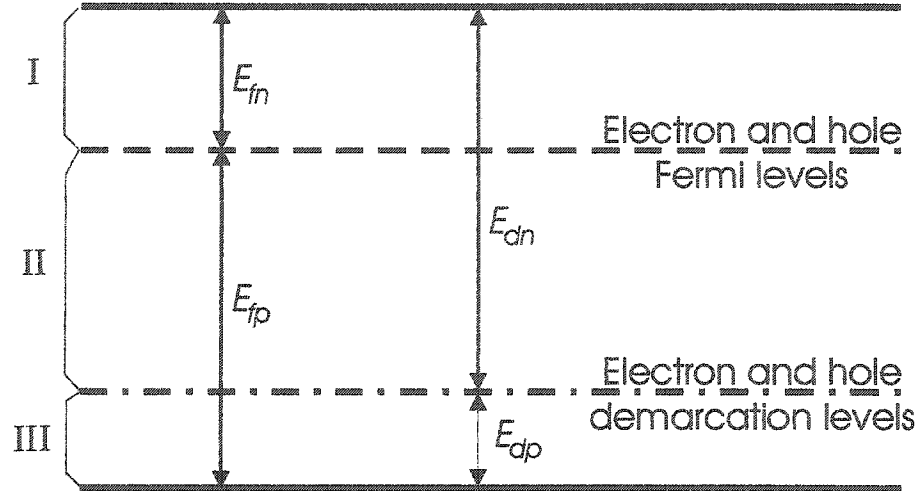
Figure 2.5. Fermi levels and demarcation levels for a semiconductor [7].

The equations relating the various levels can be derived to be [7]:

$$E_{fn} = E_{dn} + kT \ \ln\left(\frac{N_p}{N_n}\right),$$
(2.9)

$$E_{fp} = E_{dp} - kT \ \ln\left(\frac{N_p}{N_n}\right),$$
(2.10)

and,

$$E_{dn} = E_{fp} - kT \ \ln\left(\frac{S_p}{S_n}\right) - \frac{3kT}{2} \ln\left(\frac{m_h}{m_e}\right).$$
(2.11)

where E_{fn}, E_{fp}, E_{dp} and E_{dn} are the energy differences between the electron and hole Fermi levels and electron and hole demarcation levels as seen above in Figure 2.5. Also, N_p and N_n are the density of recombination centers for holes and electrons respectively.

2. Basic Principles of Photoconductivity

The conductivity of an insulator or semiconductor is expressed as

21

$$\sigma = q(n\mu_n + p\mu_p),\qquad\qquad(2.12)$$

where n and p are the densities of the free electrons and holes, respectively, and μ_n and μ_p are the electron and hole mobilitys. In a homogeneous material n and p are considered uniform throughout. The absorption of radiation energy increases the values of both n and p by raising electrons from the valence to the conduction band and, consequently, boosting conductivity—a phenomenon referred to as photoconductivity. This increase in conductivity is expressed as follows:

$$\Delta\sigma = q\big(\Delta n\mu_n + \Delta p\mu_p\big).\qquad\qquad(2.13)$$

An important differentiation can be made between semiconductors and insulators in terms of the response in the number of holes and electrons to photo-stimulation. Specifically, in insulators the values of Δn and Δp are generally much smaller than the corresponding free-carrier densities in the dark, namely n_0 and p_0, and the effect of radiation can be treated as a small perturbation. On the other hand, within semiconductors this is not the case, as the reverse is often true: Δn and Δp have a tendency to dominate. This, then, is the fundamental distinction between the theoretical treatment of an insulator and that of a semiconductor.

It is possible to effectively simplify the interaction by considering two approximations:

- By assuming that one of the carriers dominates the conductivity; the conductivity of the other can be neglected.

- The crystal is expected to stay neutral during the photoconductivity process without a build-up of appreciable space charge; i.e., $\Delta n = \Delta p$.

22

These assumptions are in fact quite popular throughout the literature and, with proper care, can greatly assist in the understanding of a rather complex interaction.

Conductivity is, in fact, a dynamic process with charge carriers constantly undergoing excitation and recombination. For this reason one of the key parameters affecting the photoelectrical properties of Cadmium Sulfide is the lifetime of the photoexcited carriers. Consider that the light falling on a photoconductor creates f electron-hole pairs per second per unit volume. Using τ_n to represent the free lifetime of an electron and τ_p for the free lifetime of a hole, we then have

$$f\tau_n = \Delta n,$$ (2.14a)

and

$$f\tau_p = \Delta p.$$ (2.15b)

Using these new definitions equation (2.2) becomes

$$\Delta\sigma = fq(\mu_n\tau_n + \mu_p\tau_p),$$ (2.16)

demonstrating the importance of lifetime within the scope of photoelectrical processes.

Although to this point we have taken *lifetime* to mean *free lifetime*, there are, as well, several other types of *"lifetimes"* requiring classification [7]:

(1) Free Lifetime

The free lifetime (as referred to above) is the time that the charge carrier is free to contribute to the conductivity. It is the time that an excited electron spends in the conduction band, or the time that an excited hole spends in the valence band. The τ_n and τ_p (of Eq. (2.3a) and Eq. (2.3b)) the free lifetimes. The free lifetime of a charge carrier can be (a) terminated by recombination, or if the carrier is extracted from the crystal by the electrical field without being replenished from the opposite electrode; (b) interrupted if the carrier is trapped, to be resumed when the carrier is freed from the trap; (c) undisturbed if the carrier is extracted from the crystal by the field at the same time as an identical carrier is injected into the crystal from the opposite electrode.

(2) Excited Lifetime

The excited lifetime is the total time the carrier is excited between the act of excitation and the act of recombination, or extraction without replenishment. The excited lifetime includes any time that the carrier may spend in traps; it is therefore usually longer than the free lifetime.

23

(3) Pair Lifetime

        The pair lifetime is the free lifetime of an electron-hole pair. If either electron or hole is captured, or is extracted without replenishment, the pair lifetime is terminated.

(4) Minority-Carrier Lifetime

        The minority-carrier lifetime is the free lifetime of the minority carrier, i.e., the carrier which makes the minor contribution to the conductivity: Electrons in p-type materials, and holes in n-type materials. Usually the pair lifetime is equal to the minority-carrier lifetime.

(5) Majority-Carrier Lifetime

        The majority-carrier lifetime is the free lifetime of the majority carrier, i.e., of electrons in n-type materials, and of holes in p-type materials. If the density of free carriers in a material is very much greater than the density of recombination centers, as is frequently true in semiconductors, the majority-carrier lifetime will be equal to the minority-carrier lifetime. But if the density of free carriers is much less than the density of recombination centers, as is most often true for insulators, the majority-carrier lifetime can be much larger than the minority-carrier lifetime.

Frequently, in an attempt to encourage photosensitivity, centers are incorporated into a material. As these centers have a much greater probability of capturing minority carriers than it does majority-carrier lifetime. As an example, in sensitive CdS while the minority-carrier lifetime is only 0.01 µs or less, the majority-carrier lifetime is increased to an order of 1 ms [7]. In our case, however, with insensitive CdS, both the majority and minority carriers have a lifetime of approximately 1 µs [7].

A term which is often utilized within the field of photoelectronics is *photosensitivity*. Although many alternate definitions of photosensitivity have arisen over the years throughout the literature, for the purpose of this thesis it will be thought of as the change in conductivity that comes about by excitation, divided by the excitation intensity. In terms or an exact definition this is given as photoconductivity per unit excitation intensity. Under the assumption that the photoconductivity of a particular material is a linear function of both applied voltage and light intensity, however, we can introduce an intrinsic property called the specific sensitivity (units: $cm^2 \ \Omega^{-1} \ V^{-1}$). The specific sensitivity of a material, as it turns out, is proportional to the free carrier lifetime, τ, and the free carrier mobility, μ.

24

In the physical world, a concept known as gain, G, is also a useful quantity when dealing with photoconductivity; this term pertains to situations in which a current passes through the photoconductor. A relation for gain is described by:

$$\frac{\Delta I}{q} = GF.$$ (2.17)

Here ΔI and q represent the photocurrent and magnitude of the carrier charges respectively. The symbol F, where $F = f \cdot$ (volume), defines the number of electron-hole pairs being created per second within the photoconductor. Naturally, then, by this definition, we can also state gain with respect to the ratios of the free lifetimes of the charge carriers (τ_n and τ_p) to the transit time, t_n and t_p, required for each charge carrier to traverse the distance between the electrodes. Thus,

$$G = \frac{\tau_n}{t_n} + \frac{\tau_p}{t_p}.$$ (2.18)

With the application of a voltage V across a distance L, the transit time can be defined in a quantitative manner by

$$t = \frac{L^2}{\mu V}.$$ (2.19)

Equation (2.6) can then be expressed as

$$G = (\tau_n \mu_n + \tau_p \mu_p)\frac{V}{L^2}.$$ (2.20)

Now consider, for a moment, a single charge carrier with thermal velocity within close proximity of a recombination center. Upon realization of the condition that the binding energy due to the coulomb attraction on this free carrier is equal or larger than

25

kT, it is assumed that the carrier is returned to the valence band of the semiconductor. A simple estimate of capture cross section, S, can then be made corresponding to

$$\frac{q^2}{r \in} = kT ,$$

(2.21)

where $\in$ is the dielectric constant. At room temperature we then obtain

$$\pi r^2 = S = \frac{10^{-10}}{\in^2} \, cm^2,$$

(2.22)

which for our case of Cadmium Sulfide the capture cross section is found to be in the order of 10^{-12} cm^2 [14]. Generally the recombination center is found to be uncharged, however, it has been found in some cases to exert a small coulomb repulsion on free carriers (see Figure 2.4 below).
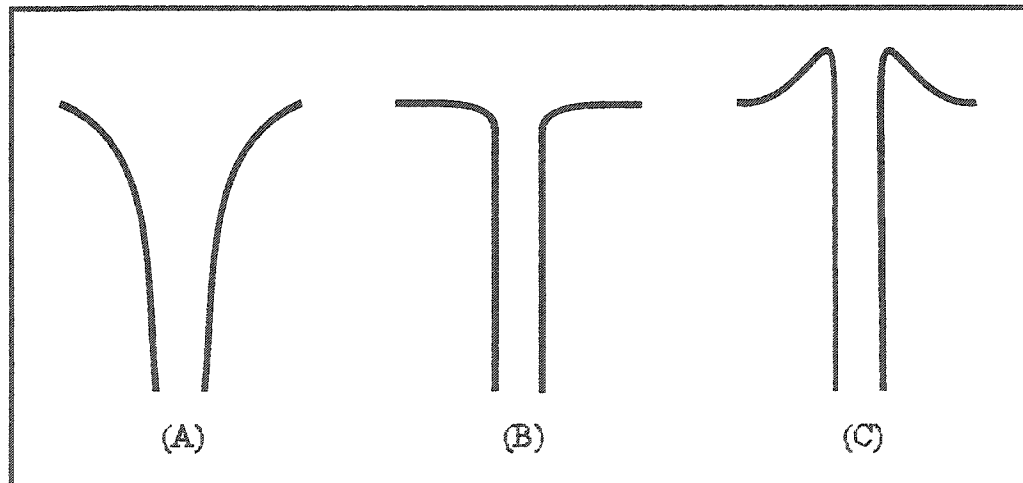
Figure 2.4. Schematic representation of coulomb forces present at recombination centers. (A) Attractive. (B) Neutral. (C) Repulsive.

Upon introducing both the concept of a recombination center and its capture cross section, the free carrier lifetime can be expressed in a greatly simplified manner:

$$\tau = (vSN)^{-1} ,$$

(2.23)

26

Within Equation (2.23) N is defined to be then density of recombination centers within a particular material and, naturally, v is the thermal velocity associated with the particular free carrier.

Optical absorption in photoconductivity is generally discussed in terms of α, the absorption coefficient. If the loss due to surface reflection is ignored, Beer's law describes the intensity of absorbed light as a function of distance x,

$$I = I_0 \exp(-\alpha x).$$ (2.24)

Penetration depth is often defined as

$$d \equiv \frac{1}{\alpha},$$ (2.25)

and hence can be described as the distance after which light intensity has been reduced by a factor of e. For indirect absorption this is typically in the range of 100 μm [13].

There is generally a close correlation between the optical absorption spectrum and the photoconductivity response. The general shape of these curves for typical photoconductors is shown below in Figure 2.5. Characterized by high absorption, in the first region the photoconductivity is dominated by the free carrier lifetime at the surface. In Region III, on the other hand, the recombination characteristics of the bulk material as well as the absorption spectrum of the particular crystal are responsible for the level of photoconductivity. The maximum seen in the second region corresponds to sample thickness.

27
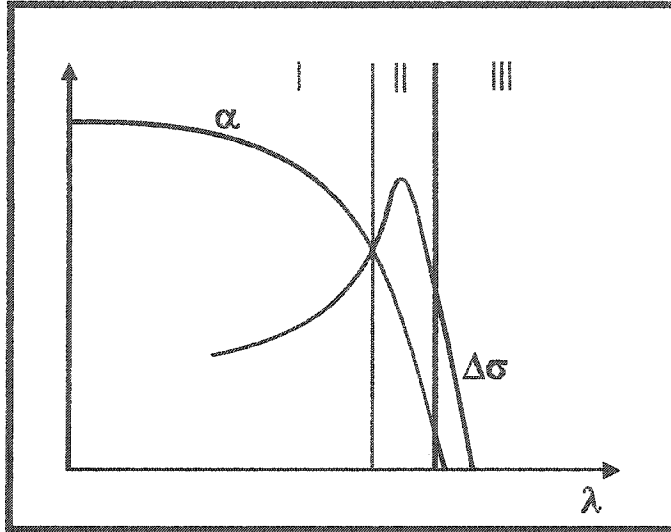
Figure 2.5. Spectral absorption and photoconductivity as a function of radiation wavelength. Here α is the absorption and Δσ represents a photoconductivity curve. The indicated regions are described in the discussion above.

3. Recombination Kinetics

To this point, although much reference has been made to excitation and recombination, little of quantitative nature has been said about the mechanisms of recombination kinetics. It is at this point that recombination, especially with respect to trapping levels, will be fully addressed. First, however, it is beneficial to discuss recombination in the absence of trapping, after all, trapping centers, although they do capture and release carriers, have only a small part in the actual recombination process itself.

For steady state levels of conductivity the rate of free-carrier generation must be equal to the rate of free-carrier recombination. For i charge carriers ($i = electrons, holes$) in the dark this is stated as

$$\sum_i g_i = n_0 \upsilon \sum_i S_i N_i \qquad (2.26)$$

28

where g_i is the rate of thermal generation, n_0 is the density of free electrons in the dark. S_i and N_i are the recombination cross-sections and densities. Upon illumination, additional free-carriers Δn are generated at a rate f. Consequently, Equation (2.18) becomes

$$f + \sum_i g_i = (n_0 + \Delta n)\upsilon \sum_i S_i N_i \qquad (2.27)$$

Under the condition of a single type of recombination center from which both optical and thermal generation originate (mathematically, this means that $N = n_0 + \Delta n$) we can derive the following relationships:

$$(n_0 + \Delta n) = \left(\frac{f + g}{\upsilon S}\right)^{1/2}, \qquad (2.28)$$

and,

$$\tau = [\upsilon S(n_0 + \Delta n)]^{-1}. \qquad (2.29)$$

In a semiconductor, as $n_0 \gg \Delta n$ and $g \ll f$, these equations reduce to

$$\Delta n = \frac{f}{2n_0 \upsilon S}, \qquad (2.30)$$

and,

$$\tau \approx (n_0 \upsilon S)^{-1}. \qquad (2.31)$$

Equation (2.30) represents the change in photocurrent caused by illumination whereas Equation (2.31) demonstrates the dependency of carrier lifetime on the change in photocurrent. As is generally the case, however, the mechanism of recombination without the effects of trapping is ineffective at adequately describing experimental results. It seems, then, that, trapping plays a large role in photoconductivity.

The existence of traps, as it turns out, effectively reduces the number of free charge carriers. In fact, the addition of traps within a particular semiconductor, means that not all excited carriers will reach the conductivity band. For this reason, it is essential to amend the theory to take into account the effect of trapping. One effective method is to define a new *drift mobility*, μ^*_d, with which all excited carriers, both free and trapped, move. In terms of the density of free and trapped carriers (n and n_t respectively) this appears as

$$\mu^*_d = \frac{n}{n+n_t} \mu.$$

(2.32)

Naturally, then, if $n_t > 0$,

$$\mu^*_d < \mu.$$

(2.33)

It can also be shown that the presence of traps both slows the observed decay time of the photocurrent, as well as decreases crystal sensitivity. Naturally, with no traps present the photocurrent decay time corresponds to the free carrier lifetime. Otherwise, upon capture from the conduction band by trapping centers, charge carriers can be thermally ejected back into an excited state. In this way, the presence of numerous shallow defects in the forbidden energy band can greatly increase the length of the free carrier lifetime. In fact, if the density of recombination centers is represented by

$$N_r = n + n_t,$$

(2.34)

where n_t is the density of centers that are specifically trapping centers, the lifetime of a free electron can be shown to be reduced from

$$\tau = \left(v S_n n\right)^{-1},$$

(2.35)

to

30

$$\tau = \left(vS_n N_r\right)^{-1}. \tag{2.36}$$

Surely then, as they play a role in photocurrent, free carrier lifetime, and effective mobility of the charge carrier, trapping centers can have a great deal of effect on experimental observations.

4. Other Defects

Although for the most part the only imperfections, or *defects*, within the forbidden energy band that have been discussed have been traps or recombination centers, there are several other types of impurities. These defects take a variety of forms [13]:

(1) native point defects, such as isolated vacancies, interstitials, or antisite atoms of the host crystal;
(2) point defects associated with the presence of isolated impurity atoms, in either substitutional or interstitial positions;
(3) defect complexes formed by the spatial correlations between different point defects, such as donor—acceptor or impurity—vacancy pairs;
(4) line defects, such as dislocations;
(5) defects associated with grain boundaries in a polycrystalline material; and
(6) defects associated with the existence of a surface or interface.

These imperfections can play many different roles, depending on the structure of the crystal and the band gap. Thus far our discussion has included recombination and absorption centers as well as traps, however, two other defects that appear in the literature have as yet been omitted. They are donors/acceptors and scattering centers. Donors and acceptors are neutral impurities within a lattice that, as their names imply, are able to either inject an extra electron into the conduction band or, conversely, accept an electron from the valence band. Both of these mechanisms leave an unoccupied hole. This hole is located in the forbidden band in the first case, or in the valence band as in the second.

31

Scattering centers, on the other hand, do not play a direct role in conductivity levels as they neither accept nor eject charge carriers, at least in general. Instead, they play a role in that they affect the mobility of free carriers if uncharged and scatter free charge carriers if uncharged.

Unfortunately, however, the theories and concepts that physicists have utilized since the middle part of the last century have been inadequate for some time in that they fail to describe some phenomena. For this reason, although they provide for an adequate understanding of the fundamental concepts of photoexcitation and recombination, they are in need of amendment. As example there are numerous citations within modern literature of what are called *metastable* levels of photoconductivity or carrier concentrations. The solution to this problem it seems, are defect formations which are of a somewhat kinetic in nature. For a more detailed explanation of modern defect physics the interested reader is referred to David Redfield's *Photoinduced Defects in Semiconductors [4]*.

5. Theory of Kinetic Photoconductivity

In crystals such as Cadmium Sulfide, slowly degrading levels of conductivity can be described in terms of a kinetic analysis. An effective preliminary mathematical model for what are called *time-dependent photochemical reactions* is described in Boer [5]:

To properly account for the slowly changing levels of photoconductivity of a semiconductor as a whole the time variant density of electrons at each band must be represented. This can be represented as

$$\frac{dn_i}{dt} = f_i - r_i, \quad n = 1, 2, \ldots \tag{2.37}$$

32

where f_i and r_i are the excitation and recombination rates for the ith level respectively. This process of electron transitions between subsequent impurity levels in the forbidden energy band is illustrated below.
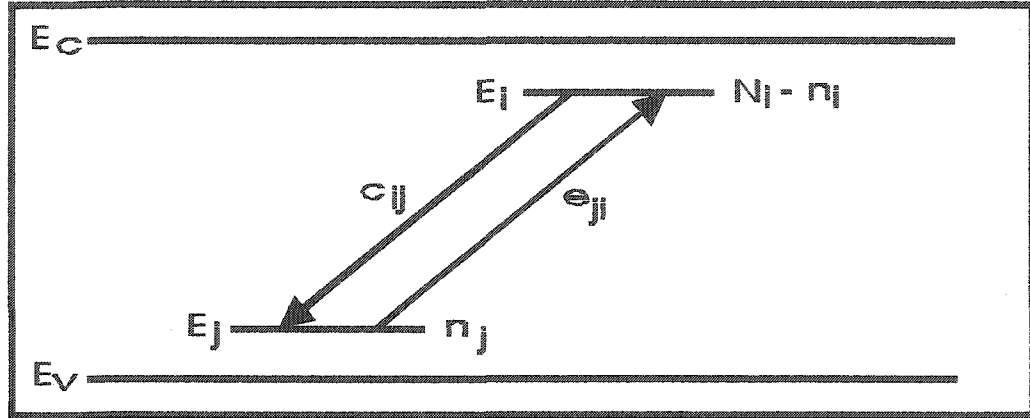
Figure 2.6. Transitions between two impurity levels in the forbidden band.

Mathematically these transitions are represented by

$$f_i = \sum_j n_j e_{ji} (N_i - n_i),$$ (2.38)

and

$$r_i = \sum_j n_i c_{ij} (N_j - n_j).$$ (2.39)

Here e_{ij} and c_{ij} are the transition coefficients between level i and level j, N_i and n_i and the density of the level i and the density of electrons on that level respectively; e represent excitation transitions and c represent capture transitions.

For an intrinsic semiconductor Equation (2.37) becomes,

$$\frac{dn}{dt} = f_{vc} - c_{cv} np,$$ (2.40)

where n and p are the density of electrons and holes and the subscript vc denotes the transition directly from the valence to conduction band. For a constant optical generation

33

rate, f_{vc}, during the time period ranging from $t_0 < t < t_1$, the solution to this equation for is a tanh function. Indeed, the photoconductivity is shown to rise as,

$$n(t) = \sqrt{\frac{f_{vc}}{c_{cv}}} \tanh\left[\sqrt{g_0 c_{cv}}(t - t_0)\right],$$ (2.41)

If at t_1 the source of excitation is shut off ($f_{vc} = 0$) then a hyperbolic function is obtained for which is Equation 2.40. The photoconductivity then decays as,

$$n(t) = \frac{1}{c_{cv}(t - t_1)}.$$ (2.42)

The speed of rise is largely dependent on light intensity for $t < t_1$. On the other hand, for $t > t_1$ the decay rate is governed by the cross sectional areas of the recombination centers particular photoconductor. A plot of these two curves can be seen below in Figure 2.7.
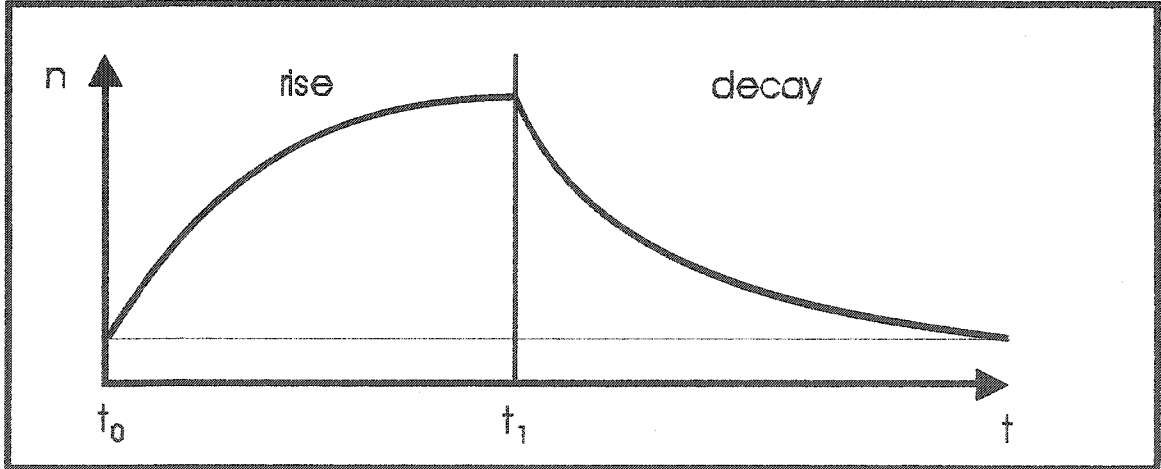
Figure 2.7. Rise and decay trends according to mathematical theory in the absence of trapping.

If there are traps introduced into this simplified model then Equation 2.40 is modified to include the possibility that transitions also include those from the valence band the trapping level. This is written as

34

$$\frac{dn}{dt} = f_{vc} - \frac{dn_t}{dt} - c_{cv}n(n + n_t),$$

(2.43)

where the succession from the trapping to the conduction band is represented by

$$\frac{dn_t}{dt} = c_{ct}n(N_t - n_t) - e_{tc}N_cn_t.$$

(2.44)
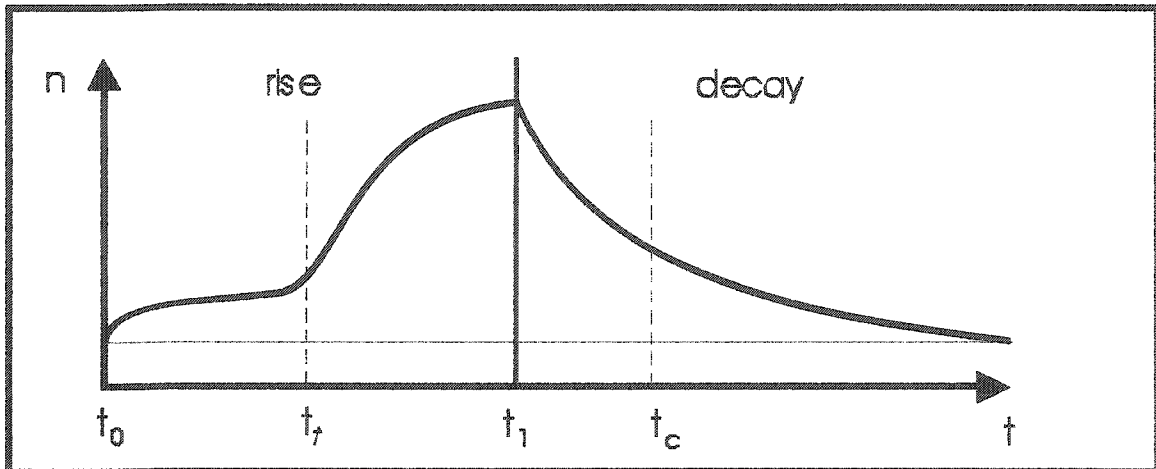
Figure. 2.8. Rise and decay trends of excitation levels with the effect of trapping.

It can be shown then (see Figure 2.8 above) that with the existence of traps further divides both the rise and decay portions of our curve. There are indeed time frames from the rise in photoconductivity. Firstly, from $t_0 < t < t_t$ the trapping levels are slowly filled, after which time we are left with a situation similar to an intrinsic semiconductor and the transitions are made to the conduction band. Similarly, the decay time is subdivided into the time during which the conduction band is vacated, $t_1 < t_c$, and the time after which all recombination takes place as a result of the trapping levels exclusively.

35

CHAPTER III

General Experimental Strategy

The fundamental purpose at the outset of this research project was the investigation of the acoustic wave interactions with free charge carriers in Cadmium Sulfide. However, before much progress could be made in this field of study it was necessary to review the fundamental understanding of the nature of photoconductivity. It was for this reason that several procedures and algorithms were given to characterize the nature of photo-excitation in CdS. The results of this study, then, carried over, and further, facilitated the development of an experimental method regarding the investigation of the acoustoelectric effect. Naturally, then, there are many experimental techniques and apparatus that are common to both the investigation of photoconductivity and the acoustoelectric effect. It is therefore beneficial at this time, before introducing becoming engaged in a discussion of either of these subjects, to commence with an introduction to the basic experimental principles and procedures that are utilized throughout this thesis project.

1. Initial Development

The central element of this thesis project is the trapezoid-shaped Cadmium Sulfide crystal itself. More specifically, in both studies, it was necessary to measure its conductivity. Naturally, the most straightforward method of determining the conductivity within the crystal is through the measurement of the resistance across it with the aid of a multimeter. In order to assure that the contacts between the ohmmeter leads and the

crystal itself were consistent between procedures, it was thought best to first affix permanent leads at opposite ends of the sample. In order to provide for the best contact possible between the leads and the Cadmium Sulfide crystal itself two rectangular aluminum thin films were vacuum evaporated onto both ends of the top face of the crystal. Chemtronics' Circuit Works conductivity epoxy was then utilized to hold fast two thin flexible copper leads onto these aluminum contacts. Also, as the resistance across the leads of the crystal was calculated at dark-level to be thousands of mega-Ohms, it was necessary to place an 8.369 MΩ resistor in parallel with the CdS crystal. By doing this it was possible to read the resistance with a Fluke 867B Graphical Multimeter. This resistor was necessary for all crystal conductivity measurements throughout all experiments in this research project. Consequently, the resistance of the crystal could be measured in a consistent manner simply through the use of an ohmmeter with alligator clips for leads.
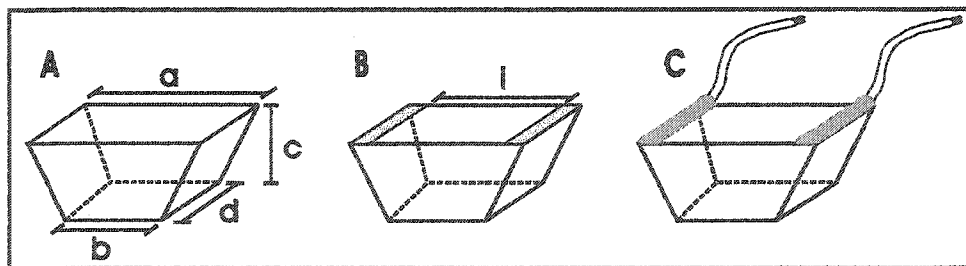
Figure 3.1 The Cadmium Sulfide crystal being prepared for resistance measurements.
A. The crystal itself.   B. Aluminum plated pads were prepared on each end.
C. Flexible leads were attached to the aluminum plated surface using conductivity epoxy.

a	b	c	d	l
2.06 cm	0.74 cm	1.06 cm	0.72 cm	1.44 cm

Table. 3.1. Dimensions of CdS shown in Figure 3.1.

37

Now that an effective and accurate method for measuring the conductivity within the crystal had been decided upon, the question as to the best method for stimulating electrons from the valence band into the conductivity band was still to be addressed. Initially the employment of an AC-powered microscope light with variable intensity output accomplished this purpose. However, as it turned out, although this was an efficient way to alter the resistance across the leads of the crystal, since it was not in fact a stable light source (due to the alternating current), it proved ineffective in maintaining a consistent conductivity value. The slight aberrations in the conductivity of the crystal, it seemed, could quite easily be attributed to the variation in light intensity—or at least, the irregularity in the light source could not be ruled out as a source for the inconsistencies within the experiment. More than this, the intensity of the microscope lamp was controlled through an analogue crescent switch on the exterior of the lamp. The inability to adequately control the value of the output light intensity greatly reduced precision within the experiments and, further, impaired repeatability. Even with the addition of an external scale on the intensity knob itself, any attempt to repeat exact intensities between experiments was a nearly impossible endeavor. Indeed then, since all experimentation to this point lacked some degree of accuracy, precision and repeatability, it brought into question the reliability of the results.

It was necessary, then, to replace the original AC lamp with a direct current light source. The Interlux DC 1100 digital light source was chosen for this task for several reasons which are discussed below. First, however, it is necessary to introduce the basic features of the lamp. Specifically, the Interlux DC 1100 lamp consists of a 120 W halogen bulb powered by a 21 volt, direct current power source. The light from the

38

halogen bulb within the lamp itself is directed through an infrared blocking filter before it is passed through the aperture on the lamp's exterior. The characteristic spectrum of this light source overlaps the visible range, as shown in Figure 3.2. Further, a Volpi, dual-arm light guide with two focusing lenses was utilized with the DC1100. This light guide was utilized almost exclusively in Chapter IV, where its primary purpose was to limit the thermal energy incident on the CdS sample; however, to limit thermal energy in this way also caused a coincident reduction in light intensity. For this reason, the light guide was removed for when investigating the acoustoelectric effect.
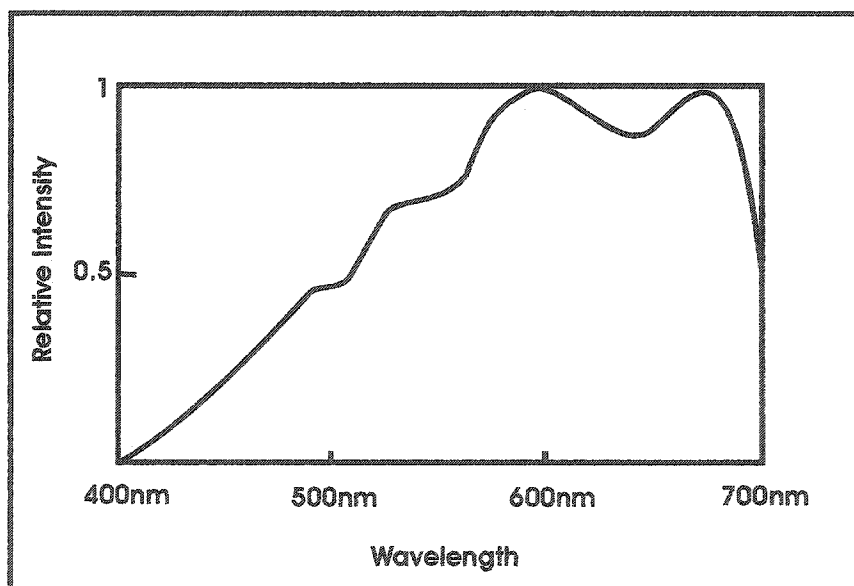
Figure 3.2. The light spectrum of the DC 1100 lamp. A brief discussion of this spectrum with respect to CdS conductivity and absorption is undertaken in Appendix D.

The most essential aspect of the DC 1100 lamp was the fact that it had a direct current (DC) power source. For this reason, the lamp manufacturer claimed a high degree of output stability, with the result that any volatility in the conductivity levels of the CdS could be attributed to variables other than that of the light source. The Interlux

DC 1100 also addressed the question of repeatability within the experiment. Because of its ability to be interfaced with a personal computer via its serial port, the light intensity output could be controlled digitally rather than through the analogue controls that also appeared on the exterior of the lamp. The lamp, in fact, allowed the user to set the output intensity at specific integer-valued steps from 0 (corresponding to no light output) to 1023 (corresponding to maximum brightness). Thus, upon determining that each lamp output setting truly corresponded to a repeatable light intensity output and, further, that this intensity was indeed steady over time, one could expect in each experiment that the light intensity could be controlled with both accuracy and precision. The replacement of the analogue microscope lamp with the Interlux DC 1100 Digital Light Source then had the potential, upon verification, to provide a great deal of consistency, and in the end, reliability to the experiment as a whole.

Now, although the Interlux Company claimed that the DC 1100 had a stable light output this consistency had yet to be quantitatively confirmed. Further, it could not be merely assumed that the inclusion of a personal computer into the experimental design to control the intensity of the light source would ensure reliable and repeatable output intensities. For this reason it was important to devise a means of both testing and monitoring the repeatability of the light intensities corresponding to the numerical output values as well as the stability of the light source over time. At this point then it is beneficial to address the repeatability of the light source.

Firstly then, prior to finalizing the initial setup of the experiment, it was important to determine the repeatability of the light intensities corresponding to the associated numerical output values in the software package that accompanied the lamp. In order to

40

establish this repeatability, a Scientech 365 Power and Energy Meter was utilized. Specifically, the process of making these determinations involved placing a focusing lens was used on each arm of the light guide to ensure that the beam of light that emerged was as nearly parallel as possible. Subsequently, each beam of light was directed toward a blank piece of paper on a flat surface a short distance away. The distance between the lens and the piece of paper, as well as the diameter of each circle of light on the paper, were carefully measured using a micrometer.

Knowing this information, the first beam of light was then focused in a similar manner at the same distance onto the detector of the power and energy meter. Using the Interlux software, the light intensity was then set to a digital value of zero. Upon zeroing the photometer, the light intensity of the Interlux lamp was set to a value of 173, a resulting photo-intensity reading was recorded in Watts and, subsequently, the lamp intensity was reset to a value of zero. Similar readings were repeated with step sizes of 25 integers from values of 173 to 1023. This procedure was then repeated three times for the first arm of the light guide and, again, three times for the second arm. Periodically, throughout the course of the various experiments, this process was repeated once for each arm.

The results from this relatively simple procedure could be examined and analyzed in a threefold manner: firstly, in keeping with the original intention of the experiment, the repeatability of the digital lamp settings can be quantitatively validated. Secondly, by comparing the original results with those taken at later dates, it can be established that the lamp intensity was not decreasing over time. And finally, as a consequence of these observations, the digital lamp intensity output values associated with the lamp's software

41

package could be related to real-world intensity values. By using the power and energy meter and also knowing the area of the lamp's beam of light, it was a simple task to then correlate a Watts cm^{-2} value for each setting of the Interlux lamp. Consequently, in each subsequent experiment, the intensity could be recorded in understandable units of measurement rather than on a scale specific to the Interlux DC 1100. These results are shown below in Figure 3.3.
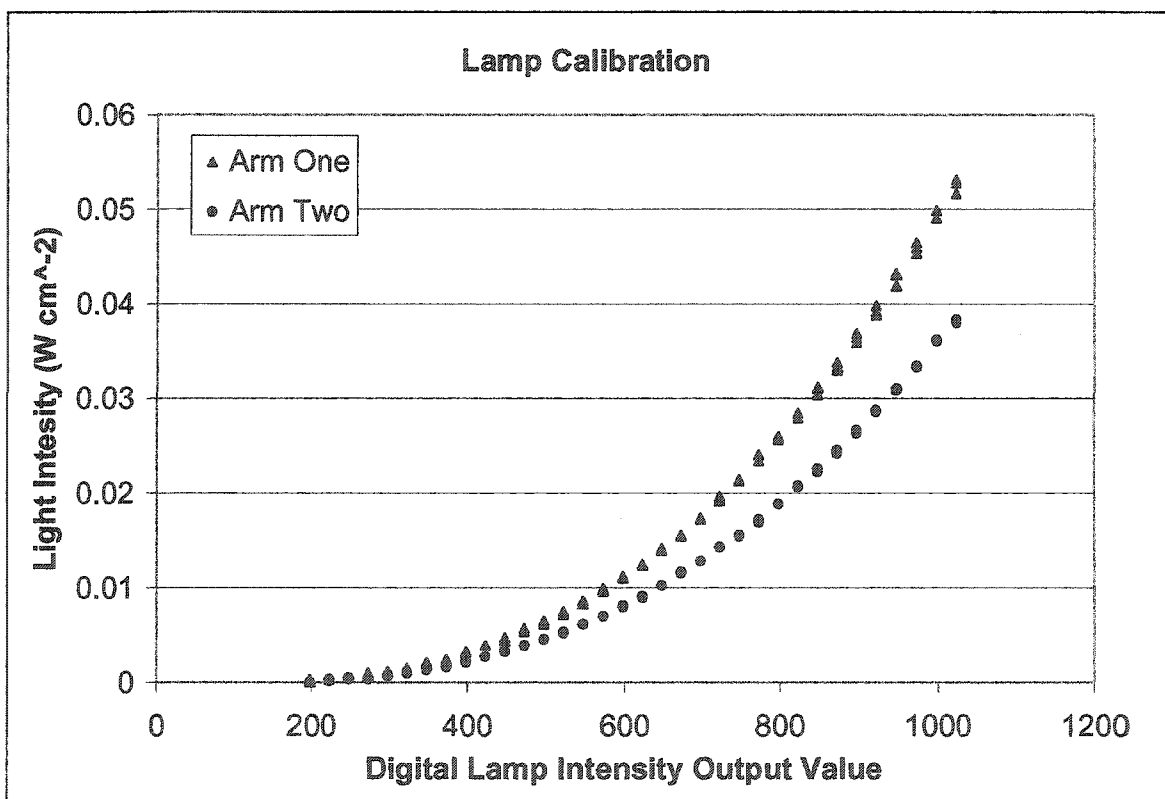
Figure 3.3. DC 1100 intensity output repeatability. Shown are three trials for each arm of the flexible light guides.

In the section of this thesis project investigating acousto-electonic interactions, as mentioned earlier, the light guide was removed in order to increase the light intensity, and, in turn, the conductivity of the Cadmium Sulfide crystal. Although the repeatability of the light source intensity was established using the light guides, it was also beneficial

42

to determine the actual increase in light intensity that resulted from their removal. For this reason a single trial of the above procedure was completed with the power and energy meter placed directly in front of the lamp's aperture. Care was taken to ensure that the distance between the light source and the power and energy meter matched that of the previous procedure. The results of this experiment are shown in Figure 3.4.

Lamp Intensity Comparison
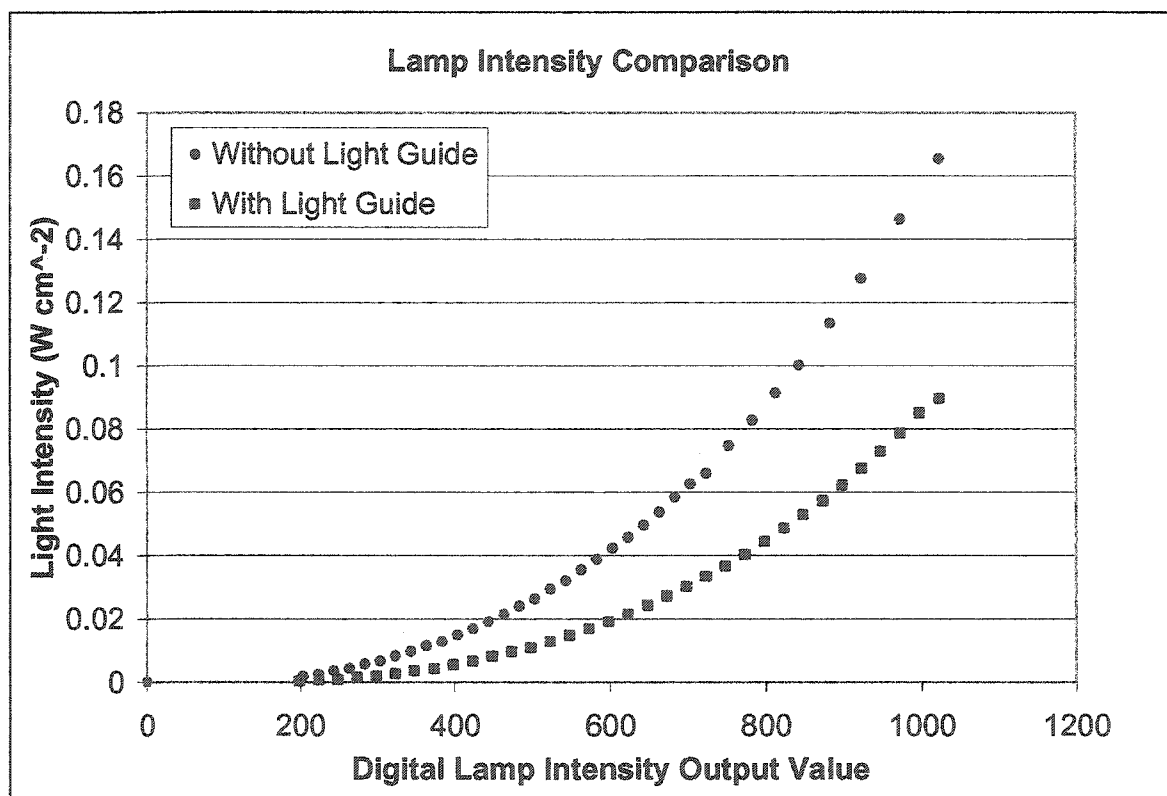
Figure 3.4. DC 1100 intensity comparison: with and without the light guide.

Using the procedures described above, the repeatability of the light output intensity was documented. However, the precision of the sustained light output had not yet been properly established. It was necessary, then, to determine an effective procedure to properly monitor the light intensity output over time in an effort to ensure that it was indeed constant. Having already determined that the DC 1100 assured a repeatable light

43

intensity that corresponded to its digital output value and further having determined the real wattage of each output level, it was now necessary only to establish that this intensity did not, in fact, change over time. That is, we needed to establish a range of precision within which the light output level could be expected to remain throughout the course of an experiment. For this reason a Vactec Photometer was incorporated into the general design of the both experiments.

Due mostly to the geometry of the experimental apparatus and the size and shape of the photometer sensor itself, however, it was not practical to utilize this photometer to directly measure the intensity of light cast upon the CdS crystal. Since it was not possible then to place it in close proximity to the crystal itself, an alternate approach was required. Examination of the design of the DC 1100 quickly revealed the existence of a ventilation grill at the end of the lamp opposite the light aperture. By placing the ultra sensitive photometer directly behind the lamp it could then be employed to measure the intensity of light that reflected off inside walls of the lamp and escaped through this opening. In this way, it was possible in an indirect manner to measure the stability of the light source over time without worry of disrupting the other components of the experiment. Records of these photometer readings could then be made during the course of each experiment to make certain that there were neither sudden changes nor gradual shifts in the intensity of the lamp. Thus, using this indirect yet undoubtedly accurate method, the steadiness of the light output intensity as a function of time could be assured.

Temperature regulation within the Cadmium Sulfide crystal was also of utmost significance within this research project. The DC 1100, along with stimulating conductivity levels within the crystal, generated considerable amounts of heat energy

that, in turn, had a considerable effect on the temperature of the crystal. Since the goal of this first set of experiments as to obtain more or less unwavering conductivity levels, it was then essential to both limit and characterize the effects of temperature changes within the experiment.
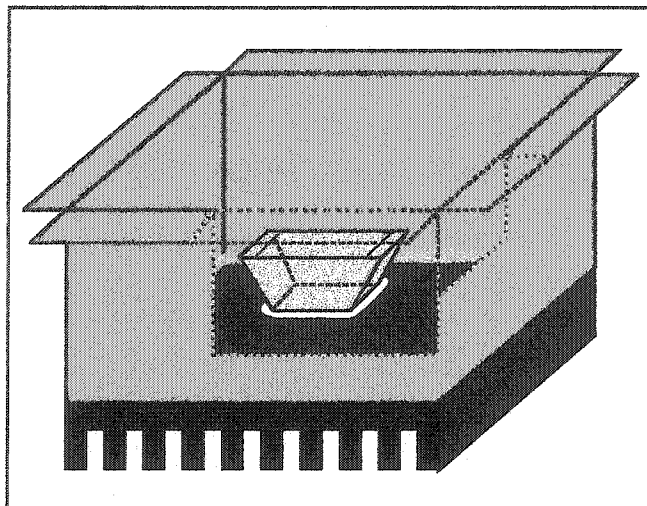
Figure 3.5. Heatsink container. Aluminum has been formed around the heat sink to form the upper portion of the box and the edges have been sealed with silicon. Within this container it can be seen that a layer of thermal couplant has been placed between the CdS crystal and the heat sink.

In an attempt to control fluctuations in crystal temperature during the course of research, the specific experimental design was developed in such a way as to permit the use of a Techne TE-10A water bath. However, to completely submerge the crystal in water would certainly give rise to numerous obstacles that would further impede experimentation—for instance the presence of the water would make accurate conductivity measurements within the crystal itself a near impossibility. To this end, an aluminum container was fabricated within which the Cadmium Sulfide crystal itself could be placed (depicted above in Figure 3.5). The entire container, with the sample inside, could be lowered into the thermoregulated water bath which could then be used to

45

influence the temperature of the crystal without interfering with crucial measurements. To create such a vessel to accommodate the CdS, a thin piece of aluminum and a heat sink were used. With the addition of some thermal couplant, then, one could expect, at least to reasonable approximation, the Cadmium Sulfide crystal and the moderating water bath to be in near thermal equilibrium.

The water bath, although itself reasonably primitive, proved to be an effective means of influencing and controlling the temperature of the Cadmium Sulfide sample. Once the crystal was placed within the silicon sealed container and lowered into the water through the small opening in the top of the bath its contents could remain insulated from and relatively unaffected by the surrounding environment. The analogue dial on the exterior of the water bath could then indirectly aid in the temperature control of the crystal. Although the scale on of the thermoregulator on the water bath was only accurate to within approximately 5°C at the top end, the insertion of a Cenco 19245 C Thermometer with precision to 0.1°C into the bath was a more than adequate means of determining its temperature for the purposes of the various experiments. Also, as the bath had the ability to rapidly circulate the water it could be assured that the whole volume of the water was in thermal equilibrium.

Although the temperature of the water bath itself was no longer in question, it was not yet reasonable to presume the effect of the bath on the crystal temperature. Despite the use of the heat sink and the thermal couplant to aid the exchange of heat between the water bath and the CdS sample, the exact temperature of the crystal still required more precise scrutiny. Due to its more precise and adaptable nature, a thermistor was selected for this task rather than utilizing a second thermometer. To monitor the temperature of

46

the crystal, the thermistor was secured directly above the Cadmium Sulfide crystal and, using additional thermal couplant, the end of this instrument was completely enclosed and, in turn, adhered to the sample. Since the conductivity of the crystal was being measured across the top face, it was also in this upper portion that the thermistor was attached. In this way one could be confident that the thermistor readings more accurately reflected a temperature that was closely associated with the intensity of light that stimulated the level of conductivity being observed. Using a second ohmmeter (Fluke 79 III True RMS Mutimeter) then, the temperature of the crystal could be gauged by measuring the resistance of the thermistor.

Before utilizing the thermistor to measure the temperature of the crystal, however, it was first necessary to develop a procedure to both calibrate it and to test its reliability. For this task, the water bath was utilized. The top of the water bath was covered, save for a small opening into which the ends of both the thermistor and the thermometer (again, accurate to 0.1°C) were lowered. Although they were immersed in rapidly circulating water a distance from the water bath's heating coil, care was taken to ensure that they were in an area of relative thermal equilibrium. For this reason they were kept in close proximity with both instruments at equal distance from the heating element.

Upon placing the two measuring devices next to one another within the water bath, the leads of the thermistor were connected to an ohmmeter in order to measure the resistance across it. The heating element within the bath was then used to slowly heat the water from 10°C to 90°C. Using the thermometer to ascertain the temperature of the water within the bath, readings from the ohmmeter were taken at 0.5°C intervals. This process was repeated a second time and these results were compared with the first to

47

ensure reading accuracy and, further, the reliability of the thermistor. In this way a scale was developed relating the resistance of the thermistor to a temperature in °C across the desired temperature range. The results of this procedure can be observed in Figure 3.6.
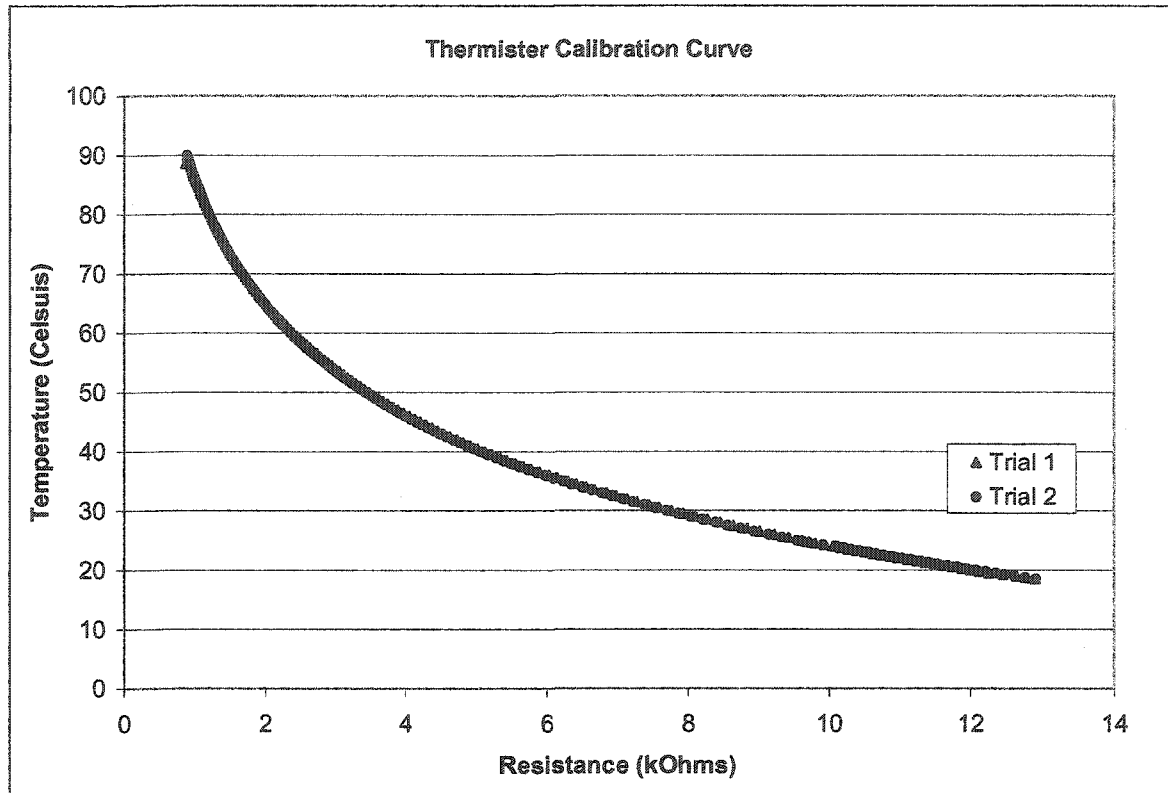
Figure 3.6. Thermistor calibration curve. The above graph shows two subsequent calibration trials relating the temperature of the water bath to the resistance of the thermistor. The exact fit of the curves is a testament to the repeatability and accuracy of the thermistor. The curves can be very closely approximated with a six degree polynomial.

Naturally, the purpose of calibrating the thermistor was to convert its temperature scale to one that is familiar. The problem with this procedure, though, lies in the fact that the thermometer and the thermistor have different levels of precision. Although the thermometer utilized to monitor the water bath temperature was accurate only to approximately 0.1°C, the thermistor has the ability to give readings on a very small scale. It is, in fact, this degree of precision, along with its considerable flexibility, that makes it a desirable instrument to measure temperature. In order to maintain this degree of

48

exactness when the thermistor is utilized to determine crystal temperature, it is necessary to have the ability to convert any resistance reading to a temperature in °C.

Once the data from the above procedure has been plotted in a graph relating resistance to temperature, by inputting the data into a curve-fitting algorithm on GNU Octave, it was fit with a tenth degree polynomial:

$$y = A \cdot x^{10} + B \cdot x^9 + C \cdot x^8 + D \cdot x^7 + E \cdot x^6 + F \cdot x^5 + G \cdot x^4 + H \cdot x^3 + I \cdot x^2 + J \cdot x + K \quad (3.1)$$

Where the coefficients are as follows:

$$A = 3.50448853624099e-8 \qquad °C \cdot (k\Omega)^{-10}$$
$$B = -3.40824932953e-6 \qquad °C \cdot (k\Omega)^{-9}$$
$$C = 1.43751664244712e-4 \qquad °C \cdot (k\Omega)^{-8}$$
$$D = -3.45149092895704e-3 \qquad °C \cdot (k\Omega)^{-7}$$
$$E = 5.20935760802194e-2 \qquad °C \cdot (k\Omega)^{-6}$$
$$F = -5.15612670768985e-1 \qquad °C \cdot (k\Omega)^{-5}$$
$$G = 3.39503125766679e0 \qquad °C \cdot (k\Omega)^{-4}$$
$$H = -1.4832587830456e+1 \qquad °C \cdot (k\Omega)^{-3}$$
$$I = 4.25789194364765e+1 \qquad °C \cdot (k\Omega)^{-2}$$
$$J = -8.22966042375066e+1 \qquad °C \cdot (k\Omega)^{-1}$$
$$K = 136580667222141e+2 \qquad °C$$

In this Equation (3.1) the x-values represent the thermistor resistances and y-values represent the corresponding temperature in °C. Thus, even a relatively simple program such as Microsoft Excel can be used to convert thermistor resistances to their corresponding temperatures.

2. Fundamental Experimental Setup

Having adequately discussed the procedures necessary to calibrate and evaluate the major elements of this research project, it is now possible to discuss the general experimental setup which serves as the foundation for experimentation. The experimental arrangement shown below in Figure 3.7 was constant throughout both experiments, save for the removal of the light guide and also the addition of acoustic apparatus when investigating the acoustoelectric effect.
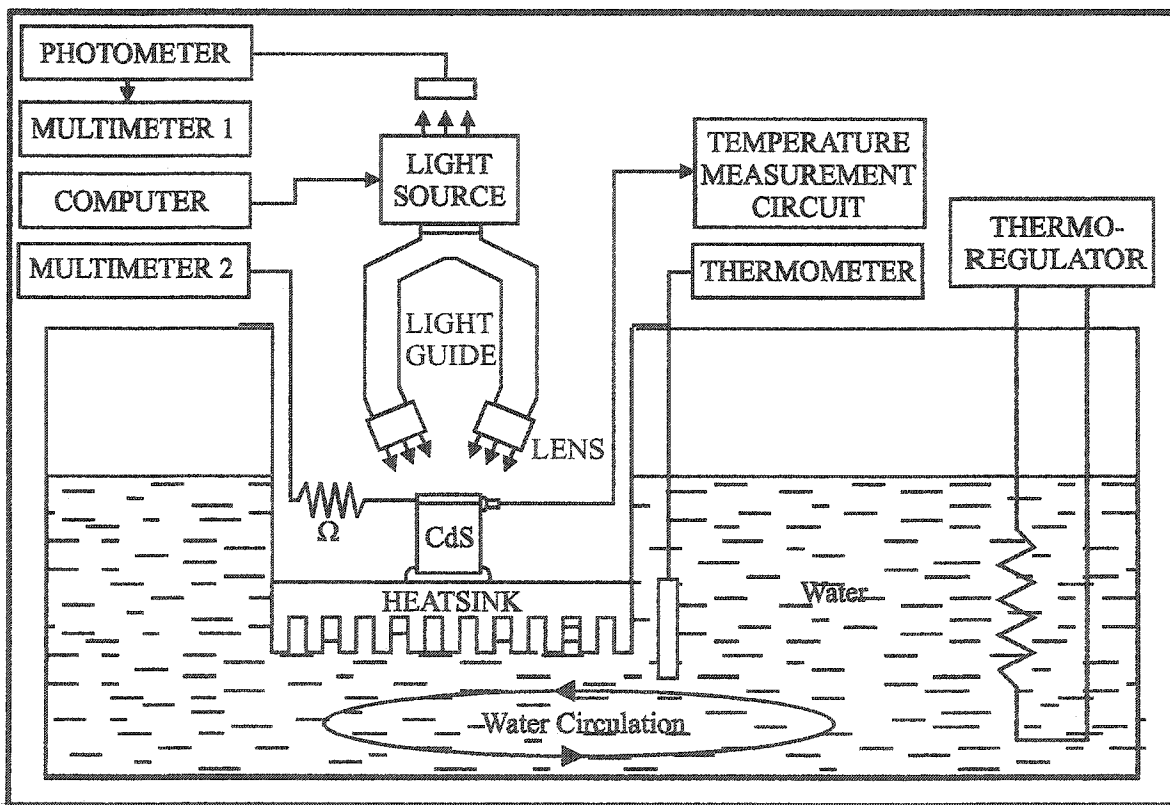
Figure 3.7. Schematic diagram of the basic experimental setup.

50

3.3 General Data Processing Procedures

At this point, upon having clarified the general arrangement of apparatus, we can switch focus to the subject of data processing. Since upon completion of most experiments some of the data was not in its final form, it was necessary to perform several simple calculations before analysing the results. Although not terribly difficult, for completeness these processes require some attention.

There were three general tasks that required completion before one could analyse the results from any given portion of research: firstly, as mentioned earlier, the reported CdS temperature was recorded in $k\Omega$ rather than in more recognizable units such as °C. Secondly, since in order to facilitate the measurement of conductivity, it was necessary to place a resistor in parallel with the Cadmium Sulfide crystal. For this reason the resistance that was recorded from the corresponding multimeter was not that of the crystal itself, but instead that of the system as a whole. Further, it is beneficial to convert this calculated resistance to crystal conductivity. And finally, although the lamp intensity had been monitored using a photometer, the output had been recorded in VDC in order to increase precision. For this reason it was necessary to convert this value to a more recognizable form. Thankfully, however, it was a relatively simple task to remedy these difficulties.

In the first case, after having completed the previously described thermistor calibration procedure, we had obtained a graphical relation between resistance and temperature. The polynomial obtained from this relationship, as described earlier, could then be used in a spreadsheet to convert these thermistor readings into temperatures in °C.

51

The process of extracting the resistance of the Cadmium Sulfide crystal itself from that of the entire system (which had included also a second resistor of fixed impedance in parallel with the CdS crystal) was also somewhat trivial. In fact, to obtain the desired result required only the application of fundamental circuit analysis concepts. With the measured resistance of the system being represented by R_T, and the resistance of the second, fixed resistor being assigned R_F, the true resistance of the CdS sample itself, R_{CdS}, could be calculated using the following equation:

$$R_{CdS} = \frac{R_F R_T}{R_F - R_T}. \qquad (\Omega) \qquad (3.2)$$

As the phenomenon with which we were most interested in was actually photoconductivity, rather than resistance, a second step was then completed. Indeed this resistance could be converted into conductivity with the following formula:

$$\sigma_{CdS} = \frac{l}{R_{CdS} \cdot A_{cross}} = \frac{l}{R_{CdS} \cdot d_p \cdot d}, \qquad (\Omega \cdot cm)^{-1} \qquad (3.3)$$

Where A_{cross} is the current cross section and d_p is the depth of penetration of the radiation, i.e.,

$$d_p = \frac{1}{\alpha}, \qquad (cm) \qquad (3.4)$$

where α is the absorption as discussed in Chapter II. As per Bube [13], for all calculations of this thesis d_p will be considered to be 100μm. Now, also, d is the width of the crystal at the top of the crystal and l is the distance between the two leads (the exact value of these numbers can be seen in Table 3.1. Thus, in a sense, we are making the approximation that the current only flows through the cross sectional area between the leads on the top of the crystal. This area is as wide as the top of the crystal but only as

52

deep as the penetration depth. This is a reasonable estimation for the intents and purposes of this thesis project.

Now, in order to convert the photometer data into units that make sense within the scope of this experiment, we may take advantage of the lamp correlation data we obtained earlier. As we are taking lamp intensity readings every thirty seconds for one hour, there is no great loss in accuracy if we approximate this first reading at t = 30s to be very nearly equal to the intensity at t = 0. Thus, if we set the value obtained from the photometer at t = 30s equal to that obtained by the power and energy meter for the corresponding lamp intensity levels, we have a basis by which to convert all other photometer readings to W cm^{-2}. The formula corresponding to this explanation can be found to be

$$I_{yx} = P_y \cdot \frac{V_{yx}}{V_{30}} \, , \qquad \text{(Watts·cm}^{-2}\text{)} \qquad\qquad (3.5)$$

where y = 223, 323,...,1023, and corresponds to lamp intensity levels of the particular experiment and x = 30, 60,...,3600 corresponding to experimental measurement times of that same experiment. Here, then, I_{yx} (Watts cm^{-2}) represents the light intensity corresponding to the measured photometer reading, V_{yx} (VDC) at time x for lamp level y. Also V_{30} is light intensity measured in DC Volts by the voltmeter which was connected to the photometer at t = 30 seconds. P_y is the light intensity in Watts cm^{-2} obtained from the initial lamp calibration data measured by the power and energy meter measured; these values differ according to whether or not the light guides were utilized. Here, again, the subscript y indicates the lamp level. Of course, V_x are the DC Volt measurements of all intensities corresponding to the measurements taken at 30-second intervals for the duration of the one hour experiment. In this way all of the data obtained

from the photometer can be converted to the corresponding level of light intensity it represents.

After performing these three corrections for any experiment, then, we obtain a CdS crystal temperature in °C, a light intensity reading in W cm^{-2}, and CdS conductivity in Ω^{-1} m^{-1}. These, in fact, are the units which are desirable for data analysis. Now, although this short list of procedures and algorithms provides a basic description of some of the data process techniques that are employed throughout this thesis, there are several other methods that have been utilized. These will be introduced at the appropriate junctures.

In this way, then, the experimental procedures and apparatus that are common throughout the remainder of this investigation have been introduced. Although by no means are these descriptions absolutely comprehensive, they provide a prologue to the individual procedures and experimental arrangements that are discussed in Chapters IV and VI.

CHAPTER IV

Experiments in Photoconductivity

Before fully exploring the nuances and, further, the explicit details of the specific experiments, it is first valuable to properly set up the problem in a more general form. Without a clear understanding, or at least a general familiarity with, the broad scope of these experiments, one can easily become lost in the details. For this reason it is important to outline the experiment as a whole before engaging in a discussion of any one particular aspect. It is with this concern in mind that we begin to introduce the nature of this research project.

The purpose of this first portion of experiments is to segregate the variables which govern photoconductivity levels in Cadmium Sulfide. Upon isolation, it will then be possible to determine which of these aspects contributes the greatest proportion to the excitation levels of this semiconductor. Hence, for future experiments we will have a better mechanism for reaching stable plateaus of conductivity.

Stimulation of charge carriers into the conduction band of a particular semiconductor is dependent on the absorption of either thermal or radiation energy. For a photoconductor, the predominant mechanism is the latter. Depending on the structure of the energy band of the particular crystal, however, thermal effects can play a significant role. For instance, the existence of trapping and other impurity levels can effectively alter the minimum requirement of energy which is necessary to influence conductivity levels. Unfortunately, the fact that radiation energy often accompanies thermal energy presents an obstacle as well.

The initial problem with which we are presented then is first to isolate these two sources of excitation energy, at least to the degree that is possible. Naturally, however, this will be extremely difficult. In fact, to completely isolate thermal heating from light energy is a near impossibility, at least within the scope of this experiment. For this reason, it is also necessary to characterize the effects of this thermal energy in the absence of illumination.

With this being said, although both portions of this experiment, in their simplest form, consist of measuring the resistance across a photo-piezoelectric semiconductor, namely Cadmium Sulfide, they are fundamentally dissimilar. The first portion of this set of experiments, *Experiment A*, correlates conductivity values with specific levels of light intensity at constant temperatures. In the second segment of this research project, conductivity is monitored with respect to consistent illumination while the temperature of the crystal is varied. In this way, upon completion of these investigations we can better characterize the independent effects of both thermal and radiation energies on crystal excitation.

1. Experimental Setup

The arrangement of apparatus common to both Experiment A and Experiment B in this chapter is, without exception, identical to that which is illustrated in Figure 3.5 of Chapter III. The major discrepancy, however, between this portion of experimentation and that concerned with the acoustoelectric effect, is the requirement that thermal radiation from the light source be limited. For this reason, as discussed earlier, the Volpi dual-arm light guide was employed. Hence, light could be focused directly upon the

Cadmium Sulfide crystal without a large degree of thermal radiation. Having previously described the experimental setup as a whole, then, in is only necessary at this time to discuss the means by which the light guide was implemented. A qualitative illustration of the light guide with respect to the CdS crystal can be seen below in Figure 4.1. Also, this figure provides a description of the specific location of the thermistor with respect to both the heatsink and the light source.
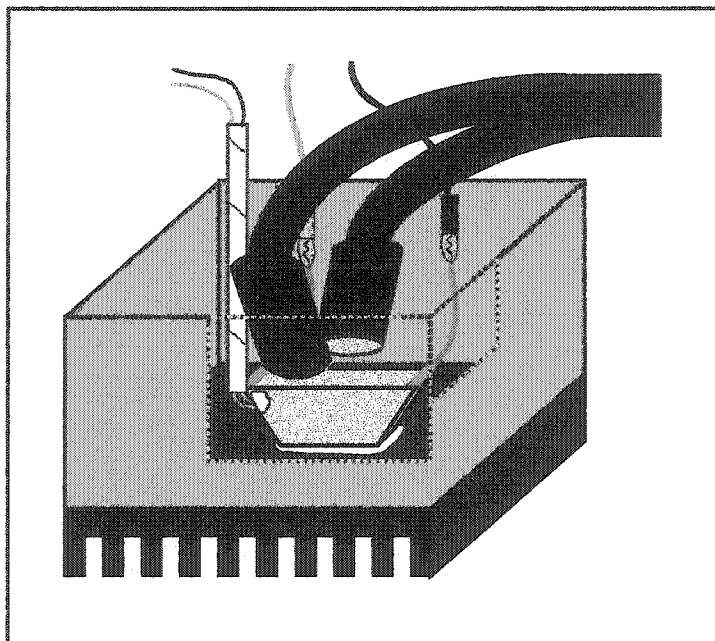
Figure 4.1. Depiction of the CdS crystal within the heatsink container. The CdS crystal is thermally coupled to a heat sink which is then surrounded with aluminum. Silicon is then used to assure the container is water tight. The thermistor (as seen on the left of the crystal) is attached to the top corner again using thermal couplant. The resistance is measured via the leads from the top corners of the CdS and light is directed upon the crystal using the flexible light guides from the DC lamp.

In order to further describe the specific geometry of the experimental setup, Figure 4.2 is included below. The numbers in the figure are only approximate. It in fact

57

proved somewhat difficult to affix the pieces of the apparatus with a great deal of precision; however, once in place, a series of clamps were utilized to assure that they remained stationary throughout the course of the experiment. It should also be noted that the light source arms were placed at a distance from the crystal that was comparable with their distance from the photometer detector by means of when they were originally calibrated. In this way, if desired, it would be possible to produce a rough estimate of the light absorbed by the crystal. This calculation, however, was not done. Finally, it should be noted that the focusing lenses also remained in an unchanged position so that the beams of light emerged in a reasonably parallel manner.
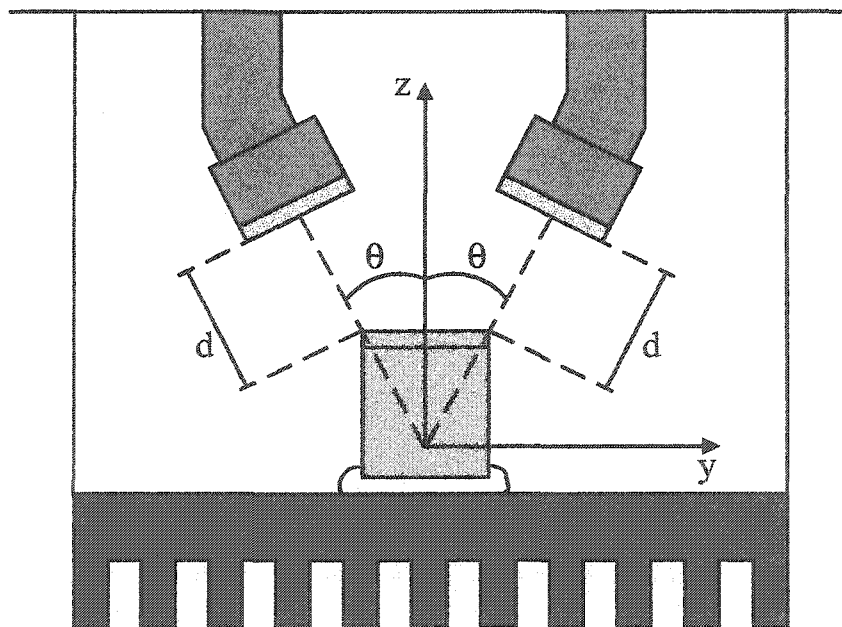
Figure 4.2. The geometry of the light guides with respect to the CdS Crystal. Here $\theta \sim 27.5°$ and $d \sim 2.5$ cm.

58

2. Procedure: Experiment A

At this point, having completed clarification of the general arrangement of apparatus, we can switch focus to the subject of experimental method and procedure. Within this particular section of research, two major experiments were performed, both having the fundamental purpose of investigating the properties of Cadmium Sulfide affect conductivity. In this set of experiments, the amount of light stimulating conductivity within the crystal was held constant as the crystal resistance was monitored over time. While the water bath was used to maintain the sample at a constant temperature in the first procedure, the second test utilized the bath in such a manner as to slowly increase the temperature of the crystal over the course of the experiment. By monitoring the response of the Cadmium Sulfide sample to such variables as light intensity variations and temperature changes throughout each procedure, its behavior could be more accurately characterized and, in turn, better understood.

The first experiment that was performed in an attempt to better understand the conduction characteristics of the CdS sample was rather comprehensive. More than merely completing the somewhat involved procedure of this experiment, great care was taken to ensure a consistent environment in which it was performed. With this in mind, the experiment was carried out during four consecutive days. Care was taken to ensure that neither the apparatus had not shifted, nor had the elements of the external environment experienced significant change. By assuring that the secondary or peripheral components of the experimental setup remained relatively constant, the results of this extensive procedure could be regarded with a greater level of confidence. This being said, explanation of the explicit details of this first experiment can be made.

59

As described earlier, the Cadmium Sulfide crystal was thermally coupled to the specially designed container and, in turn, was lowered into the water bath. The temperature of the bath was then set to 20°C and the entire room was made dark, save for the negligible light from a small lamp and the muted glow of the computer monitor. The crystal would remain in this constant state for approximately 1 hour, after which time the lamp intensity output was set to a value of 223. Using a stopwatch to standardize observations, at the end of each 30-second interval (beginning ½ minute from the initial powering of the lamp) the crystal temperature, crystal resistance and light intensity were simultaneously recorded. Even this task of taking concurrent measurements from three separate instruments, however, required some degree of design. The fact that both the crystal resistance and the light intensity values had a tendency to vary at a rapid rate made it extremely difficult to clearly distinguish even one distinct value from a single multimeter, let alone from two or three simultaneously. Due to the necessity of synchronized measurements, it was then necessary to develop a repeatable procedure that would preserve the accuracy and integrity of the data.

The simple algorithm that would remedy this difficulty utilized the 'freeze' buttons on two of the multimeters. Also, it took into account the nature of the fluctuations in the crystal's temperature. Because the crystal would remain at each temperature for several seconds at a time before changing, it was possible to discern an exact value from the ohmmeter with little difficulty. Thus, upon reaching each ½ -minute interval, the reading on the ohmmeter designated to monitor crystal 1 temperature was memorized while simultaneously pushing the 'freeze' button on each of the remaining two multimeters was simultaneously pushed. Immediately, the temperature value could

60

be keyed into a spreadsheet while the other values were frozen on the screens of their respective instruments awaiting observation. Subsequently these values were recorded alongside the corresponding temperature of the crystal in the same spreadsheet. This procedure was then repeated every 30 seconds for the remainder of the hour, at which time the lamp was reset to a value of zero.

In order to encourage the crystal to once again return to its original level of conductivity, it was allowed to remain in a state of darkness for ½ hour between stages of the experiment. Once this ½ hour had passed, the light source was once again turned on, this time with an intensity output value of 323 (an intensity increase of one hundred units). For a second time, simultaneous measurements of temperature, light intensity and resistance were taken every 30 seconds for 1 hour, before the lamp was again shut off. This procedure was repeated over the course of several hours for lamp intensities at intervals of 100 units, ranging from 223 to the maximal intensity value of 1023. Upon completion of an equivalently performed experiment for water bath temperatures of 40°C, 60°C, and 80°C over the next three days, the data from this portion of the research were complete. The data were then thoroughly scrutinized in an attempt to determine the relationships between these variables and to identify which, if any of them, play a major role in the photo-interactions that take place within the Cadmium Sulfide crystal.

3. Results: Experiment A

Upon completion of this rather onerous set of experiments, the next step was to analyze this data in an efficient and effective manner. Although not terribly difficult, this process was not entirely straightforward. Accordingly, it was important to wade through the material in a vigilant manner. Attention was paid to the fact that this data was not in

61

its final form; for this reason, the steps described in Chapter III were utilized to convert the data series to an operational form.

After performing these three calculations, we obtained a series of data whose complete set consisted of 36 similar charts, an example of which can be seen below (Table 4.1). Comparable tables were assembled for lamp intensity output values from 223 to 1023, in step sizes of 100 units for each of the four experiments completed with water bath temperatures of 20°C, 40°C, 60°C and 80°C.

Light Intensity Setting: 1023							
Time (min)	Thermister Reading (kOhms)	Calculated Crystal Temperature (Celsius)	Recorded Resistance (MOhms)	Calculated CdS Resistance (MOhms)	Calculated CdS Conductivity (10^3 Ohm m)^-1	Photometer Reading (VDC)	Calculated Light Intensity (W cm^-2)
0.5	11.41	21.07	1.839	2.357	8.486	1.093	0.090
1	11.29	21.13	1.821	2.327	8.593	1.091	0.089
1.5	11.19	21.22	1.811	2.311	8.654	1.100	0.090
2	11.2	21.18	1.841	2.360	8.474	1.104	0.091
2.5	11.13	21.22	1.844	2.365	8.456	1.105	0.091
.	.	.	.	.	.	.	.
.	.	.	.	.	.	.	.
.	.	.	.	.	.	.	.
58	11.02	21.62	1.883	2.430	8.232	1.033	0.085
58.5	11.04	21.64	1.891	2.443	8.187	1.032	0.085
59	11.04	21.58	1.880	2.425	8.249	1.032	0.085
59.5	11.02	21.64	1.873	2.413	8.288	1.031	0.085
60	11.04	21.66	1.885	2.433	8.220	1.032	0.085

Table 4.1. Table showing the finalized data from Experiment A, for a lamp output intensity setting of 1023. The columns denoted by the word 'Reading' or 'Recorded' indicate that they are the measured values from their respective multimeters. All other values are calculated values. The processes of data acquisition and calculation are discussed at length in Chapter III.

Now, to digress for a moment or two, it is important to revisit the purpose behind this portion of the research project. After all, without a clear understanding of objectives it is difficult to achieve a relevant analysis of the data. With this in mind, let us once again describe the nature of the experiment. We have, with this particular set of procedures, attempted to stimulate the conductivity levels of the CdS crystal with constant light intensity while maintaining a relatively stable crystal temperature. The

62

focus of this effort was, in the end, to determine which variables had the greatest influence on changes in photo-stimulation within the crystal. It is with this intention in mind that we will then examine the results of this experiment.

Let us first evaluate the stability of one of the major variables within the experiment, namely that of the Interlux DC 1100 Digital Light Source. Already having established the fact that, due to its serial port interface and digital scale, the initial light intensity output is highly repeatable, we need now only assess the consistency of this intensity output over time. Fortunately, as described earlier, this variable could be monitored indirectly through the use of a Vactec photometer. Accordingly, then, accompanying each and every section of the various experiments performed throughout this portion of the research project, there were simultaneous readings of the relative light intensity. Since the findings related to light intensity were nearly identical throughout the course of the experiments, the analysis of only two such sets of this data is sufficient. As such, the photometer readings for the trials corresponding to water bath temperatures of 20°C and 80°C are shown on the following page in Figures 4.3 and 4.4.

Initial comparison of the two graphs reveals the almost absolute repeatability of the light source intensity through the duration of the hour in which the various experiments took place. The two graphs are, in fact, nearly identical. More than this, one can see that at the lower lamp levels—from 223 to 623—the intensity of the light source is unwavering. Indeed, at these intensities the lamp is steady to within a standard deviation of 0.0005. On the other hand, at the higher lamp levels—from 723 to 1023— the standard deviations gradually increase. An example of this decline in stability can be observed in the particular example of the highest lamp intensity, 1023. As can be seen in

both of the graphs shown below, the light output decays slightly during the first 20 minutes of the experiment. There is, in fact, a change in intensity of nearly five per cent. Remnants of this deterioration of light intensity can also be visibly verified (although to lesser degrees) for levels 923 and 823. After about 20 minutes, however, the lamp intensity seems to more or less stabilize to a standard deviation of less than 0.004, even at the highest levels. In fact, a considerable decrease in the standard deviation of the recorded light intensities can be seen for the remaining 40 minutes of the experiment for all but the first two lamp levels, whose standard deviations are negligible throughout.
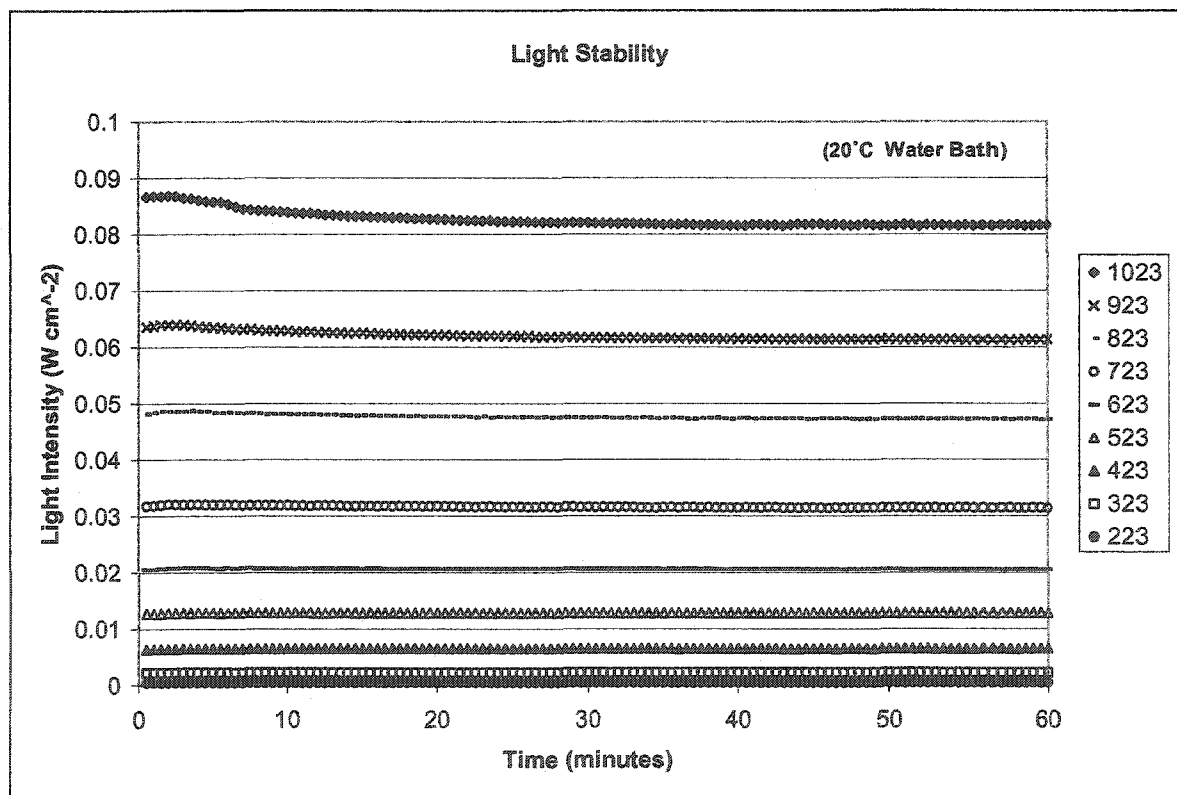
Figure 4.3. Light stability for the 20°C water bath trial in Experiment A.
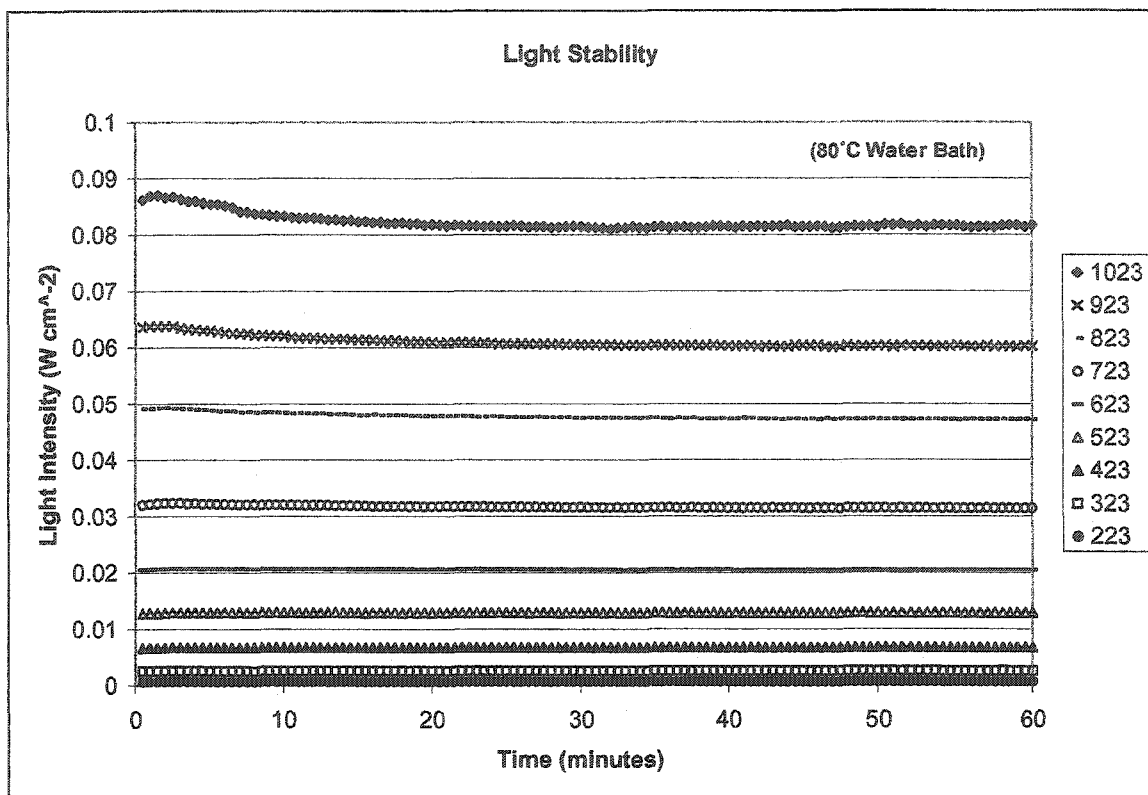
Figure 4.4. Light stability for the 80°C water bath trial in Experiment A.

A comparison between the standard deviation of values falling within the first 20 minutes of the experiment, and those of the remaining values can be seen in Table 4.2. To obtain the values given in the fourth column, the absolute value of the difference in standard deviation was divided by the standard deviation from the first 20 minutes.

Standard Deviation Comparison (20°C Water Bath)			
Lamp Output Value	First 20 Minutes	Last 40 Minutes	% Reduction
223	1.75E-05	1.78E-05	~ 0
323	7.80E-05	2.17E-05	72.20
423	2.10E-04	7.50E-05	64.37
523	4.01E-04	1.78E-04	55.76
623	6.65E-04	4.53E-04	31.94
723	1.32E-03	1.09E-03	17.36
823	3.61E-03	1.89E-03	47.70
923	7.39E-03	3.13E-03	57.60
1023	1.72E-02	3.71E-03	78.46

Table 4.2. Standard deviation of lamp stability. The standard deviation of the light intensity values for the first 20 minutes are compared with those of the last 40 minutes.

65

Thus, it has been determined that the lamp intensity output cannot truly be considered stable until it has been running continuously for 20 minutes, especially at high intensities. The question then remains as to how this slow deviation in light output affects the other aspects of the experiment—particularly the conductivity levels within the Cadmium Sulfide crystal itself. In order to determine the consequences of this instability, we now turn our attention to an inspection of the CdS conductivity as a function of time. In this case, it needful to study the data from only two of the four experiments, as the results were similar throughout. In order to be stay consistent, and also for comparison purposes, we will again choose the first (water bath temperature 20°C) and the last (water bath temperature 80°C) data sets. The graphs specific to these particular results can be seen below in Figure 4.5 and Figure 4.6.
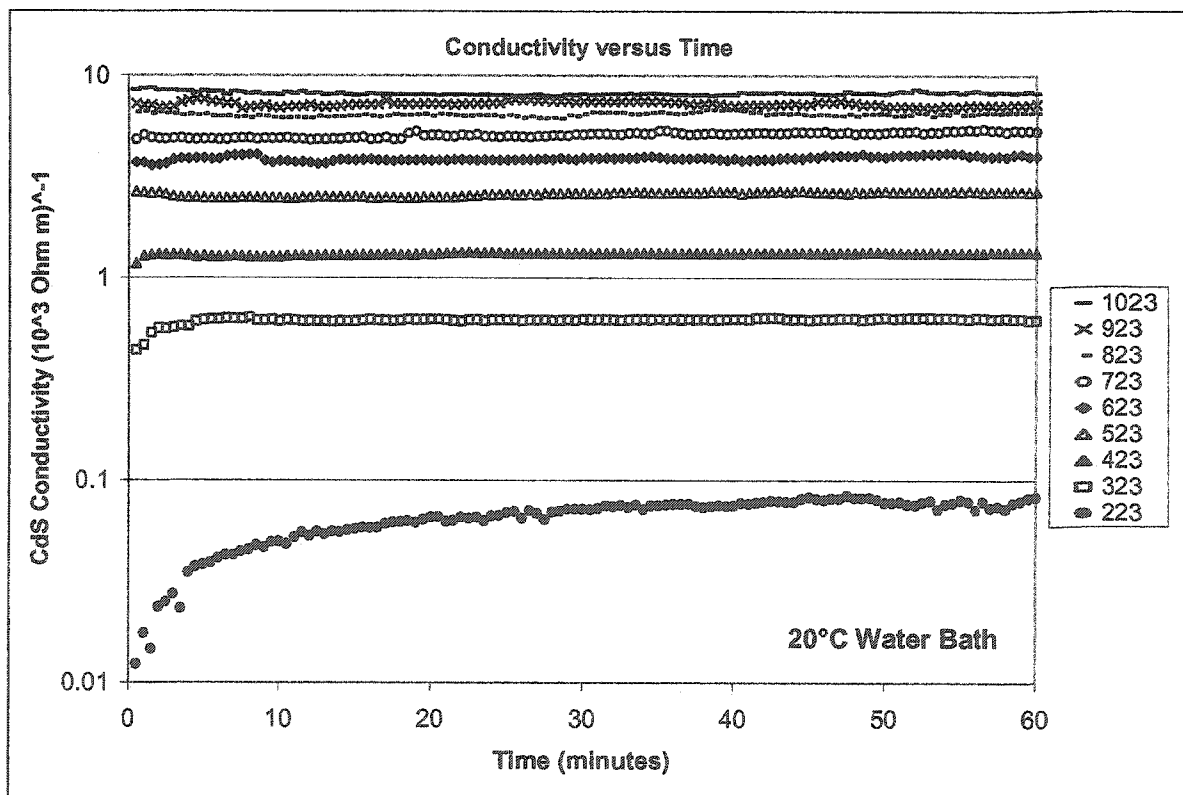
Figure 4.5 Crystal conductivity versus time for the 20°C water bath trial in Experiment A.
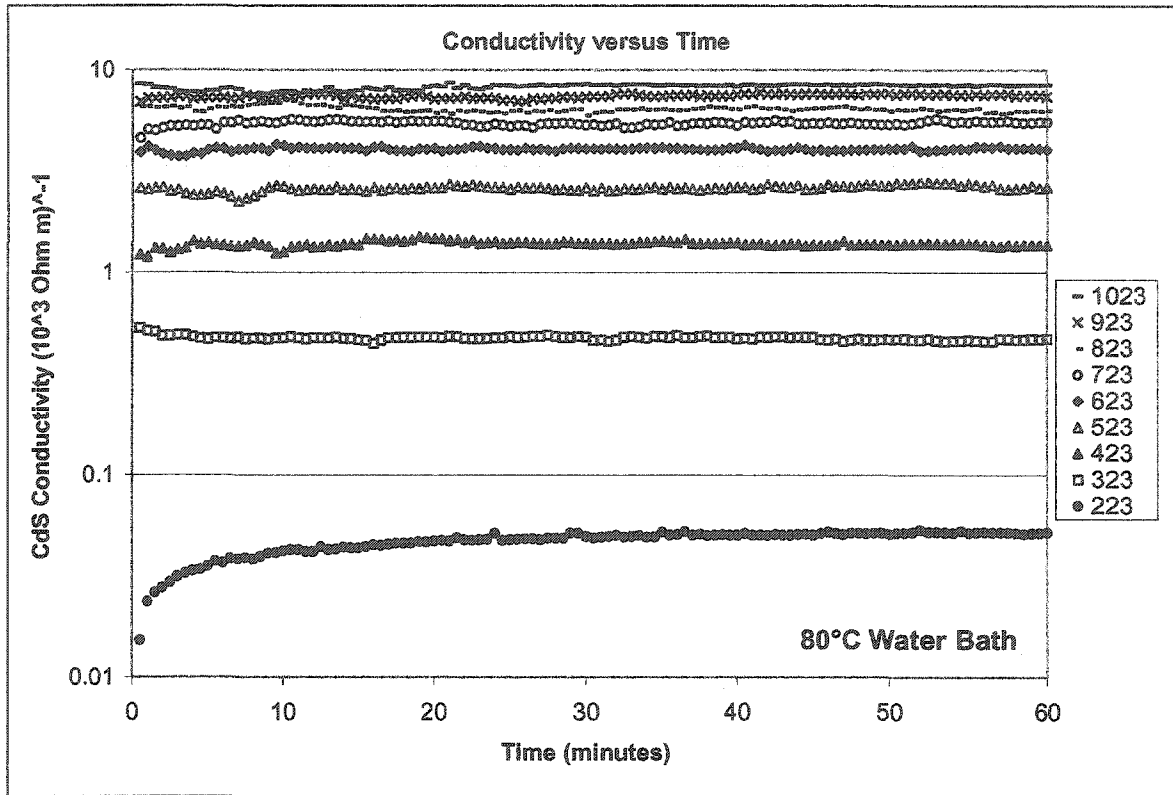
Figure 4.6. Crystal conductivity versus time for the 80°C water bath trial in Experiment A.

It is perhaps beneficial, before jumping into an in-depth analysis, to first state the more qualitative aspects of Figure 4.5 and Figure 4.6. Firstly, one of the subtle, yet quite intriguing, aspects of the experiment is the great swing in conductivity, or inversely, the resistivity of the crystal between the various levels of lamp intensity. Indeed, the difference in conductivity between a dark crystal and one that is maximally stimulated is in the approximately two orders of magnitude—a considerable increase. One notices also on these graphs that fluctuations within the conductivity of the crystal take place, for the most part, within the first 20 minutes of the time interval. To see some of the more subtle trends of this graph it is beneficial to engage in a more quantitative analysis.

At this point we should check whether there is indeed a trend in the stabilization of the conductivity levels of the Cadmium Sulfide crystal. Indeed, if this, metastable level of conductivity shown in Figure 4.5 and 4.6 does 'settle down', at which point does

67

it do this. To distinguish this behaviour, it is convenient to analyze the relative standard deviations within the nine curves. In other words, if we calculate the standard deviation for a section of each curve and divide that standard deviation by the average conductivity for that section, we have a reasonable method for comparing the relative deviations between the various levels of light intensity. Further, if we break the hour-long experiment into five-minute intervals we could then quantitatively monitor what appears to be a gradual calming of the variance in the conductivity values. The results of this particular data analysis procedure for the 80°C water bath temperature are presented in graphical form below in Figure 4.7. Similar results can be found for the remaining three water bath temperatures.
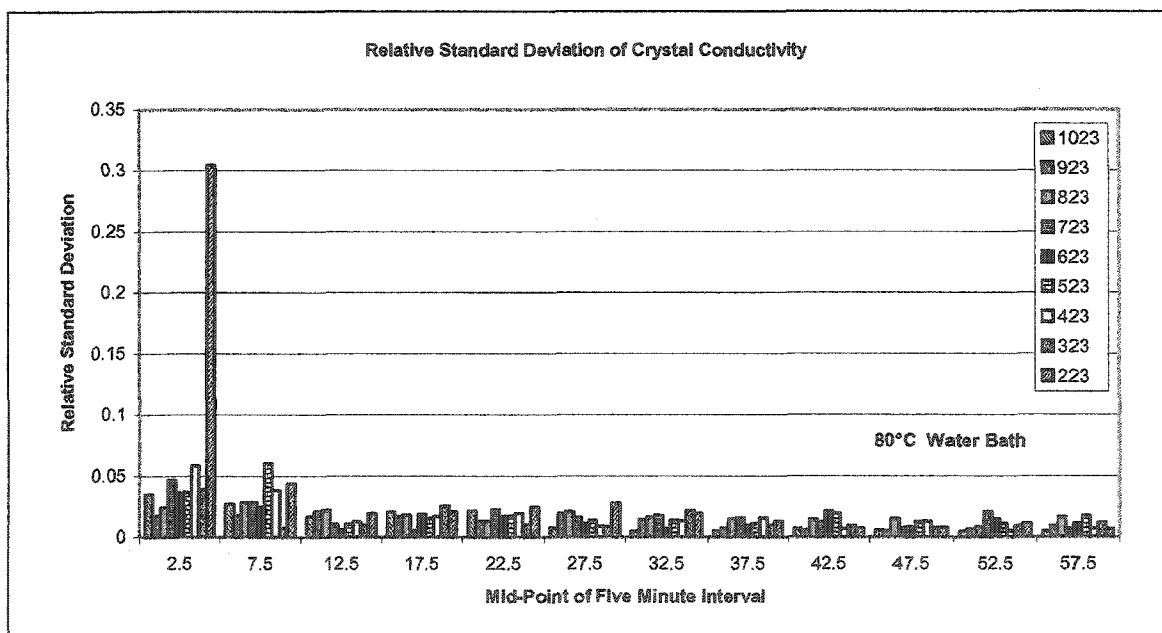
Figure 4.7. Relative standard deviation of CdS conductivity. This graph quantitatively shows the 'calming' of the Cadmium Sulfide crystal to a relatively steady level of conductivity. As can be seen, the standard deviation of the crystal resistance moves to a lower, relatively stable level between the 10 and 15 minute marks.

Inspection of this new set of data reveals that the relative standard deviation values for each of the lamp intensities settle to a constant level shortly after the 10-minute

mark. This graph then provides a quantitative analysis of Figure 4.6. It suggests that, although the levels of conductivity that are induced by the light source are somewhat turbulent in the first several minutes of the experiment, they reach more stable and consistent levels at a point between the 10- and 15-minute marks. This level of measured resistance then remains reasonably steadfast for the remainder of the time period.

Just as this new set of data demonstrates the metastability of the crystal conductivity, it in some ways seems to refute the existence of a simple correlation between the initial changes in the conductivity levels and the instability of the light source. If there were in fact a direct relationship between the lamp's inconsistency and the crystal's fluctuations in conductivity, there would then also be a more immediate connection between the two standard deviations. This is not the case. In fact, if we compare the relative standard deviation for the light intensity with the average standard deviation of the crystal conductivity, we can validate whether or not there is a correlation. Before comparing these deviations, however, they should be further subdivided into low, medium and high light intensities for greater accuracy. Thus, the relative deviations of the three lowest light intensities (corresponding to lamp levels of 223, 323, and 423), the three medium light intensities (523, 623 and 723) and the three highest intensities (823, 923, and 1023) can be averaged together for each 5-minute interval of the various experiments. Likewise, the standard deviations of the crystal conductivity levels associated with these lamp intensities can also be averaged for the same 5-minute intervals. The subsequent comparisons of each of these relative deviations are shown in Figure 4.8, Figure 4.9 and Figure 4.10 below. If in fact there was a correlation between the instability of the lamp and that of the Cadmium Sulfide crystal, it would be reflected

in that the graphs would appear to 'level out' at corresponding times. This, however, is not the case. In actuality, the crystal conductivity seems to stabilize before the light intensity does. Thus, as can be readily seen in the graphs below, there is no connection between these two instabilities.

Relative Deviation Comparison: Light Intensity vs. Crystal Conductivity
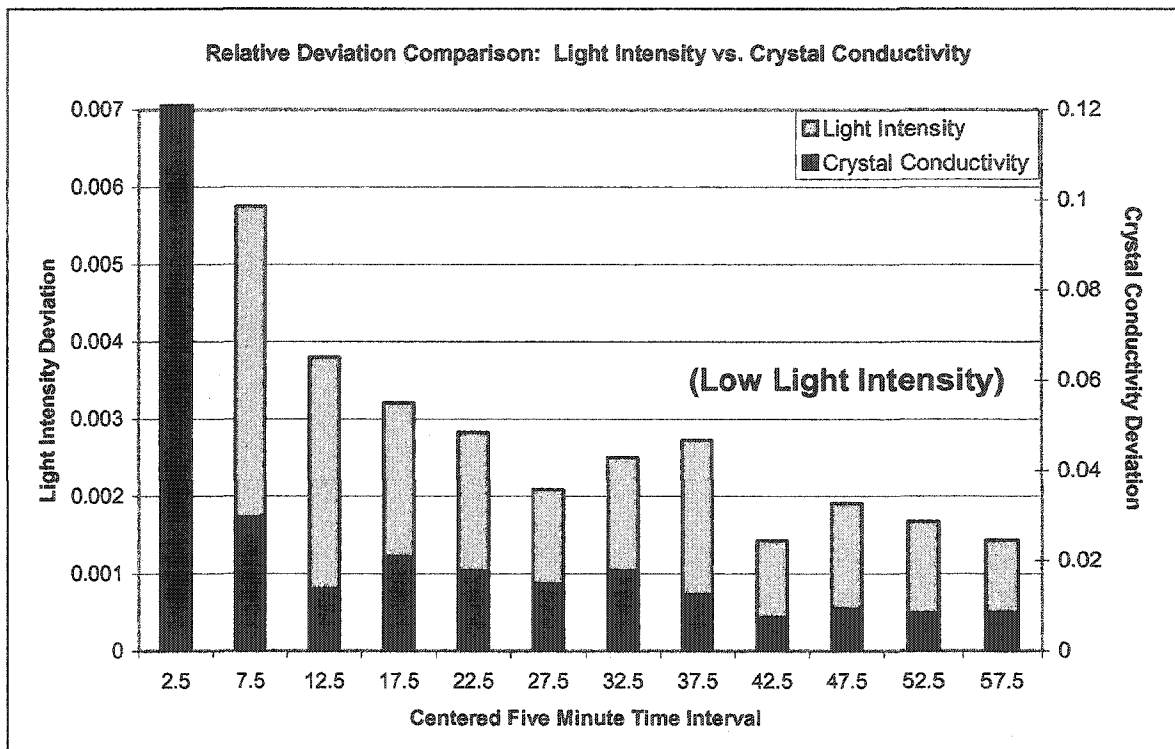
Figure 4.8. Relative standard deviation comparison of light intensity and crystal conductivity for low light intensity. The chart above demonstrates the simultaneity of the 'calming' of the standard deviations of the Cadmium Sulfide crystal to more stable levels with the steadying of the light output intensity. Here the results for the three lowest light levels are averaged. The average standard deviation for all photo-stimulations levels in each 5-minute interval are compared with those of the light intensity levels. As can be seen, the crystal resistance and the light intensity become more stable at separate times.

70
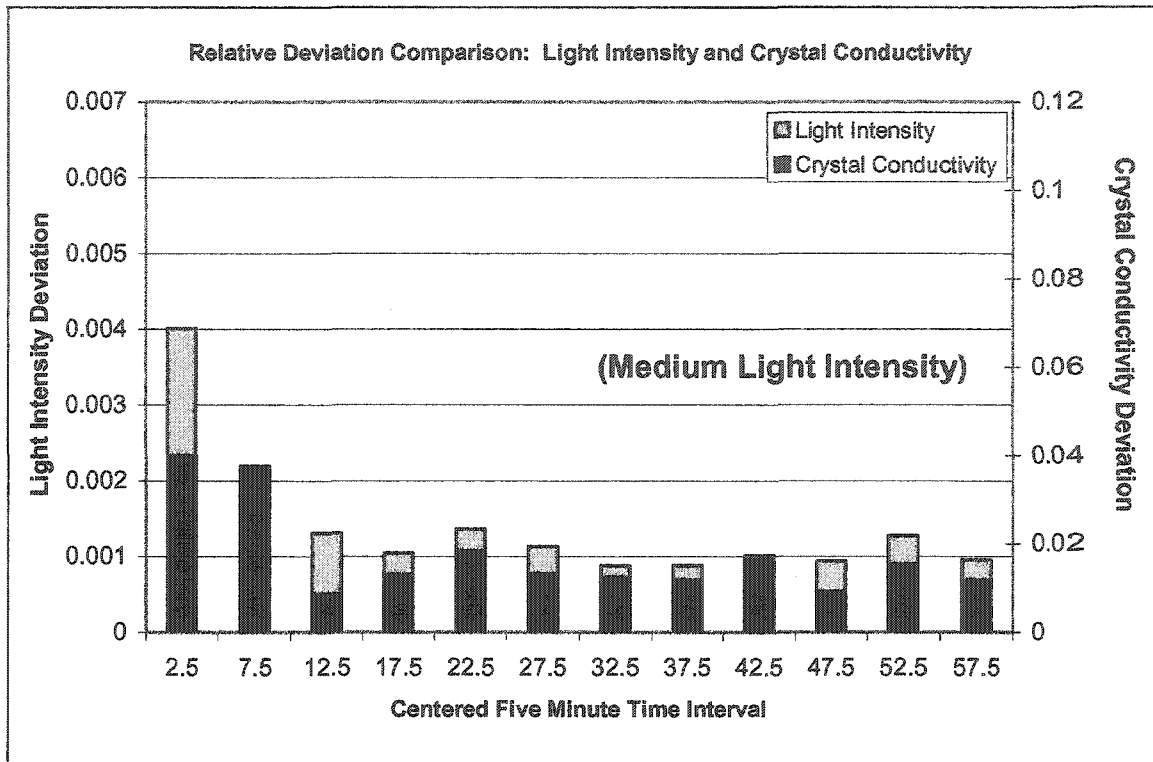
Figure 4.9. Relative standard deviation comparison of light intensity and crystal conductivity for mid-range light intensity.
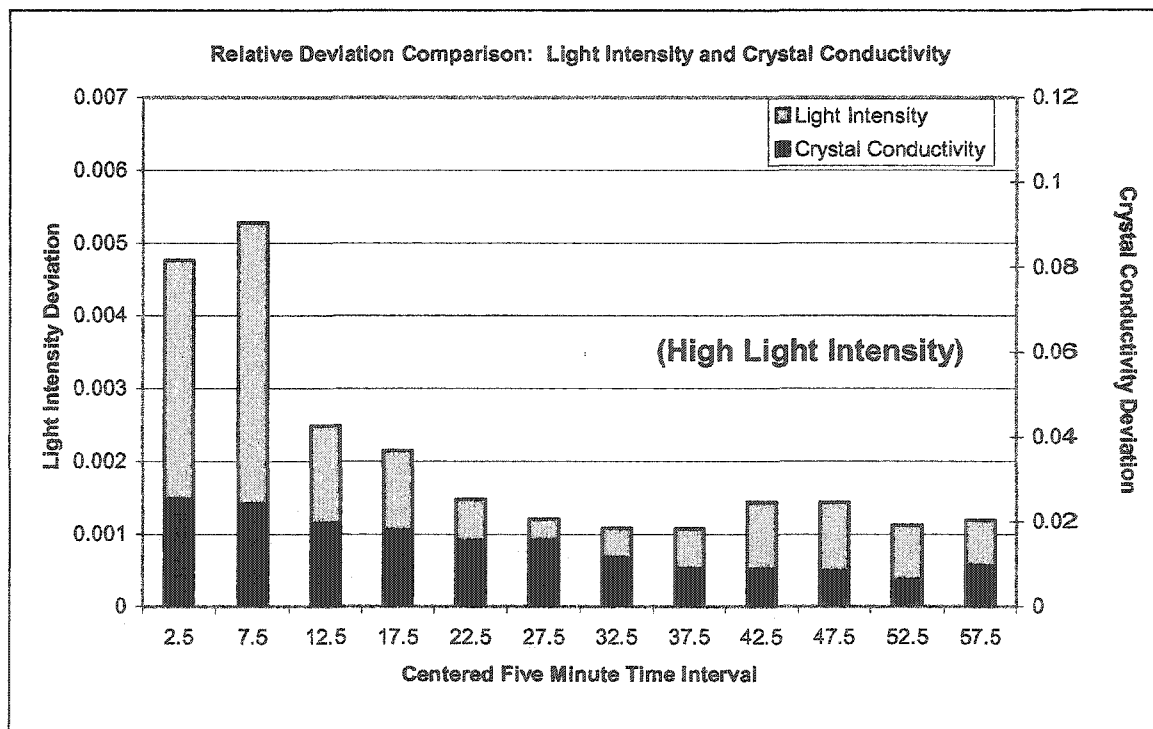
Figure 4.10. Relative standard deviation comparison of light intensity and crystal conductivity for high light intensity.

71

If we take a moment to reflect on the experiment as a whole and, further, on the results that have been presented so far, we can quickly see that, as of this point, we have omitted a relatively fundamental graph. With some thought, we can create a chart that is of great appeal in that it nicely summarizes the basic principles of the experiment in a visual manner. The two most primary variables in this portion of experimentation are crystal conductivity (or inversely, resistively) and light intensity. Indeed, after all, at the core of this entire field of research is the assertion that an increase in light intensity stimulates electrons within the CdS crystal, and consequently lowers the resistance across it. We have, indeed, already seen proof of this phenomenon in Figure 4.5 and Figure 4.6, where CdS resistance was plotted against time. It is evident from those charts that, with increasing light intensity, there is a corresponding decrease in resistance. By further manipulating the data that accompanies these graphs, however, we can present what is perhaps a more revealing look at the nature of the Cadmium Sulfide crystal.

Earlier in this section, based on experimental results, we established that the levels of conductivity within the CdS crystal reach more or less stable levels after being photo-stimulated for 20 minutes. After this time, the crystal resistance remains relatively constant. Upon averaging the crystal resistance values over some time period, then, we are able to gauge the conductivity level that specific lamp output settings can be expected to stimulate. Given the earlier investigation mapping the digital lamp output levels of the DC 1100 onto true light intensities (as discussed in Section 4 of this chapter), we are, further, able to map these levels of conductivity to corresponding levels of photo-stimulation in Watts per cm^2. The results of this investigation corresponding to all four

72

of the various water bath temperatures can be seen in Figure 4.11. The resistances shown are, in fact, the averaged resistance values taken from the final 10 minutes of each experiment.
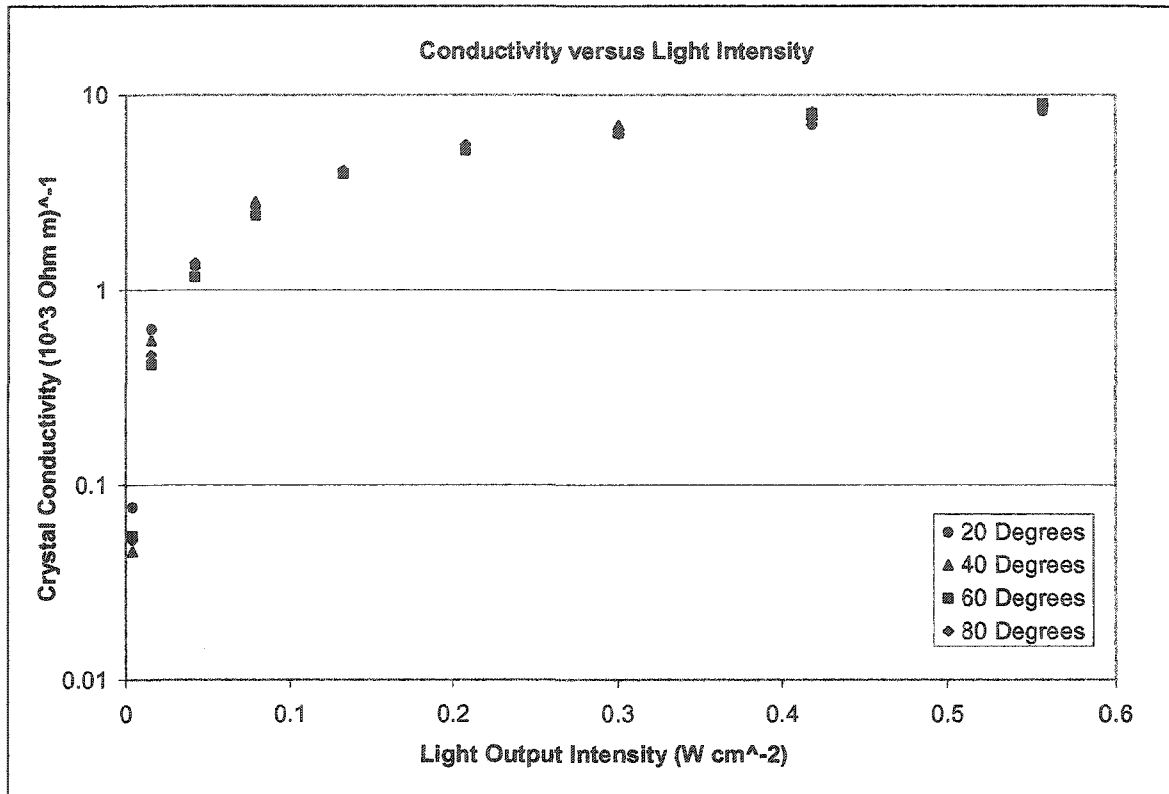
Figure 4.11. CdS conductivity with respect to specific light intensities. The crystal conductivities shown represent the average levels of stimulation during the final 10 minutes of each experiment

Now, recall that the water bath was first incorporated into the experimental design with the purpose of limiting the effects of crystal heating due to the light source itself. Nothing has yet been said about how effective this water bath has been. For this reason, at this point it is appropriate to analyze the effect of light intensity on crystal temperature. To commence the analysis of temperature within the experiment, let us first present the results from our thermistor data.

During the course of each experiment, resistance readings were taken from the thermistor that was thermally coupled with the crystal itself. Upon converting these

73

resistances to temperatures in °C, we then have an accurate record of the temperature of the crystal at ½ -minute intervals throughout each of the four experiments. The first chart, shown below (Figure 4.12) contains complete crystal temperature information for each experiment. For simplicity, details delineating explicitly the specific temperature curves within the various experiments, as well as a qualitative discussion of temperature considerations, have been left to Appendix B. A few remarks, however, are beneficial at this time.
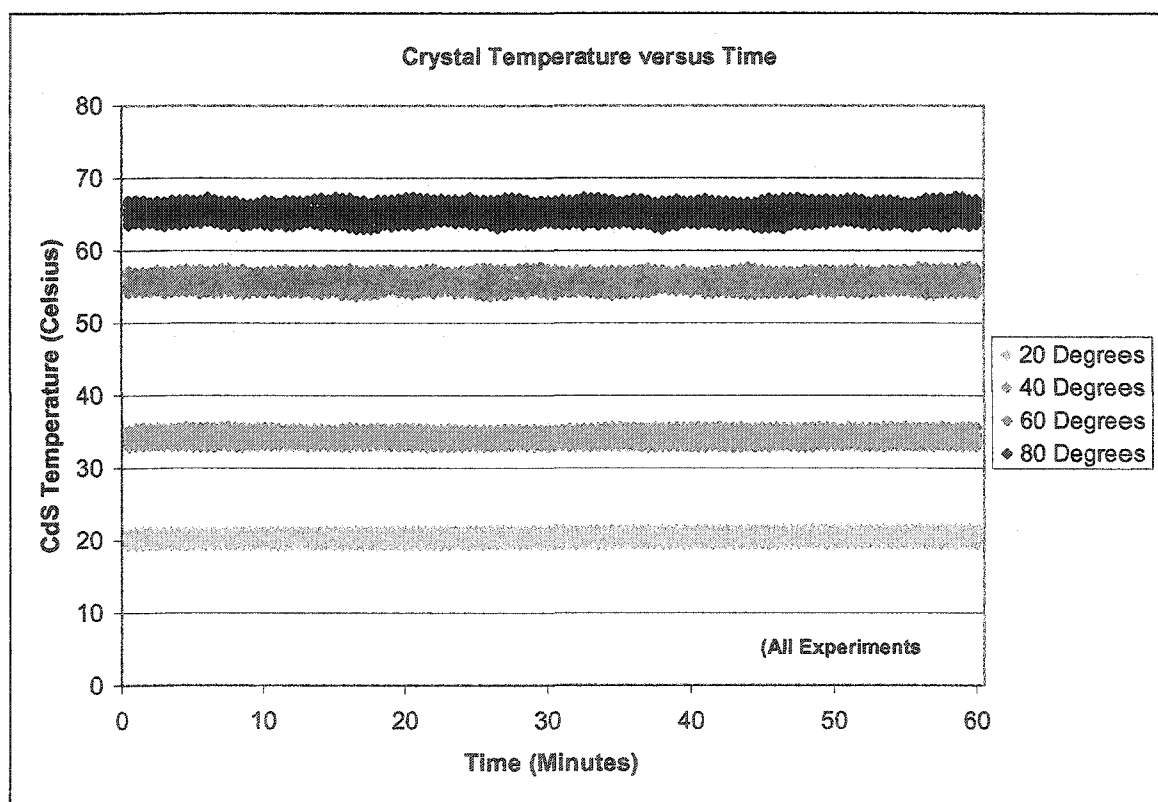
Figure 4.12. Crystal temperature versus time: all water bath temperatures. Specific details from each particular experiment can be seen more readily in Figure 4.13 and 4.14 below.

The first comment that should be made about Figure 4.12, is the discrepancy between the crystal temperature and that of the water bath for the various experiments. This difference in temperature simply reflects that the water bath in unable to keep the CdS crystal in thermal equilibrium for all temperature ranges. Surely, as bath

74

temperature increases the temperature of the crystal, it also increases the temperature gradient between the crystal and the surrounding air. This is most likely the reason behind this discrepancy. However, this is not a major concern at this point, as we were merely interested in running the experiment at different temperatures.

Also, it can be seen that the various curves representing the four different experiments have dissimilar thicknesses. In fact, the broader curves seem to correspond to experiments performed with higher water bath temperatures. To determine if this is indeed the case, however, it is necessary to look more closely at each individual experiment. The two experiments which were performed with the highest and lowest water bath temperatures are presented in Figure 4.13 and 4.14 below.
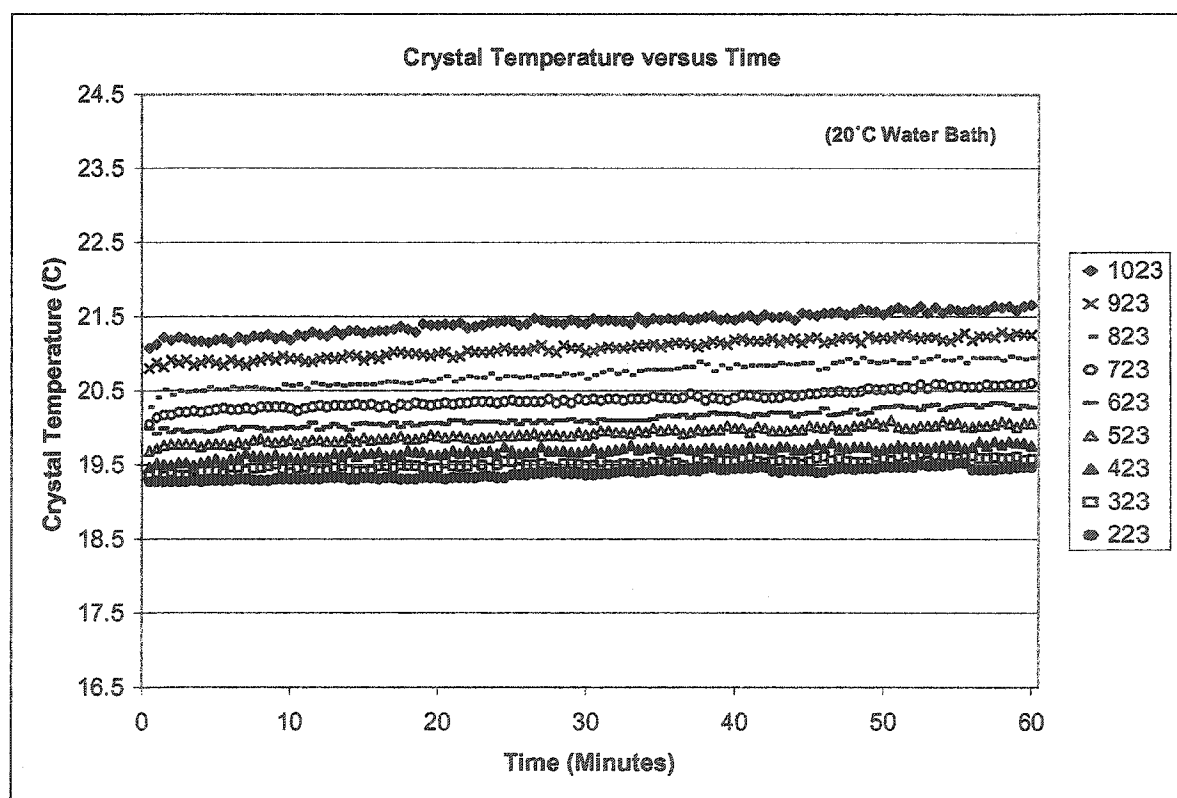
Figure 4.13. Crystal temperature versus time: 20°C bath temperature.

75
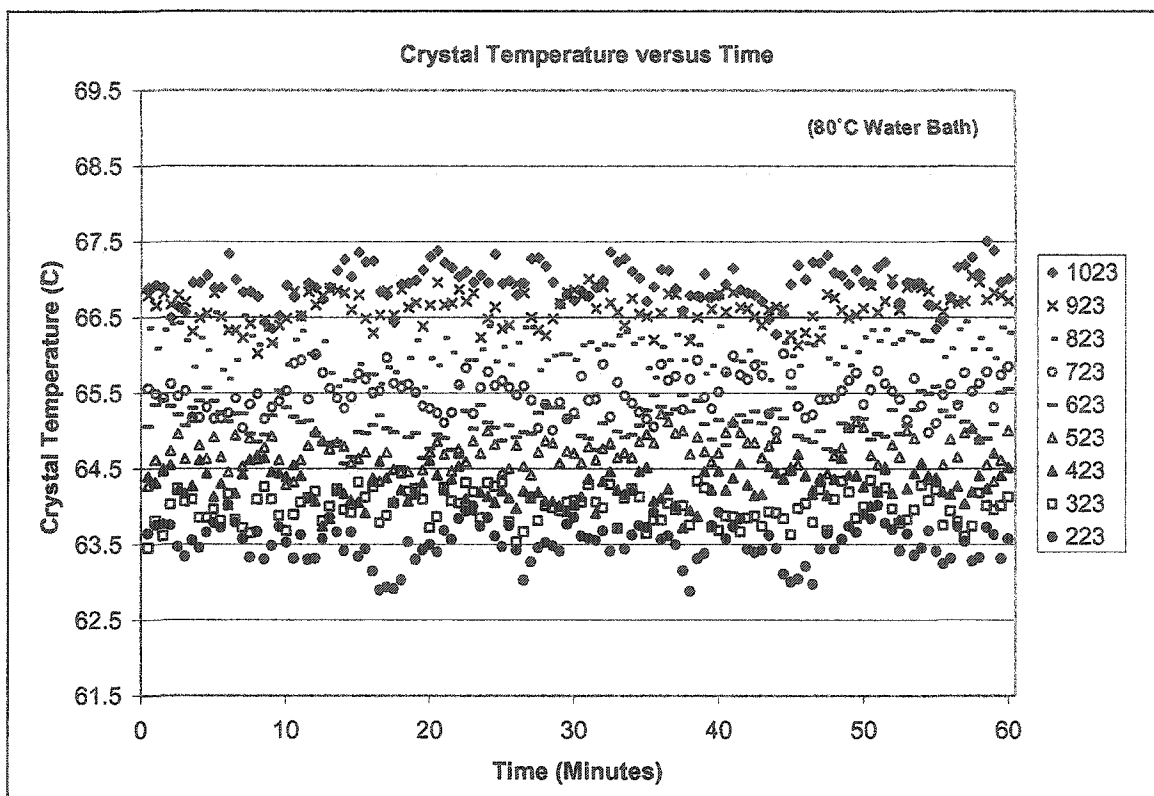
Figure 4.14. Crystal temperature versus time: 80°C bath temperature.

As can be clearly seen, there seems to be a definite dissimilarity between the two graphs. The most obvious is that while the temperature versus time curves in Figure 4.13 are reasonably 'well behaved', they seem to oscillate in a seemingly random fashion in Figure 4.14.

Perhaps most interesting with respect to the purposes of this particular experiment, however, is the fact the temperature difference between the top and bottom curve in the first experimental study is nearly double that of the first. It should be mentioned at this time that this overall temperature difference within each graph represents the fact that for high lamp intensities, the crystal is at higher temperature. This seems to make logical sense; as the intensity of light increases, so should the radiated thermal energy.

76

Another peculiarity that seems to exist between the overall patterns depicted in these graphs is the difference in their slopes. At low bath water temperatures, the crystal seems to undergo a heating process over the course of the hour long experiment.

Although each of these observations are engaging on their own (as witnessed by their inclusion in Appendix B), there is a fundamental statement that should be made at this time. It is this: efforts to limit the effect the lamp had on crystal temperature have to this point in the experiment been unsuccessful. Despite the inclusion of the light guide, as well as the water bath, there is still a pronounced variance in temperature between high and low light intensities. For this reason, the effect of temperature on conductivity must be further examined.

4. Procedure: Experiment B

The procedure for the second portion of this investigation, as mentioned earlier, was developed only after having analyzed the data obtained from the first. With a more complete understanding of the nature of the crystal, this next task could be completed with a more efficient and accurate approach. In order to fully understand which elements of the crystal's nature came into play in this second procedure, it is certainly beneficial to first sketch out the general scheme of experimentation. The experimental arrangement in this section was identical to that of the Experiment A (as seen in Figure 3.5); the method, however, was to be modified slightly. At the heart of this segment of research was the investigation of the effects of temperature on the levels of conductivity within the crystal. Accordingly, in this procedure, the lamp intensity was held constant while the water bath temperature was slowly raised from 20°C to 80°C; this, in turn, produced a change in the

temperature of the CdS crystal. By simultaneously monitoring both the resistance and the temperature of the crystal during this change in water temperature, the relationship between these two variables could be explored.

In order to generate an appropriate procedure with which to characterize this relationship between conductivity and temperature, however, it was first necessary to possess at least a basic understanding of the behaviour of Cadmium Sulfide conductivities. Having already scrutinized the data from the previous experiment indeed proved to be indispensable. Perhaps most importantly, through the full analysis of this data, the observation was made that the inherent aberrations in both the intensity of the light and the crystal resistance were greatly reduced after the first 20 minutes of photo-stimulation. After this point, in fact, crystal resistance leveled out and stabilized considerably. Given that the most effective way to examine the effects of thermal changes on the resistance of the crystal would be to compare the new data with that of a crystal in relative thermal equilibrium, this observation would prove to be indispensable in perfecting the specifics of the next procedure.

The modus operandi, then, consistent with the findings of the first experiment, progressed in the following manner: the experimental apparatus remained in an arrangement identical to that shown in Figure 3.5. The water bath was adjusted to an initial temperature of 20 °C and the light source remained off. The Cadmium Sulfide crystal was allowed to remain in this state of darkness and relative equilibrium for ½ hour at which time the DC 1100 lamp was set to an intensity output level of 223. Consistent with the findings of the proceeding experiment, this effectively provided more than sufficient time for conductivity to become relatively constant. At this time the DC 1100

78

lamp was set to an intensity output level of 223 and again ½ hour was allowed for stabilization. By means of the method utilizing the 'freeze' buttons on the multimeters discussed earlier, simultaneous recordings were made of crystal temperature, crystal resistance, and the intensity of the light output from the DC 1100. Upon completing this task, the temperature of the water bath was steadily increased from 20°C to 80°C over the course of approximately 1 hour. Using the thermometer within the water bath as a gauge, similar data was subsequently taken at each 1°C increment in water temperature.

Once the final reading had been taken for the corresponding water temperature of 80°C, the light source was again returned to an intensity output setting of zero. At this time, the hot water was emptied from the bath, and it was refilled with 16°C tap water which was then heated to 20°C. The process of changing and reheating the water generally took approximately 5 minutes. The CdS crystal would then remain in this darkened condition for 30 minutes, allowing it once again to reach a stable level of conductivity and relative thermal equilibrium. At the end of this time period, the DC 1100 lamp was then set to a level of 323 (an increase of 100 units from the previous trial) and the entire procedure was repeated, increasing the bath temperatures and taking readings again up to 80°C. The lamp was then returned to a zero value and the water was once again removed from the bath. This entire process was then repeated for lamp levels at increments of 100, up to a final value of 1023, thus completing this segment of experimentation. Once all of this data had been obtained, the thermistor readings, photometer readings and crystal resistance readings were converted to temperature, light intensity and crystal conductivity as described for Experiment A. The table resulting from the experimental readings of one lamp intensity setting is shown below in Table 4.8.

Light Output: 1023							
Temperature			Conductivity			Light	
Water (C)	Thermister Reading (kOhms)	Calculated CdS (Kohms)	Resistance Reading (Mohms)	Calculated CdS Resistance (Mohms)	Calculated CdS Conductivity (10^3 Ohm m)^-1	Photo-meter Reading (VDC)	Light Intensity (W cm^-2)
20	12.05	20.10	2.026	2.670	0.7282	0.4748	0.090
21	11.43	21.22	2.043	2.658	0.7316	0.4754	0.090
22	10.75	22.48	2.020	2.658	0.7316	0.4738	0.090
23	10.14	23.70	2.020	2.782	0.6990	0.4747	0.090
.	.	.	.	.	.	.	.
.	.	.	.	.	.	.	.
.	.	.	.	.	.	.	.
77	1.574	71.27	1.989	2.719	0.7152	0.4705	0.090
78	1.532	72.06	1.954	2.697	0.7209	0.4714	0.090
79	1.502	72.65	1.989	2.746	0.7082	0.4725	0.090
80	1.484	73.01	2.001	2.665	0.7296	0.4702	0.091

Table 4.3. Table showing the finalized data from Experiment B, for a lamp output intensity setting of 1023. The columns denoted by the word 'Reading' indicate that they are the measured values from their respective multimeters. All other values are calculated values. The processes of data acquisition and calculation are discussed at length in Chapter III.

Results: Experiment B

Throughout this chapter—particularly in the results section of Experiment A—we have discussed at length the effect that the moderating bath has on crystal temperature with respect to the thermal energy transmitted to the CdS sample by the lamp. Indirectly from the data obtained from this graph, we can determine the relationship between crystal conductivity and the temperature of the water bath at specific increments; i.e. 20°C, 40°C, 60°C and 80°C water bath temperatures. Although preliminary remarks have been made in the past section with respect to Figure 4.1 concerning the effectiveness of the water bath in moderating crystal temperature, Experiment B provides a perfect opportunity to observe this exact relationship. That is, how close is the correlation between the temperature of the crystal and that of the water bath for a given temperature range. This data is presented in Figure 4.15. It can be readily seen in

the graph that the temperature of the water is closely paralleled by the resultant temperature of the CdS crystal.
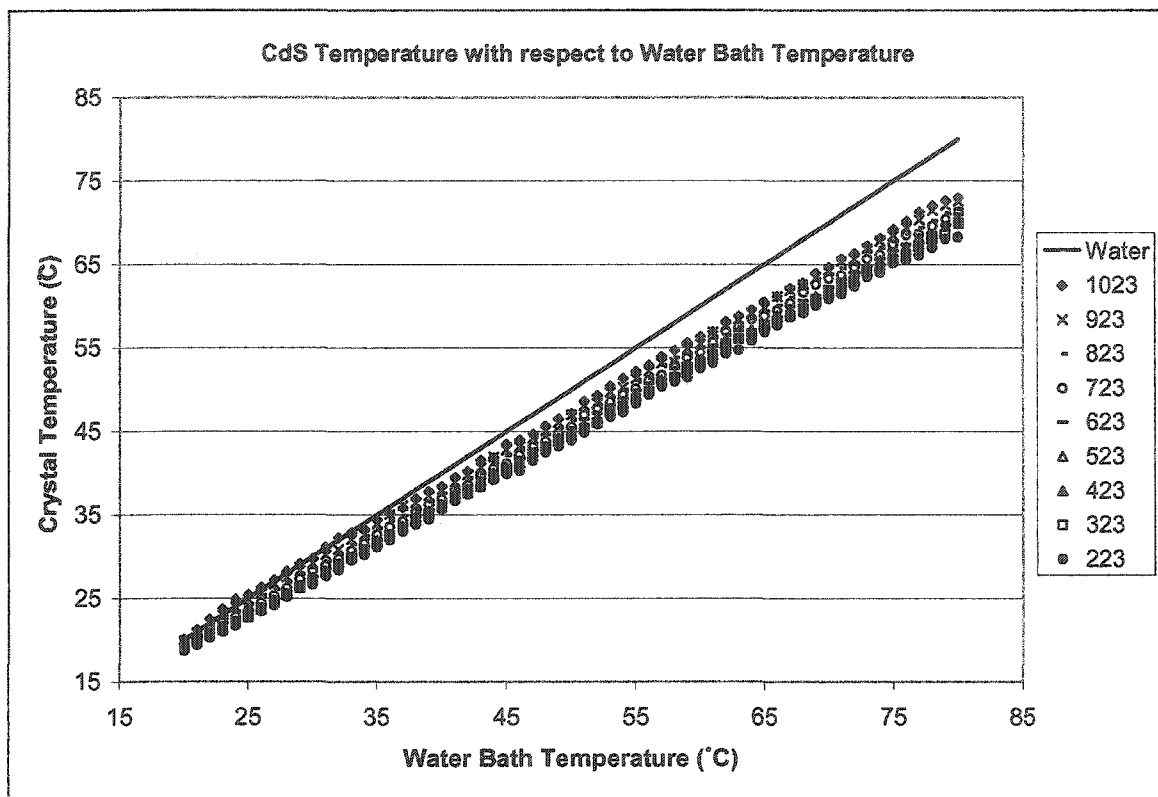
Figure 4.15. Crystal temperature versus water bath temperature. It can be seen that as the water bath temperature increases it is less able to control the temperature of the crystal.

The fundamental purpose of this portion of the research project was to determine the nature of crystal conductivity as a function of light and temperature, each as an independent variable. We have already discussed the relationship between conductivity and light intensity while limiting the temperature fluctuations of the CdS crystal. Having determined indirectly in the Experiment A that we can only limit this variability to

81

within a few degrees Celsius, it is then necessary to determine the effect of thermal energy on conductivity.

Below, Figure 4.16, CdS conductivity is presented as a function of crystal temperature. This data reflects the conductivity of the crystal after it has been excited by the light source for ½ hour prior to the temperature being increased. For this reason, based on the results from Experiment A, we can expect at this time that Cadmium Sulfide crystal had reached 'equilibrium' conductivity. After this time then, it is reasonable to expect that any significant conductivity changes can be logically attributed to the effect of thermal energy alone.
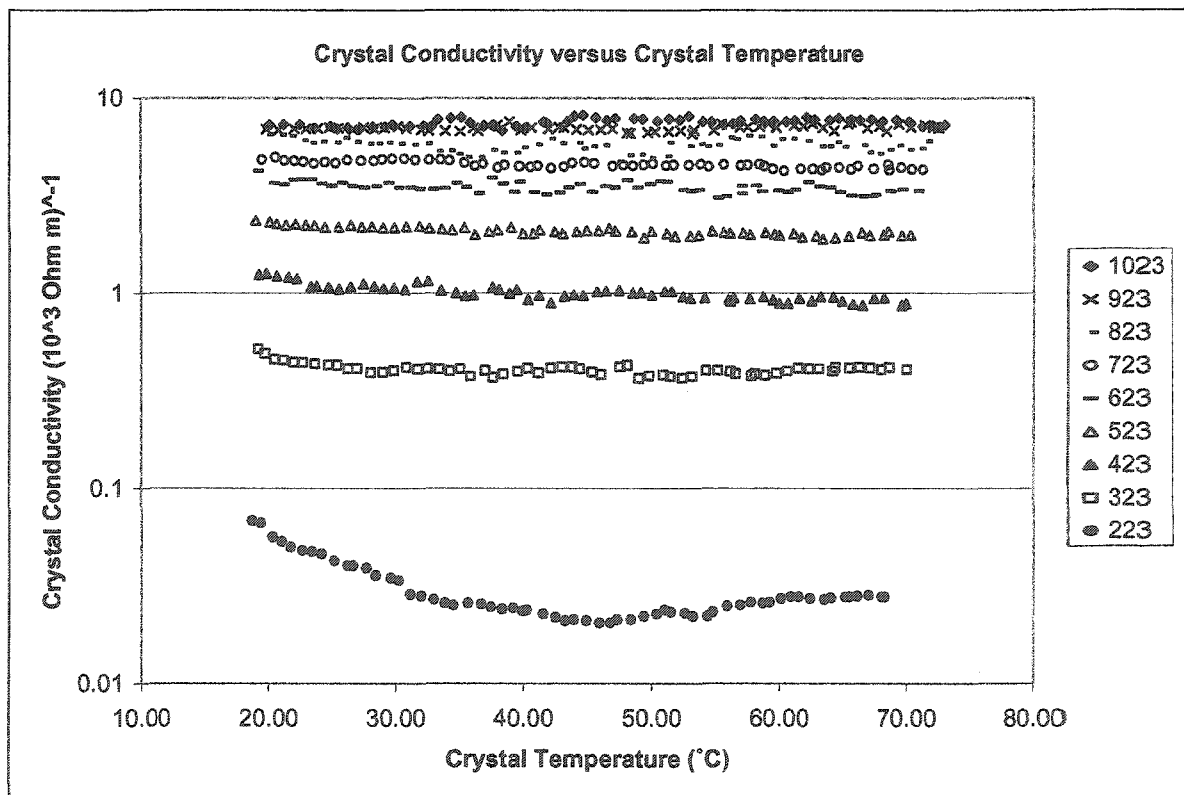
Figure 4.16. CdS conductivity as a function of crystal temperature. The temperature of the crystal was increased, using the water bath, after it was allowed to reach stable levels of conductivity.

As can be seen above, there do seem to be some slight changes in crystal conductivity with respect to temperature. In fact, as can be seen clearly by the curve corresponding the '223' lamp level, conductivity is in fact changing. Although, having said this, the exact effect of temperature has yet to be fully characterized. Indeed, after all, it can be similarly said of this plot that conductivity also is changing with time. For this reason an additional, and perhaps altogether more useful, comparison is needed.

Indeed, in order to properly classify whether or not the effect of heating the crystal some 50°C affects conductivity, we must necessarily have something distinctive with which to compare Figure 4.16. In one regard we are already prepared to create such a figure. The procedure of Experiment B was, in fact, developed in such a way as to provide an opportunity to properly make such a comparison. The results from Experiment A, specifically the conductivity versus time graph (Figure 4.5) provides such a resource. It was determined that after the first 30 minutes of illumination, the measured crystal conductivity seemed to stabilize. After such a point it could be expected to remain more or less steady for the duration of the hour. With this in mind, then, the last 30 minutes of the conductivity versus time data pertaining to a 20°C water bath can be compared to the data obtained in procedure B. It is first, however, necessary to assure ourselves that this is a reasonable endeavour. After all, while the data in the first experiment were recorded with respect to time, in the second crystal temperature was the primary independent variable.

Albeit not factored into the original design of the experiment, the time required to heat the water bath from 20°C to 80°C was coincidentally in the range of 35-40 minutes. For this reason, then, it is possible to compare the two experiments based merely on their

83

duration. Further, for the procedure in Experiment A conductivity readings were taken every 30 seconds for 1 hour, constituting 60 measurements. In a similar manner, procedure B recorded a single conductivity reading for every 1°C that the water bath was increased. In this way, the two experiments have an almost one-to-one correspondence, both in terms of the number of readings and in their duration. Admittedly, however, this does not necessarily suggest that the two experiments can be compared quantitatively point for point. On the other hand, this point for point analysis is not a necessary requirement. In order to deduce the extent to which thermal energy affects conductivity we need only qualitatively compare the two plots. This is done in Figure 4.17.
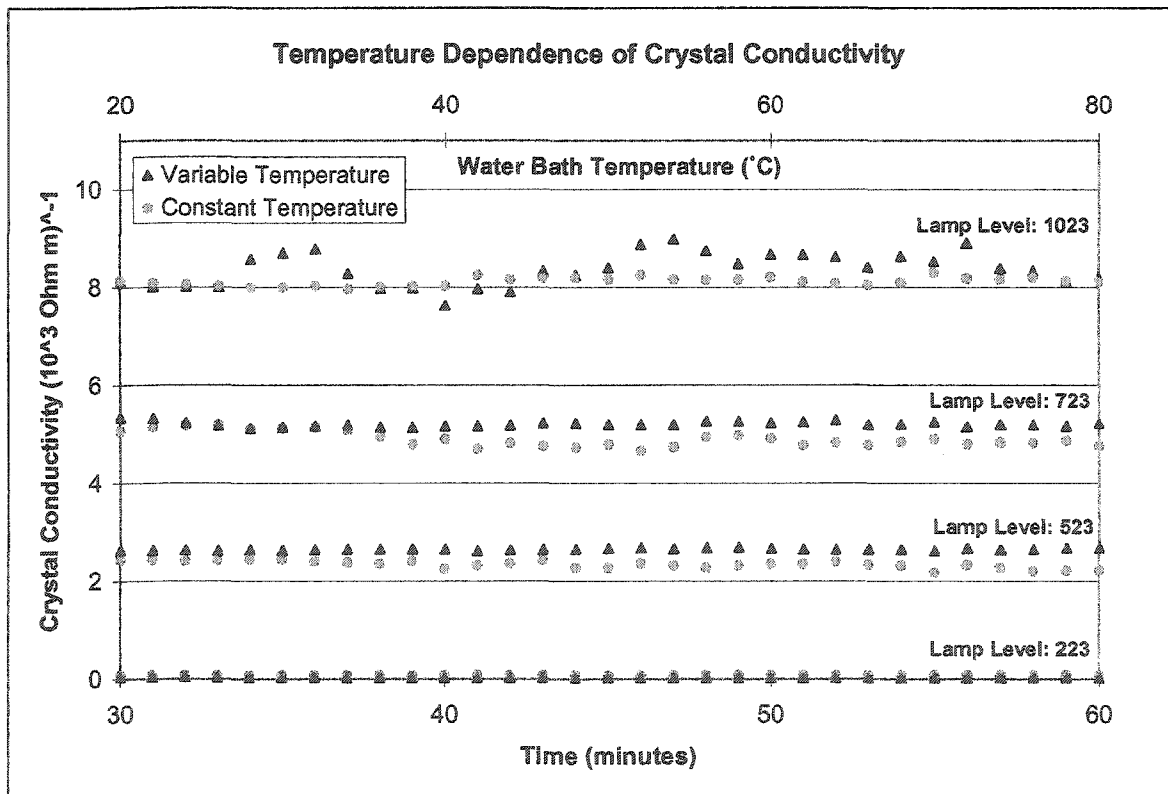
Figure 4.17. CdS conductivity as a function of both time and crystal temperature. This graph provides a basis for the qualitative determination of the effects of limited increases in thermal energy on CdS conductivity. Here selected curves from the last 30 minutes of Figure 4.5 are plotted alongside their counterparts in Figure 4.16. A minor additive constant was utilized to ensure that the first two points coincided. Further, the variable temperature curve is plotted with respect to the 'water bath temperature' axis, whereas the constant temperature curve is plotted with respect to time.

84

Before summarizing the results depicted within the above plot, it is perhaps necessary to discuss the specific steps that were used to create it. For each recorded crystal resistance in the data set obtained from procedure B, there are two temperature values by which it could be differentiated. Each of these measurements, in fact, corresponds to both the specific crystal temperature, as well as the water bath temperature at which it was recorded. Naturally, the most precise way to document the effect that temperature has on crystal conductivity is to plot it with respect to its simultaneously recorded temperature. For the sake of a greatly simplified and ordered graph, however, conductivity was plotted, instead, as a function of the water bath temperature. This decision can be justified in two ways: first, as can be seen in Figure 4.20, there is a close correlation between the temperature of the bath water and that of the crystal. And, second, in this procedure we require only a qualitative description of thermal effects. For this reason Figure 4.17, as it is plotted, is more than adequate.

In the above figure, then, the circular data represent conductivity measurements taken at constant temperature. These values correspond to the lower, time-axis. The triangular shaped points are plotted relative to water bath temperature which is shown on the top axis. Also, in order to further simplify this graph only a select few conductivity levels are shown; these curves, however, provide enough data from which to draw conclusions.

As a final note, it should be mentioned that the two curves did not fall immediately fall so perfectly upon each other. In fact, in order to facilitate their comparison, the conductivity curves in Figure 4.16 were slightly displaced in order that their first data point coincided with that of Figure 4.5. This displacement, although

slightly different for each pair of curves, was in each case comparable to the deviation of the conductivity readings for the data measured under increasing temperature.

The most significant detail that can be ascertained from Figure 4.17 is the fact that an increase in crystal temperature of up to 50°C has little effect on Cadmium Sulfide conductivity. Indeed, at lower conductivities, the curves follow almost exactly the same pattern. In the middle ranges of the light intensity levels there is seen to be a slightly higher conductivity level throughout. The fact that the averaged values of these conductivity curves are nearly parallel suggests that this is more coincidence than indications of some thermal phenomena. Even more pronounced is the deviation of the two curves at the highest intensity; the departure of the variable temperature conductivity readings from those obtained under constant temperature, however, seem to be more a consequence of instability. Indeed, as no two curves are substantially divergent, this figure supports the assumption that thermal exchange of this magnitude plays no significant role in conductivity. If this were the case, one would expect a constant and continued departure of the two curves as a function of the increased temperature discrepancy between the two experiments with respect to time.

6. Concluding Remarks

Having completed individual discussions regarding the investigation of long-range photoconductive behaviour, it is appropriate to summarize the observations that have been made. First, however, it is perhaps beneficial to restate the purpose of this study. In fact, the fundamental goal within this portion of research was not to present a comprehensive exploration of the many nuances of Cadmium Sulfide. Nor were

86

quantitative models expected as an outcome. In actuality, this portion of experimentation had the modest intention of characterizing the temperament of conductivity with respect to radiation and thermal excitation. Through a better understanding of this specific crystal, it was believed the long term stability of this Cadmium Sulfide crystal could be characterized and, further, predicted. It is believed that this objective has been accomplished.

Within the first portion of experimentation, while attempting to limit the effect of temperature, the conductivity of a particular Cadmium Sulfide crystal was measured over the course of one hour. Several data sets were taken with respect to different levels of photo-excitation. In this way, then, upon completion of these procedures, the excitation levels, resulting from stable illumination, could be examined as a function of time. Through the processing and evaluation of data, two generalized conclusions were drawn: first, it was determined that after a period of 20 minutes, the standard deviation of the measured conductivity was greatly reduced. It was also found that an increase in temperature due to radiation energy was, within the scope of this experiment, unavoidable.

It was primarily for this reason that, in the second procedure, an effort was made to evaluate the effect temperature had on the conductivity. Specifically, a method was developed by which the conductivity data which taken at relatively constant temperatures could be compared with that corresponding to an increasing crystal temperature. From these results it was determined that within the parameters of this particular experimental setup, the effects of heating due to the light source had negligible effect on crystal conductivity.

87

Thus, with these results, the goal at the outset of investigation had been accomplished. It was determined that the metastability of Cadmium Sulfide crystal was unavoidable, even in the absence of thermal equilibrium. Further, and perhaps most relevant within the scope of this research project, it was concluded that these fluctuations did plateau after a relatively short period of time. After this point, then, it could be expected that crystal conductivity would remain in this state.

CHAPTER V

Acoustic Wave Interactions in Cadmium Sulfide

The interesting, and sometimes challenging, properties of Cadmium Sulfide stem from the fact that it is simultaneously a photo-semiconductor and piezoelectric. For this reason, an acoustic wave propagating in this extraordinary medium gives rise to several interesting phenomena. In order to build a model of Cadmium Sulfide, then, it is beneficial to develop the properties associated with an acoustic field in each medium separately before putting them together in their final form.

1. Bulk Wave Propagation in a Piezoelectric Medium

At this stage of development, there are abundant resources available which expound upon acoustics and the piezoelectric effect. For this reason this section need only be devoted to the summary of the well documented fundamentals which describe piezoelectricity and, further, wave propagation within a piezoelectric medium. If desired, considerably more comprehensive analyses can be found in Auld [5] or Ikeda [4].

Consider a plane wave propagating in a non-piezoelectric crystal. The equation of such a wave is given by

$$u_k(x_k,t) = u_0 p_k \exp\left[j\left(k_i x_i - \omega t\right)\right] , \qquad (5.1)$$

where p_k is the polarization vector and the summation convention over repeated indices is employed. Also, the wave vector is defined in the usual manner as $k_i = |k| n_i$, with n_i representing a unit vector parallel to the direction of propagation.

89

The equation of motion (in tensor notation) for this medium is

$$\rho \frac{\partial^2 u_i}{\partial t^2} = \frac{\partial T_{ij}}{\partial x_j},$$

(5.2)

where ρ is the material density, and T is the strain. Hooke's Law defines the relationship between stress, T, and strain, S, in this situation as

$$T_{ij} = c_{ijkl} S_{kl} = c_{ijkl} \frac{\partial u_k}{\partial x_l},$$

(5.3)

where constant c_{ijkl} is the elastic moduli, or stiffness, a fourth rank tensor represented in matrix notation by

$$c_{ijkl} = \begin{bmatrix} c_{11} & c_{12} & c_{13} & c_{14} & c_{15} & c_{16} \\ c_{21} & c_{22} & c_{23} & c_{24} & c_{25} & c_{26} \\ c_{31} & c_{23} & c_{33} & c_{34} & c_{35} & c_{36} \\ c_{41} & c_{42} & c_{43} & c_{44} & c_{45} & c_{46} \\ c_{51} & c_{52} & c_{53} & c_{54} & c_{55} & c_{56} \\ c_{61} & c_{62} & c_{63} & c_{64} & c_{65} & c_{66} \end{bmatrix}.$$

(5.4)

Substitution of Equation (5.1) and (5.3) into Equation (5.2) yields the Christoffel equation,

$$\left(\Gamma_{ik} - \rho v_0^2 \delta_{ik} \right) p_k = 0,$$

(5.5)

where v_0 is the acoustic wave speed, δ_{ik} is the Kronecker delta, and

$$\Gamma_{ik} \equiv c_{ijkl} n_j n_l = \begin{bmatrix} \Gamma_{11} & \Gamma_{12} & \Gamma_{13} \\ \Gamma_{21} & \Gamma_{22} & \Gamma_{23} \\ \Gamma_{31} & \Gamma_{32} & \Gamma_{33} \end{bmatrix}$$

(5.6)

is defined as the Christoffel tensor or Christoffel matrix.

Due to the symmetry properties nature of a piezoelectric material, however, an acoustic wave in this medium behaves in a slightly different manner. The alternating

90

regions of high and low stress associated with an acoustic wave, in fact, contribute to polarization changes within the crystal, which in turn generate an electric field. Consider, for example, the following one-dimensional model (see Figure 5.1). As an area of high pressure from the acoustic wave passes through this portion of the medium, the charges associated with the constituent particles experience a compressive force. The polarization within this segment of material is then temporarily changed and, accordingly, an electric field is generated.
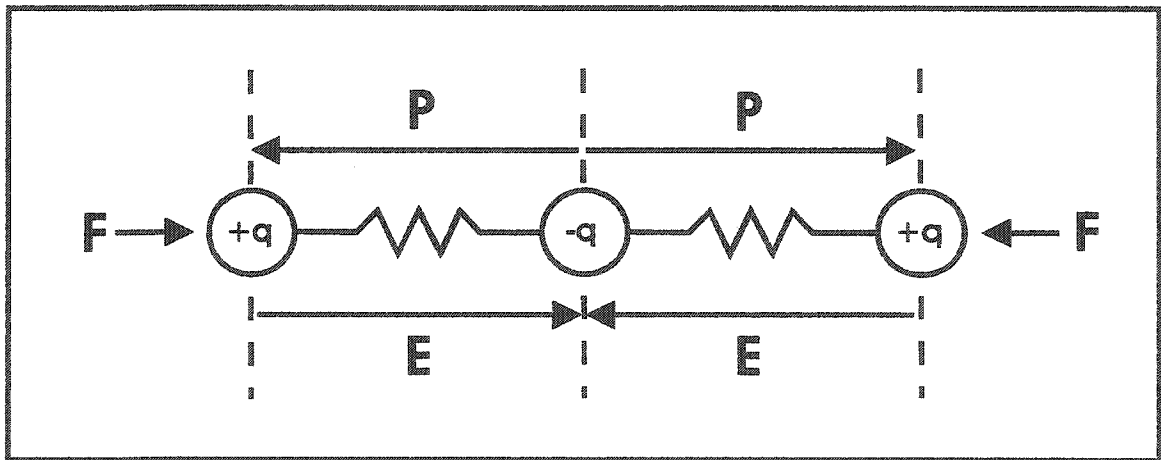
Figure 5.1. Schematic diagram of the piezoelectric effect. The above diagram demonstrates in one-dimension the mechanism by which an acoustic wave creates an electric field within a piezoelectric medium. The force, F, associated with the wave causes a displacement the charged particles of the material to displace from their equilibrium position. This displacement causes a polarization between the particles, in turn giving rise to an electric field.

Hence, due to the coupling between acoustic and electric fields within a piezoelectric semiconductor, the constitutive equations which describe the nature of wave propagation must be altered. These fundamental relations are

$$T_{ij} = c^E_{ijkl} S_{kl} - e_{mij} E_m,$$
(5.7)

and

$$D_n = \varepsilon^S_{nm} E_m + e_{nkl} S_{kl}.$$
(5.8)

91

With these equations we can directly observe the consequences of the change to a piezoelectric medium. An additional term has been added to Hooke's Law to account for the electric field, E_i, that accompanies an acoustic wave. Further, an electric displacement equation must also be considered. In equation (5.8) the electric displacement, D_i, is related to the electric field in the usual way save for an allowance specific to the influence of an acoustic wave. In these equations c_{ijkl} is, as before, the elastic stiffness matrix, ε_{nn} are the electric permittivity constants, and e_{mij} are the piezoelectric stress constants. The superscripts E and S denote that these constants were measured under conditions of constant electric field and constant strain respectively.

The most prominent distinction between the two theoretical bases is the fact that a piezoelectric medium couples the acoustic and electromagnetic fields. Therefore, along with the modifications of Hooke's Law and the electric displacement equation, Maxwell's equations make their appearance for the first time. In a piezoelectric insulator without net charge these take the form

$$rot\, E_i = -\frac{\partial B_i}{\partial t}, \qquad \text{(Faraday's Law)} \tag{5.9}$$

$$rot\, H_i = \frac{\partial D_i}{\partial t}, \qquad \text{(Ampere's Law)} \tag{5.10}$$

$$div\, D_i = 0, \qquad \text{(Gauss' Law)} \tag{5.11}$$

$$div\, B_i = 0, \qquad \text{(no magnetic monopoles)} \tag{5.12}$$

where B_i is the magnetic field and H_i is the magnetic intensity. Also, the medium is assumed to be nonmagnetic,

$$B_i = \mu_0 H_i, \tag{5.13}$$

92

where μ_o is the magnetic permeability of free space. Often, in what is called the quasi-electrostatic approximation, $\dot{B}$ is set to zero. Together equations (5.9)-(5.13) can be used to modify the Christoffel equation for a piezoelectric medium:

$$\left(\Lambda_{ik} - \delta_{ik} \rho v_0^2 \right) u_k = 0 .$$

(5.14)

In this equation Λ_{ik} is the new Christoffel tensor with

$$\Lambda_{ik} = \bar{c}_{ijkl} n_j n_l = \begin{bmatrix} \Lambda_{11} & \Lambda_{12} & \Lambda_{13} \\ \Lambda_{21} & \Lambda_{22} & \Lambda_{23} \\ \Lambda_{31} & \Lambda_{32} & \Lambda_{33} \end{bmatrix} , \qquad (5.15)$$

where the $\bar{c}_{ijkl}$ are often referred to as the stiffened elastic constants and

$$\bar{c}_{ijkl} = c_{ijkl} + \frac{n_m e_{mij} n_n e_{nkl}}{n_r \varepsilon_{rs} n_s} . \qquad (5.16)$$

In other words, the appropriate corresponding acoustic wave velocities can be determined using the eigenvalues of equation (5.14) along with

$$v = \left(\frac{c_{eff}^{(\lambda)}}{\rho} \right)^{\frac{1}{2}} . \qquad (5.17)$$

Here $c_{eff}^{(\lambda)}$ are defined as the effective elastic constant corresponding to the particular acoustic mode (λ).

To this point, we have undertaken a discussion of the behavior of an acoustic wave in a piezoelectric insulator. This, however, is not the situation with which we are faced. Indeed, as Cadmium Sulfide has the properties of a semiconductor, we must now amend the theory to allow for the existence of free charge carriers. The mechanism by

93

which these charge carriers are created within the medium has already been outlined in Chapter II.

With the introduction of free charge carriers into a piezoelectric medium Faraday's Law and Gauss's Law must both be altered. If q represents the magnitude of electronic charge and n the variation in conduction band electrons caused by an acoustic wave, equations (5.9) and (5.11) become

$$rot E_i = 0,\tag{5.18}$$

and

$$div D_i = -qn,\tag{5.19}$$

respectively. Here we have made a considerable simplification: while the assumption has been made that all the instantaneous space charge is indeed mobile, this is generally not the case. More sophisticated treatments account for fractionally mobile charge, however, this simpler approach is sufficient for our purposes. Further, a continuity equation must be added to represent the conservation of charge within the system. This is given as

$$div J_k - q\frac{\partial n}{\partial t} = 0, \quad \text{(continuity equation)}\tag{5.20}$$

where

$$J_k = \sigma E_k, \quad \text{(Ohm's Law)}\tag{5.21}$$

is the conductivity relation with J_k being the current density and σ the crystal conductivity. Altogether, then, the free carrier charge influences the equation for electric displacement within the system. This can be shown to become

94

$$D'_n = D_n - \left(\frac{j\sigma}{\omega}\right)E_n. \tag{5.22}$$

The influence of the charge carriers can be seen explicitly in this form. Consequently, the constitutive relations for a piezoelectric semiconductor become

$$T_{ij} = c^E_{ijkl}S_{kl} - e_{mij}E_m, \tag{5.7}$$

as before, and

$$D_n = \varepsilon^*_{nm}E_m + e_{nkl}S_{kl}, \tag{5.23}$$

where

$$\varepsilon^*_{nm} = \varepsilon^S_{nm} - \frac{j\sigma_{nm}}{\omega}, \tag{5.24}$$

clearly demonstrates the modification of the dielectric constants.

For purposes of future discussion, it is useful to qualitatively consider the case of an acoustic wave propagating along an arbitrary axis within a piezoelectric medium. Dependent, of course, on the specific piezoelectric tensor and the axis of propagation, the addition of the second term containing the electric field in Equation (5.7) implies that this mechanical wave will give rise to an electromagnetic wave. These electromagnetic and acoustic waves will then propagate together as a *quasiacoustic* wave whose phase velocity is only slightly dispersed its initial value. The mechanical energy within this quasi-acoustic wave dominates the associated electromagnetic energy. In a similar manner equation (5.23) expresses the fact that electromagnetic waves stimulate mechanical waves, in turn pairing together to create a *quasielectromagnetic* wave. Thus, within a piezoelectric semiconductor, there is a specific coupling between the three (one longitudinal mode and two transverse modes) modes of an acoustic wave and the two (transverse) modes of an electromagnetic wave.

95

Although these slight changes in wave velocity that result from the union of electromagnetic and acoustic waveforms exist mathematically, the most remarkable phenomena arise from the electrostatic fields accompanying the piezoelectric polarization. While polarization configurations are specific to variables such as wave mode and direction (as well as the structure of the crystal itself) it can be demonstrated [5] that an acoustic wave engenders an electric field only in the circumstance that

$$\overline{D}^{(piezo)} \| \overline{k}. \tag{5.25}$$

Here the superscript denotes that we are looking only at the piezoelectric contribution to the electric displacement. If the condition of Equation (5.25) is met then the wave corresponding to this mode is termed to be *piezoelectrically active*. It is this geometry that is of particular interest and, in turn, is the focus of most papers on the subject of acousto-electric interactions within semiconductors.

2. Linear Wave Dispersion and Attenuation

The major papers which correspond directly to the experimentation within this particular research project were written by Kyame [10] as well as by Hutson and White [32]. In a review article outlining the initial progress within the specific field, McFee [34] effectively summarizes the theoretical and experimental contributions of several authors and it is the approach therein which is outlined below.

Before undertaking a complete theoretical analysis, some simplifications can be made, upon consideration of the experimental parameters specific to this thesis project. First, the waves generated within the particular experiments ranged from a minimum frequency of around 2 MHz to a maximum of just over 20 MHz. In CdS, these

96

correspond to wavelengths of approximately 2 mm and 0.2 mm respectively. Thus, for a wave propagating within CdS, $k\bar{l} \ll 1$, where $k = 2\pi/\lambda$ is the usual wave number and $\bar{l}$ is the mean free path of the carriers. As a result, quantum mechanical effects need not be considered. The acoustic wavelength is, in fact considerably larger than the lattice constants as well as the mean free path of the charge carriers thereby enabling a continuum mechanics approach. On the other hand, the wavelength is macroscopically small as compared to the dimensions of the crystal itself. Second, the CdS crystal is considered to be an extrinsic semiconductor and the electron distribution is assumed to be governed by Maxwell-Boltzmann, nondegenerate statistics. Also, the role of holes in conductivity is ignored. Perhaps the greatest simplification—and perhaps one of the largest sources of error—is the assumption that every charge carrier within the conduction band is entirely free. Both this case and the case where only a portion of the space charge escape the bound states in the energy gap are described by Hutson and White [32]. With these three approximations in effect, many of the theoretical complexities are greatly reduced without an unreasonable sacrifice in accuracy. Indeed, this theoretical approach provides a sufficiently detailed and accurate description for comparison with measured data within the limits of the experimental method.

With this being said, we can further reduce the complexity of the theory by taking into account the fact that the truly significant effects of piezoelectricity are dependent on the existence of these piezoelectrically active waves. Thus, without any loss in precision analytical analysis can be addressed with a one dimensional model. Indeed, the acoustic interaction along the piezoelectrically active (piezo-active) axis moves to the forefront of evaluation. With this in mind the desired constitutive equations become

$$T = cS - eE ,$$ (5.26a)

$$D = \varepsilon E + eS ,$$ (5.27b)

where all superscripts have been dropped to simplify notation. By inserting Equation 5.26a into the usual wave equation,

$$\frac{\partial T}{\partial x} = \rho \frac{\partial^2 u}{\partial t^2} ,$$ (5.28)

we can arrive at a modified wave equation—one that accounts for the piezoelectric nature of the medium:

$$\rho \frac{\partial^2 u}{\partial t^2} = c \frac{\partial^2 u}{\partial x^2} - e \frac{\partial E}{\partial x} .$$ (5.29)

With the addition of a current density equation,

$$J = q(n_0 + n)\mu E + q \wp \frac{\partial n}{\partial x} ,$$ (5.30)

where $\wp$ is the diffusion constant, as well as two equations defining the space and time dependencies of the electric field and electric displacement:

$$E = E_1 \exp[j(k_s x - \omega t)] ,$$ (5.31a)

$$D = D_1 \exp[j(k_s x - \omega t)] ,$$ (5.31b)

we have all the tools to properly determine the fundamental relationships between the acoustic and electronic fields within a piezoelectric semiconductor. It should be noted that in the above equations n_0 represents the equilibrium density of charge carriers in the conduction band, μ is the electronic mobility and $\wp$ is the electronic diffusion constant. Further, E_1 and D_1 represent the maximum variation of the field two fields.

98

By inserting Eq. (5.31a) into Eq. (5.30) we can begin to distinguish and, in turn, isolate the linear theory from that of the nonlinear. For the linear approximation we obtain

$$J = q\mu \left(n_0 \cdot E_1 \right) \exp\left[j(k_s x - \omega t) \right] + q \wp \frac{\partial n}{\partial x},$$ (5.32)

where the product of the two wave amplitudes (the source of the nonlinearity) has been neglected. From this point these algebraic relations can be manipulated in such a way as to yield a wave equation to replace equation (5.29):

$$\rho \frac{\partial^2 u}{\partial t^2} = c' \frac{\partial^2 u}{\partial x^2}.$$ (5.33)

Notice that in this equation the electric field term is conspicuously absent. Also, the crystal stiffness has been modified. The new complex elastic constant appears as [34],

$$c' = c \left[1 + \frac{e^2/c\varepsilon}{1 + \frac{j(\sigma/\varepsilon\omega)}{1 + j(k_s^2/\omega)\wp}} \right].$$ (5.34)

Observing that

$$\kappa^2 \equiv \frac{e^2}{c\varepsilon},$$ (5.35)

where κ^2 is the square of the electromechanical coupling coefficient [34]. Typically

$$\kappa^2 \ll 1.$$ (5.36)

The acoustic wave velocity is given by

$$v = \frac{\mathrm{Re}\sqrt{c'}}{\sqrt{\rho}} = v_0 \frac{\mathrm{Re}\sqrt{c'}}{\sqrt{c}},$$ (5.37)

and the attenuation coefficient is given by

$$\alpha = \frac{\omega}{v_0} c^{\frac{1}{2}} \, \mathrm{Im}\left(c'^{-\frac{1}{2}} \right). \tag{5.38}$$

Upon solving for the acoustic wave velocity and attenuation coefficient it follows that [34],

$$v = v_0 \left[1 + \frac{\kappa^2}{2} \cdot \frac{1 + \frac{\omega}{\omega_D}\left(\frac{\omega_C}{\omega} + \frac{\omega}{\omega_D}\right)}{1 + \left(\frac{\omega_C}{\omega} + \frac{\omega}{\omega_D}\right)^2} \right], \tag{5.39}$$

and,

$$\alpha = \frac{\omega}{v_0} \left[\frac{\kappa^2}{2} \cdot \frac{\frac{\omega}{\omega_C}}{1 + \left(\frac{\omega_C}{\omega} + \frac{\omega}{\omega_D}\right)^2} \right]. \tag{5.40}$$

Within these equations the following abbreviations and definitions have been used:

$$\omega_C \equiv \frac{n_0 \, q\mu}{\varepsilon}, \qquad \text{(conductivity relaxation frequency)} \tag{5.41}$$

$$\omega_D \equiv \frac{v_0^2}{\vartheta}. \qquad \text{(electron "diffusion" frequency)} \tag{5.42}$$

It is interesting at this point in the discussion to analyse Equations (5.39) and (5.40) with respect to the experimental procedures of this thesis project. As a first step let us scrutinize the major constituents of the relationships between the constants and variable in these equations. We will, however, only outline the general consequences of these equations.

The conductivity relaxation frequency, as defined in Equation (5.41), can be further simplified in that the conductivity with respect to free electrons is

100

$$\sigma = n_0 \, q\mu \,.$$ (5.43)

If ε is considered constant then we have

$$\omega_C \propto \sigma \,.$$ (5.44)

More specifically, in fact, the conductivity relaxation frequency is a linear function of only conductivity, as can be seen if Figure 5.2.
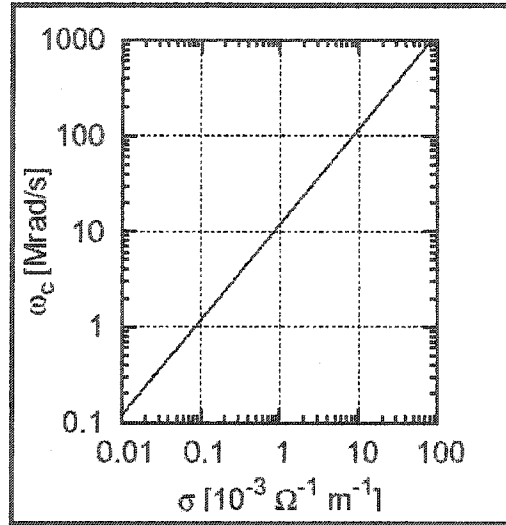
Figure 5.2. Conduction relaxation frequency versus conductivity.

In a similar manner, we can examine the electron "diffusion" frequency equation. Within the denominator in this relation is the so-called Einstein equation,

$$\wp = \frac{\mu \, kT}{q} \,,$$ (5.45)

where kT is the thermal energy of the charge carrier. Taking into account the parameters consistent with the experimental scope of this research project Equation 5.45 and, consequently, Equation 5.42 can be considered to be essentially constant with respect to the other variables.

Finally, then, with Equation 5.35 reflecting the constant nature of the electromechanical coupling constant, Equation 5.39 can be written as

101

$$v = F(\omega, \sigma), \tag{5.46}$$

$$\alpha = G(\omega, \sigma). \tag{5.47}$$

Thus, for the purposes of this thesis project we can view both velocity and attenuation as functions of wave frequency and crystal conductivity alone.
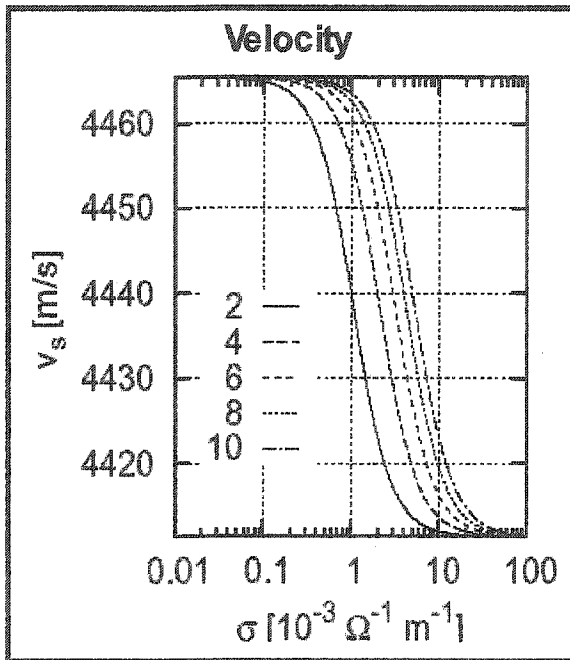
Figure 5.3a. Wave velocity versus conductivity curve with frequency as a parameter. Material parameters are given in Appendix B.
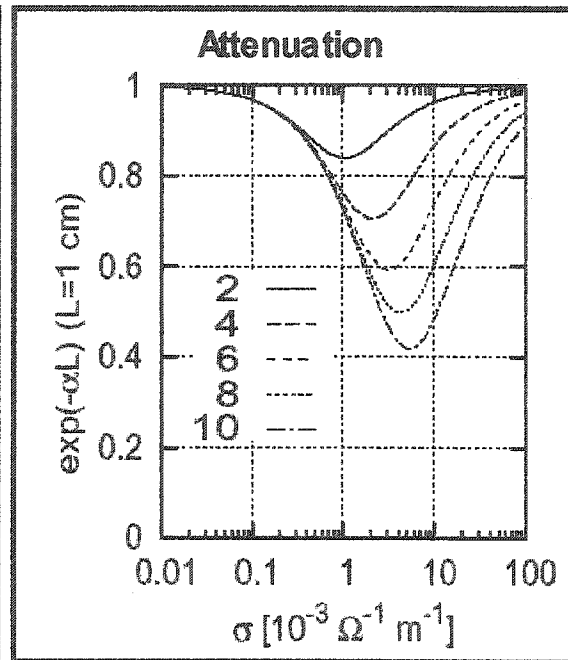
Figure 5.3b Amplitude attenuation versus conductivity with frequency as a parameter. Material properties are given in Appendix B.

As can be seen by Figure 5.3a, there can be considerable changes in wave velocity due to the interaction of acoustic waves with free charge carriers. Also, the frequency of a wave can play a significant role in determining the carrier concentration necessary to observe the acoustoelectric effect. The expected wave attenuation expected for a given frequency as a function of conductivity is also plotted in Figure 5.3b.

102

2. Nonlinear Consequences

Several papers have discussed the origin and consequence of the nonlinear aspects of the acoustoelectric effect [43-46]. For the purpose of this research paper, however, we desire only a qualitative explanation for this phenomenon. For this reason, in the following discussion, McFee [24] is provided as a reference.

Recall that in the linear approximation, Eq. (5.31a) was inserted in to Eq. (5.30) and the $(n \cdot E_1)$ term was ignored in Eq. (5.32). This approximation was realistic for small wave amplitudes, where in Eq.(5.30), $n_0 >> n$ and n is variation in the density of the free electrons caused by the acoustic wave. For large signals this is no longer the case. Thus, Equation (5.30) remains (in expanded form)

$$J = q\mu n_0 E + q\mu n E + q\wp \frac{\partial n}{\partial x}.$$ (5.48)

The nonlinear term that was absent from Eq. (5.32) is defined as

$$J_{ae} = q\mu nE,$$ (5.49)

where J_{ae} denotes the *acoustoelectric current* which accompanies the acoustic wave. By expanding all wave amplitudes into Fourier series and determining the average value of the acoustoelectric current, Equation (5.49) can be expressed in terms of Equation (5.40), the linear attenuation coefficient [24]:

$$J_{ae} = -\frac{\mu I(2\alpha)}{v_0},$$ (5.50)

where I is the acoustic energy flux.

In this way, then, Equation (5.50) provides a physical interpretation of the acoustoelectric effect. As the acoustoelectric current is proportional to attenuation

103

coefficient, linear wave attenuation can be thought of as the transfer in acoustic energy to this acoustoelectric current which travels along with the wave. Thus, the acoustic loss due to the conduction electrons is directly attributable to nonlinear phenomenon. In addition, the nonlinear theory can give rise to harmonic generation [43] which will be demonstrated in the next chapter.

104

CHAPTER VI

Experiments Exploring Acousto-electric Interactions

While the experimental procedure of Chapter III had as its primary focus the study of photoconductivity, specifically within Cadmium Sulfide, this section of research is concerned with the phenomena associated with the acoustoelectric effect. That is, having already explored the effects of both radiation and thermal energy on the level of free charge carriers within a photoconductor, concentration can now be shifted to better understanding the behavior of an acoustic wave with respect to these levels. In this way the experiments that have been presented to this point have helped to lay the foundation for this portion of research. It is in light of the previous results, then, that all experimental procedures within this section have been developed.

In order to properly investigate the acoustic properties of CdS, experimental methods have been divided into two separate components: linear and nonlinear. It is in this way that the results will be presented. The first half of this chapter develops such aspects of acoustic wave attenuation and velocity dispersion, while the second portion has as its focus the study of harmonic generation. Finally, connections are drawn with respect to the relationship between these two aspects of the acoustoelectric effect.

1. General Experimental Setup

Preliminary experimentation regarding the nature of acoustic waves within the Cadmium Sulfide crystal began with an arrangement of apparatus that was nearly identical to that which was described in Chapter III. In fact, with respect to Figure 3.5,

the only significant modification was the inclusion of apparatus pertaining to the generation, reception and observation of ultrasonic waves. The typical experimental setup can be seen below in Figure 6.1. This layout, however, is specific to the investigation of linear phenomenon. Naturally, this design was modified in order to observe the nonlinear aspects of the acoustoelectric effect.
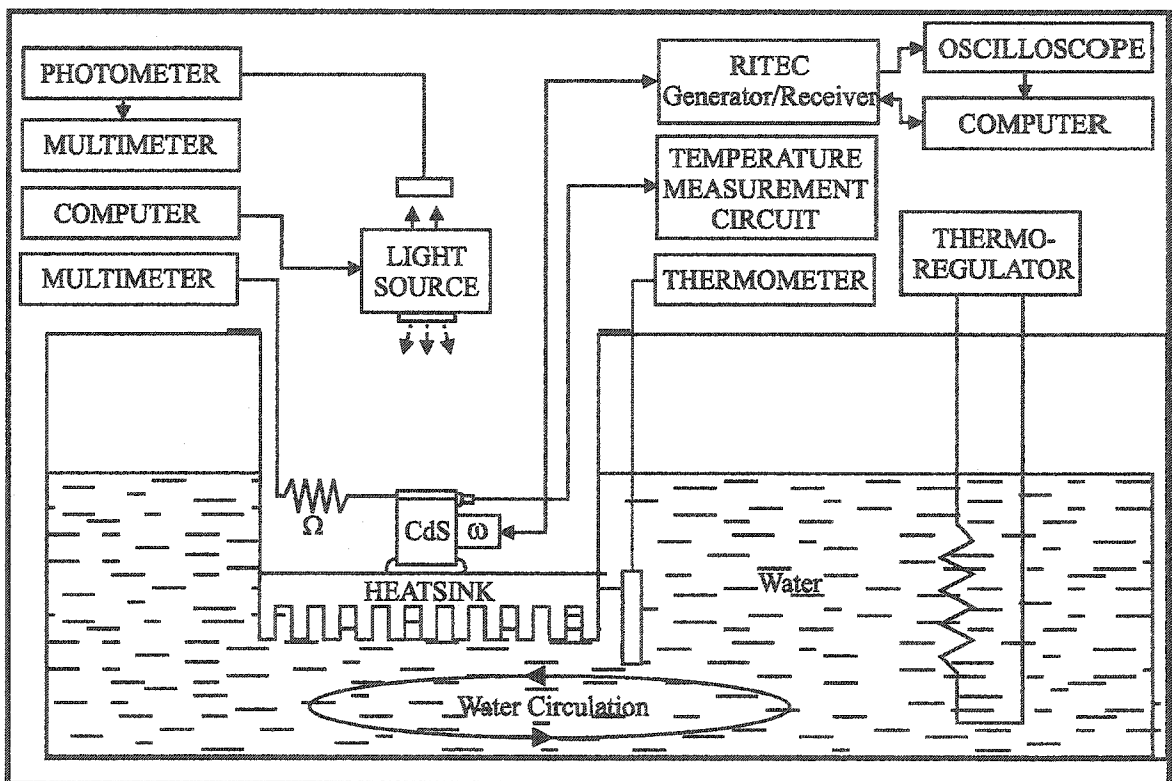
Figure 6.1. Experimental arrangement for all linear acoustic experiments. An identical setup is used for the nonlinear portion of this research project with a second transducer of frequency 2ω added to receive the pulse.

In order to generate, receive and process the acoustic signal that was passed through the CdS crystal the Ritec Acoustic Measurement System Snap-1-30 (hereafter referred to simply as the *Ritec system* or *Ritec Machine*) was utilized. The Ritec system is a state-of-the-art high-frequency measurement system whose features lend it perfectly

106

to the study of nonlinear phenomenon. The broadband gated R.F. amplifier is able to generate ultrasonic waves up to a frequency of 30 MHz and the Ritec system has a considerably refined receiver. Features include phase sensitive detectors, gated integrators as well as multiple frequency synthesizers. In short, the Ritec system allows for the generation of acoustic pulses at specific frequencies. Further, the sophisticated receiver and detailed software package allows for the processing of the received signal; in many ways, then, the Ritec machine facilitated the necessarily precise nature of this research project. Included within this package were all the necessary filters required to perform the various experiments in this chapter. A LeCroy LT342L Digital Oscilloscope was implemented to visually monitor and quantitatively measure the received signal. Along with several features common to most oscilloscopes, the LeCroy LT342L model allowed for all wave data to be stored in an ASCII format. This tab delimited file could then be processed externally. The transducers were manufactured by Xactex (3.5 MHz) and Aerotech (7.5 and 15 MHz). Also, a second computer was implemented into the original experimental design in order to both manage the Ritec system and, also, to process the data received from the LeCroy oscilloscope.

Aside from the above mentioned apparatus, as alluded to in Chapter III, there was in actuality another major discrepancy between the fundamental experimental setup and the present description that is presented in Figure 6.1. That is, the exclusion of the dual arm light guide which was implemented into the original design to reduce thermal radiation. This, however, was as a consequence of necessity. In fact, preliminary experiments concerning the attenuation of acoustic waves had suggested that it was necessary to increase conductivity levels within the CdS crystal in order to achieve more

107

complete results. For this reason it was essential to remove the light guides that had been utilized throughout the previous procedures. Instead, the lamp aperture was centered directly above the sample, in this way increasing the intensity of light incident on the crystal. Unfortunately, as a direct consequence of this alteration, there would also be a decided increase in thermal energy being directed towards the crystal. The results of the previous experiments concerning conductivity as a function of temperature, however, suggested that even rather substantial increases in crystal temperatures had little effect on the conductivity levels of CdS. Further, the thermister readings which accompanied each experimental procedure quantitatively demonstrated that the increase in temperature due to the close proximity of the lamp aperture was negligible when viewed with respect to the results of Chapter IV.

At this point, then, the experimental arrangement that accompanied each specific procedure was exactly as described above. The only dissimilarity between the designs of the linear and nonlinear experiments came as a result of the necessary rearrangement of transducers and filters and, naturally, the methods which were particular to each investigation. The nuances of each experiment are described below.

2. Linear Domain: Experiment

The specific arrangement of the acoustic apparatus with respect to all linear experimentation is depicted below in Figure 6.2. As can be seen in this diagram, a pulse-echo technique was employed in this portion of the research project. It was thought that by employing only a single transducer and receiving the sequential pulses that echoed from the back face of the crystal we would effectively lengthen the acoustic path. In this

108
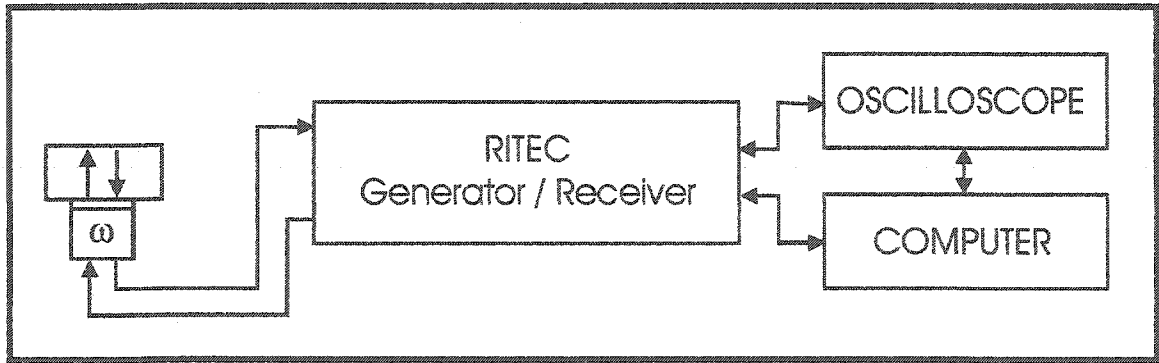
Figure 6.2. Arrangement of acoustic apparatus for linear acoustic experimentation

way the consequences of the acoustoelectric effect have a more significant effect between

subsequent echoes. A longitudinal wave was employed along the hexagonal axis of the

Cadmium Sulfide crystal. In this way an *acoustically active wave* was assured.

Ultrasonic coupling gel was utilized at the interface between the transducer and the CdS

crystal in order to increase the amplitude of the received pulse. Various transducers were

initially tested in order to determine which was most effective to utilize as a fundamental

frequency for both the linear and nonlinear portions of this thesis project. In the end, at

least in the case particular to this specific experimental arrangement, it was determined

that the best results were obtained when driving 3.5 MHz Xactex transducer at 4.1 MHz.

Also, in the second trial of the linear procedure a 7.5 MHz Xactex transducer was utilized

to produce a 8.2 MHz waveform.

Now, before venturing to explain the particular procedure developed to measure

the amplitude and velocity of the received waveforms, it is first beneficial to provide a

brief qualitative description of the observed phenomenon. Figure 6.3, as seen below,

illustrates a single pulse received from a fundamental waveform of 4.1 MHz sample

oscilloscope reading for several different levels of crystal illumination. As can be seen,

the level of illumination, and in turn, the quantity of free charge carriers in the conduction

109
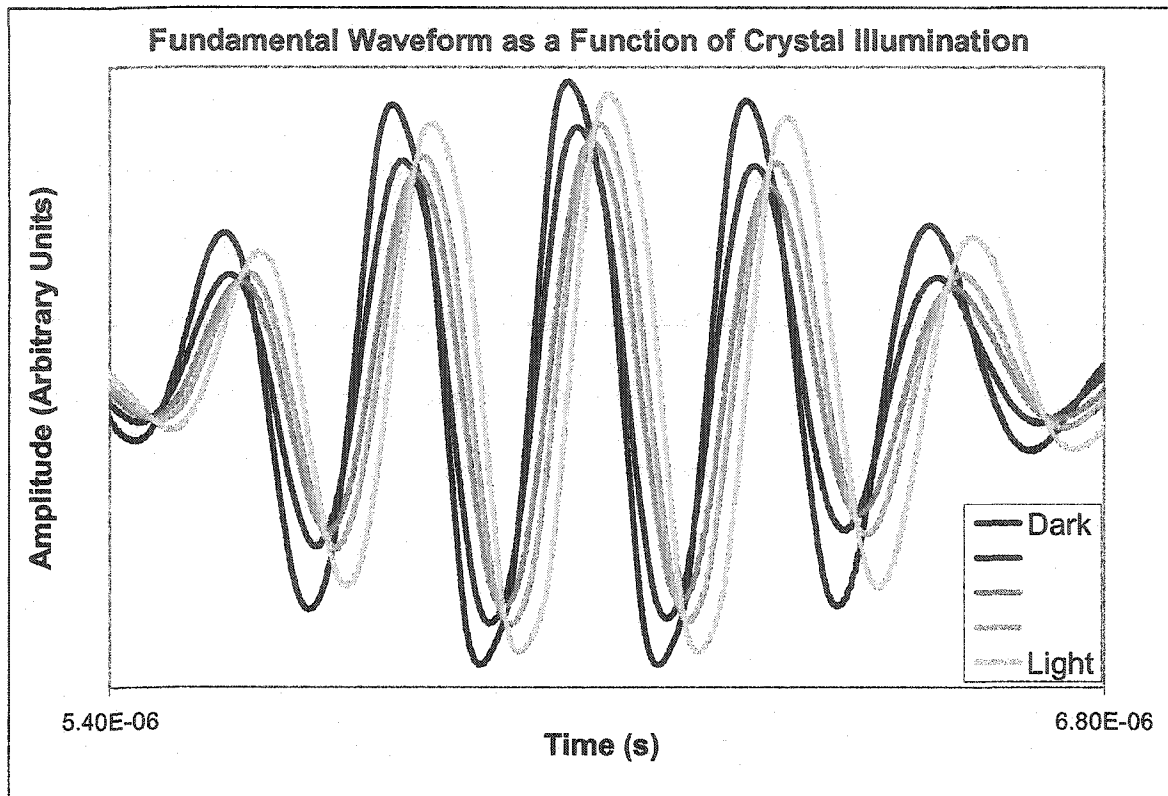
Figure 6.3. Typical waveforms for fundamental frequency with illumination as a parameter. As can be seen, the increased number of charge carriers affects both the velocity and attenuation of the wave.

band of CdS, can have a profound effect on both the velocity and amplitude of an appropriately polarized wave. Indeed, as the light levels increase from dark to bright, the waveform undergoes two observable changes: first, the wave amplitude can be seen to move through a minimum before once again nearing its original magnitude. And second, the time delay of the waveform slowly increases with the light intensity. The physical interpretation of this time-shift is, of course, a decrease in wave velocity. In this way, then, Figure 6.3 demonstrates both the wave attenuation and velocity dispersion that results from the acoustoelectric effect. In order to quantify this effect, however, a more specific and exact procedure is required.

110

3. Linear Domain: Procedure

Having arranged the experiment in the form discussed above, a procedure was developed which took advantage of the results of Chapter IV, as well as the knowledge gained from several initial qualitative investigations. Although several trials of this experiment were repeated, the results and procedures of one particular instance will be discussed. Indeed, all trials yielded similar results. Also, this particular experiment was performed with identical procedures for frequencies of 4.1 MHz and 8.2 MHz. In this case, we explore case corresponding to an initial pulse of 4.1 MHz.

Initially, before performing any procedures specific to the investigation of the acoustoelectric effect, some initial adjustments were required. For this reason the external environment was set to match the conditions within which the experiment was performed. The water bath temperature was set to 20°C and the overhead lighting was shut off. All external sources of light such as the computer monitor and a small desk lamp were directed in such a manner as not to disturb the Cadmium Sulfide. Also, the DC 1100 light source was also set to a value of zero.

At this point the transmitted and received wave was adjusted using the Ritec system which had been fitted at this time with a 3.5 MHz Xactex transducer. The software which controlled the Ritec machine was set in such a manner as to generate a an 8-cycle, 4.1 MHz modulated wave pulse. Further, the software set the receiver to track the fundamental frequency. Using the LeCroy oscilloscope as a guide, the output pulse was amplified to the maximum value that could be transmitted before any form of saturation was detected in the received pulse. On the oscilloscope, then, appeared a wave-train similar to the one pictured below in Figure 6.4.

111
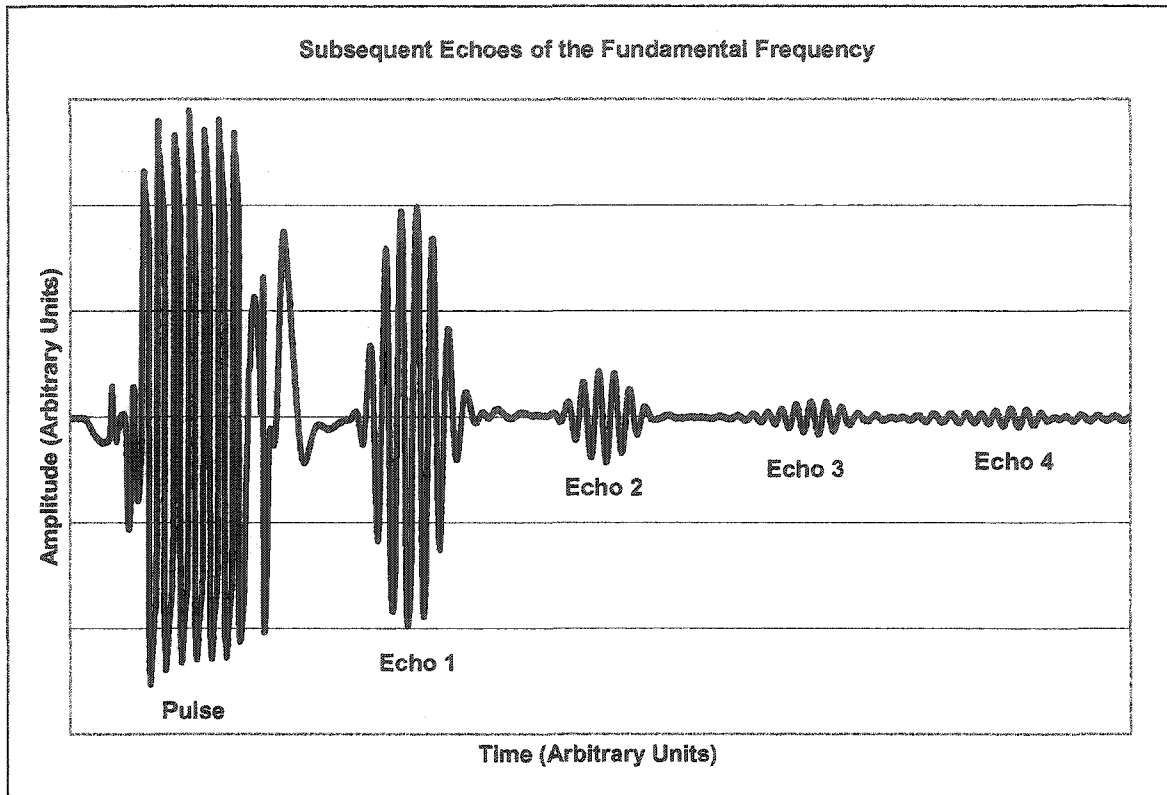
Figure 6.4. Subsequent echoes of the fundamental frequency. The above figure plots the data from the LeCroy oscilloscope. Depicted are the initial pulse and subsequent echoes of the fundamental frequency.

The pulses that appeared on the oscilloscope display represented numerous echoes from the back face of the crystal. In order to determine both the wave velocity and the attenuation, however, we required only two of these echoes. For this reason the *time-base* of the oscilloscope was then adjusted so that only the first and second echoes appeared on the oscilloscope screen. Also, the *volts-per-division* scale was adjusted in such a manner that the amplitude of the first pulse almost completely filled the vertical extent of the display. Upon completing this task, the light source was then set to a value of 1023, corresponding to its maximum level. The subsequent form of these echoes was once again examined to assured that, due to the decrease in velocity, no part of the second echo had crept off the display. In this way, without adjusting the display of the

112

oscilloscope screen, the full extent of two subsequent echoes could be observed for all levels of illumination (see Figure 6.5).
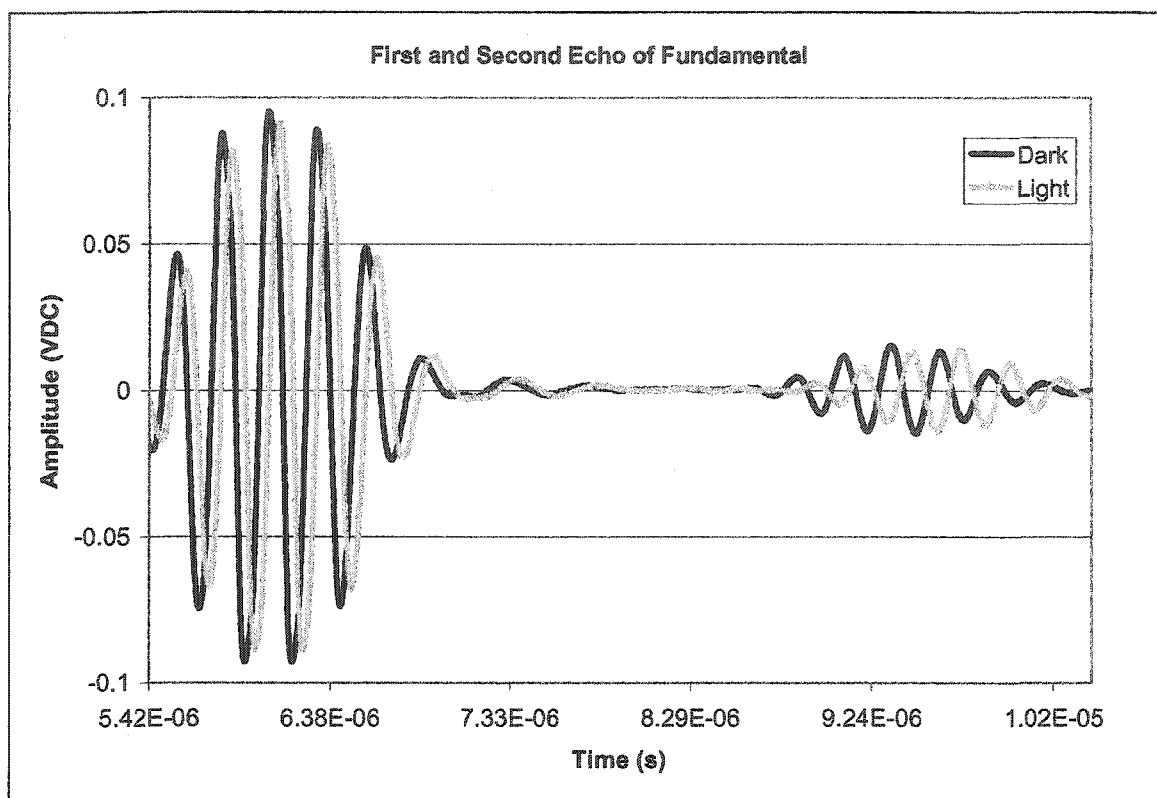
Figure 6.5. First and second echo of fundamental frequency for dark and light crystal. By adjusting the oscilloscope so that the entirety of these two waveforms were visible through the entire experiment the data could be stored in the digital oscilloscope for alter processing.

Upon completion of this preliminary procedure the lamp intensity was once again returned to a null value and the CdS sample was allowed to remain in this darkened state for one half hour. This time period, according to the results of Chapter IV would provide ample time for the conductivity levels within the crystal to reach a relatively stable level. At this time, utilizing one of the math functions from the LeCroy digital oscilloscope on a second channel, 2500 sweeps were averaged; this resultant waveform was then stored in ASCII form in the memory of the oscilloscope for later evaluation.

113

The resistance of the Cadmium Sulfide crystal was also recorded at this time so that for each stored waveform there would be a means of determining the corresponding level of conductivity. In a similar manner two additional waveforms were also recorded together with the crystal resistance. These three readings were spaced with time periods of 20 seconds between them.

The lamp level, at this time was set to a level of 223 and the crystal was allowed 30 minutes for the levels of conductivity to stabilize. Once again, three of the waveforms were stored into memory and the crystal resistance was recorded. Following these readings, the light source was shut off and the conductivity levels within the CdS crystal were allowed to return to their original, dark levels. Upon remaining in this state for several minutes, the lamp intensity was set to the next level of illumination and the procedure was repeated. Light intensities corresponding to lamp levels of 0, 223, 273, 323,..., 923, 973, 1023 were chosen in order to have appropriately and effectively spaced conductivity levels.

In this way, then, upon completing this procedure, three ASCII files had been recorded for each conductivity level stimulated by the light source. The ASCII files contained the time and amplitude data corresponding to the oscilloscope display. In fact, this procedure had effectively recorded the amplitude and form of the first and second echo at each level of excitation. This data, then, could be properly analyzed at any point.

4. Velocity Dispersion and Wave Attenuation

Having completed the procedure described above, we were left with series of oscilloscope data. For each lamp level, then, there existed three similar tab delimited

arrays from which the corresponding waveform could be obtained. From this data, then, a Microsoft spreadsheet could be created and; in this form, then, the relationship between wave velocity and conductivity could be properly scrutinized, whether graphically or analytically. A portion of one of these spreadsheets is shown below in Table 6.1.

| Time (s) | Amplitude (Volts) | | | | | | Average C |
| | Average Crystal Resistance: 4994 MOhms | | | Average Crystal Resistance: 1086 MOhms | | | |
	Trial 1	Trial 2	Trial 3	Trial 1	Trial 2	Trial 3	Trial 1
5.40E-06	-0.0121807	-0.0122661	-0.0121868	-0.0114482	-0.0097148	-0.0074321	-0.0036968
5.40E-06	-0.0137615	-0.0137859	-0.0136821	-0.0128643	-0.0111003	-0.0087017	-0.0051128
5.40E-06	-0.0146038	-0.0145793	-0.0144817	-0.0135479	-0.0115825	-0.0092083	-0.0054607
5.41E-06	-0.0144268	-0.0144817	-0.0143718	-0.0133708	-0.0114177	-0.0089885	-0.0052166
.	.	.	.	.	.	.	.
.	.	.	.	.	.	.	.
.	.	.	.	.	.	.	.
1.04E-05	-0.0002727	-0.0002239	-0.0002117	-0.0001018	-0.0001812	-0.0001934	-0.0003704
1.04E-05	0.00013623	0.00018506	0.00017285	0.00020337	0.00016065	0.00013013	-4.69E-05
1.04E-05	-0.0004741	-0.0005107	-0.0005657	-0.0005718	-0.0006511	-0.000761	-0.0009014

Table 6.1. Sample spreadsheet showing the compiled data the Lecroy digital oscilloscope during the linear portion of experimentation.

Further, alongside these three data sets were the corresponding crystal resistances. Using this above data, the waveforms resulting from any level of conductivity could be plotted. Two such these waveforms have already been presented earlier in Figure 6.5; the first of the data series was taken from a dark crystal reading while the second corresponds to a fully illuminated crystal. From the data corresponding to particular echo pairs, then, we can calculate with relative ease both the amplitudes of the echoes, as well as the velocity of the wave. As an example, then, this will be done for the waveform corresponding to the dark crystal.

115

Two subsequent echoes are plotted below from the oscilloscope data corresponding to a conductivity of approximately 10^{-3} Ω^{-1} m^{-1} (Figure 6.6). The process

Oscilloscope Data for Dark Crystal
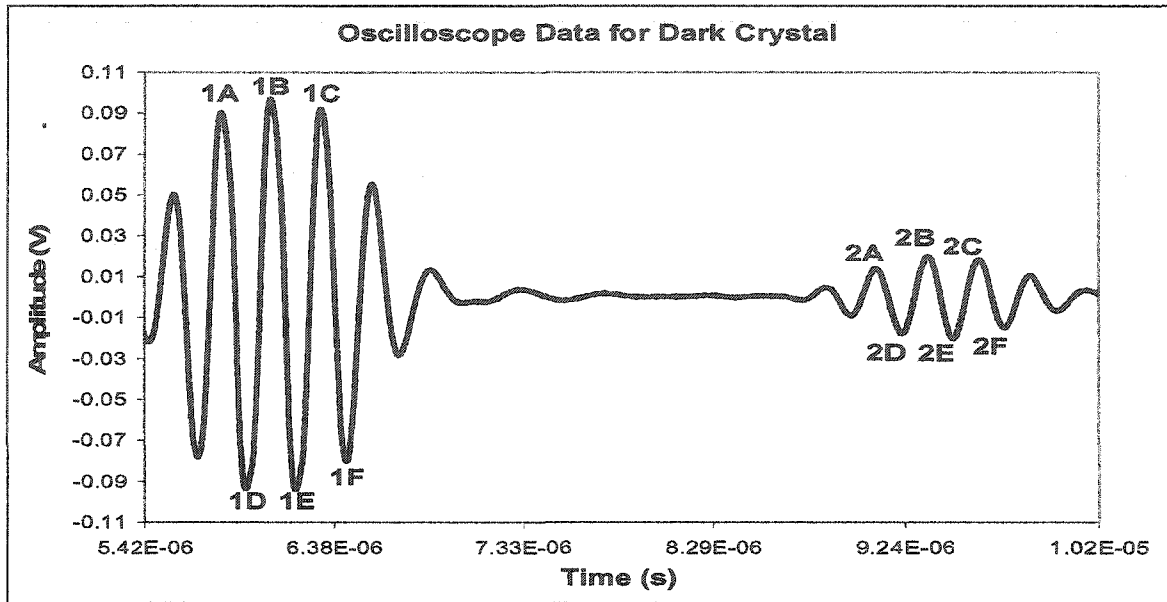
Figure 6.6. First and second echo of fundamental frequency with labels for calculation. The notation above the two waveforms denote the corresponding peaks between the two echoes.

by which both the amplitude and the wave velocity is determined from this graph begins in a similar manner. Within each pulse the individual peaks are labeled in such a way that they may be correlated: *1A, 1B,..., 1F,...,2A, 2B,...2F*. The number in each label denotes the echo number to which it belongs, whereas, the letter labels the specific peak. A correspondence can be found between the letters in that 2A is the same peak as 1A shown at a later time; i.e., after a second pass through the crystal. In order to determine the peak-to-peak amplitude of the first pulse, we need merely take the maximum amplitude between peaks *1A, 1B* and *1C* and add the magnitude of the minimum amplitude between peaks *1D, 1E* and *1F*. The peak-to-peak amplitude of the second pulse can be found in a similar manner. Upon completing this calculation for each particular trial, the three resultant amplitudes were then averaged for each echo. This average value, then, corresponded to the average of the conductivity levels recorded for

116

each trial. Thus, for a specific conductivity level, we obtained the amplitude of the first and second pulse. Upon repeating this calculation for the tree trials at all light intensities we could plot the amplitude of each pulse as a function of conductivity for both 4.1 and 8.2 MHz. This graph appears in Figure 6.7., where for both trials the initial wave amplitude was normalized to one. For both frequencies the subsequent amplitude the second echo has been scaled with respect to the normalized amplitude of the first.
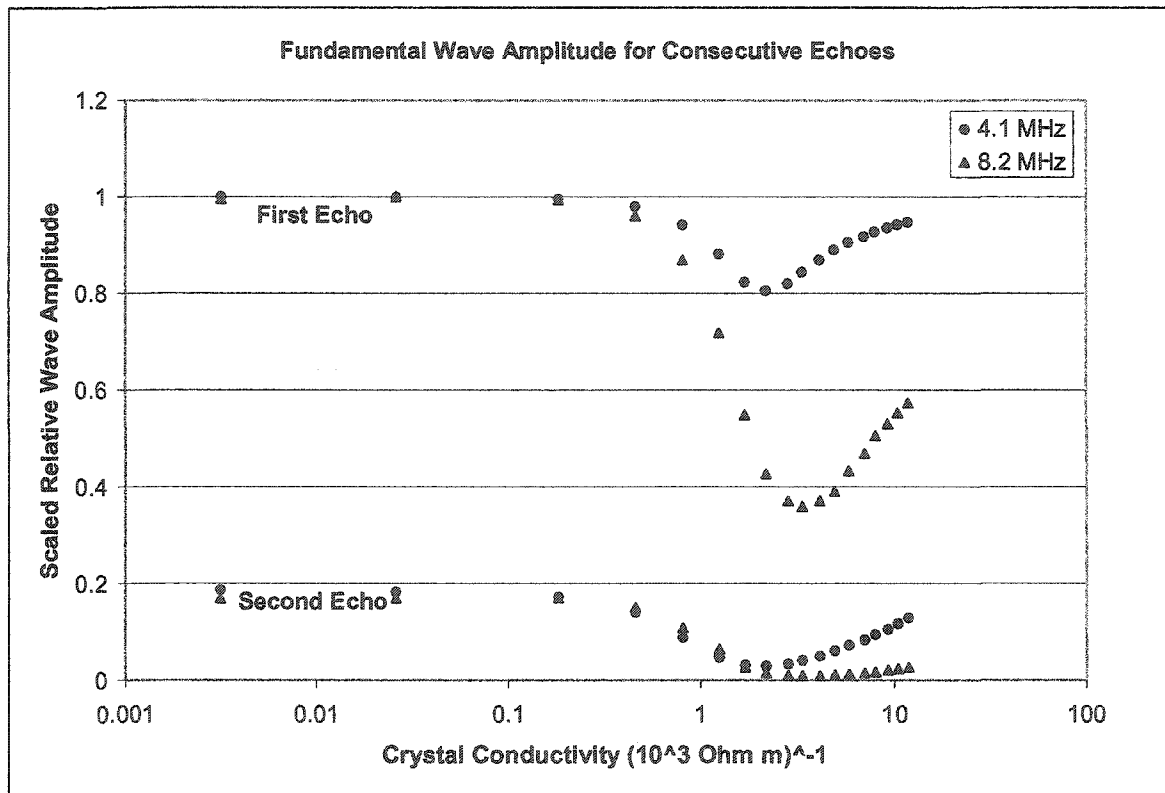
Figure 6.7. Fundamental wave amplitude versus conductivity for consecutive echoes. The first echoes for both frequencies were normalized and the second echoes were scaled accordingly.

From these amplitude values we can then calculate the attenuation coefficient using

$$\alpha = -\frac{1}{2d}\ln\left(\frac{A_2}{A_1}\right) , \tag{6.1}$$

117

where A_2 and A_1 are the amplitudes of the second and first echo respectively, and d is the distance from the front to back face of the crystal. This plot is shown below in Figure 6.8.
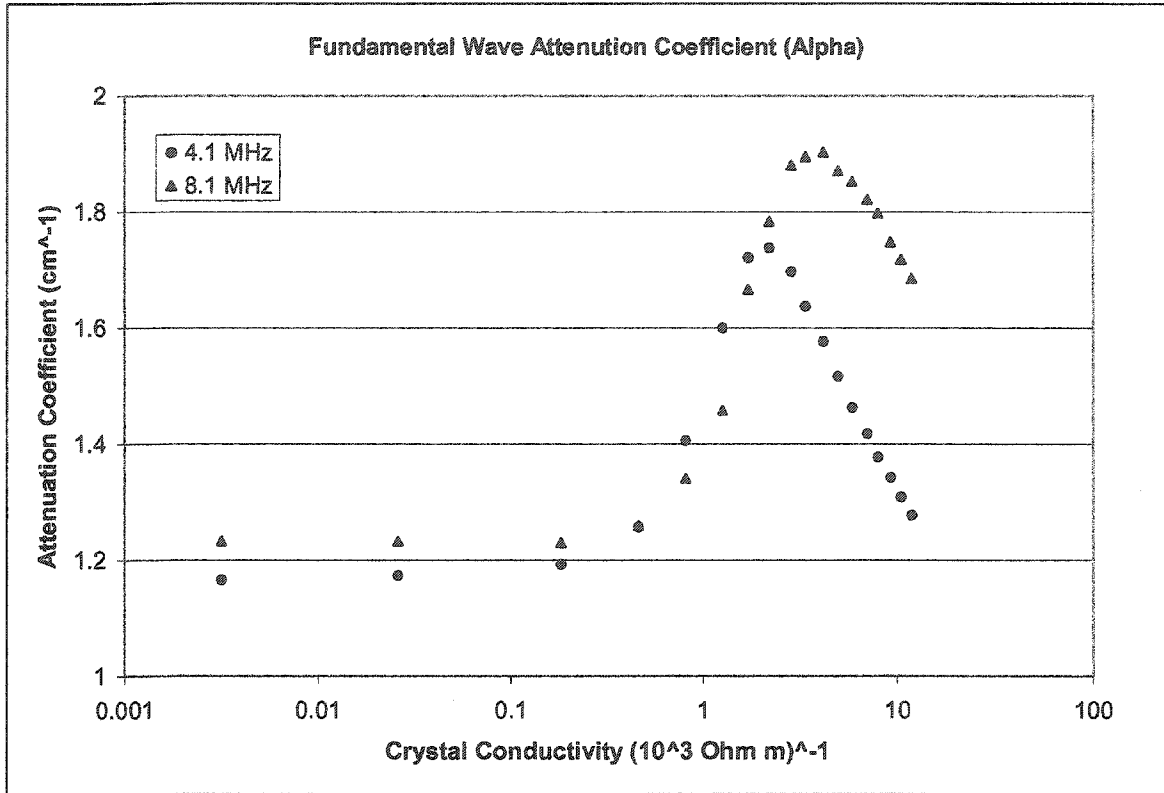
Figure 6.8. Fundamental wave attenuation coefficient versus conductivity. The relative amplitude between the first and second echo was utilized to calculate α.

In order to calculate the wave velocity with respect to crystal conductivity, a similar, yet appropriately modified procedure was used. Let us consider for a second time an example from the trial with a dark crystal (Figure 6.6.). For each of the individual peaks within the first and second echoes (*1A, 1B,..,1F, 2A, 2B,..., 2F*) it is possible to determine the amplitude. Using the Excel spreadsheet, then, the time corresponding each of these amplitudes can also be determined. We will label these T_{1A}, $T_{1B},...,$ T_{1F}, T_{2A}, $T_{2B},...,$and T_{2F} respectively. Hence, the *time-of-flight*, T_X, for each of these individual peaks can be calculated as

118

$$T_X = T_{2X} - T_{1X},$$ (6.2)

where the subscript X denotes the individual peak. Hence, if d is again the width of the crystal, the wave velocity for each trial can be calculated as

$$v = \sum_X \frac{2d(T_X)^{-1}}{6} \quad X = A, B, C, D, E, F.$$ (6.3)

In this way, then, we have averaged the time-of-flight information of six individual peaks within the echoes, thus improving the accuracy of our velocity calculation. Further, upon averaging the three trials together, we have calculated the wave velocity with respect to conductivity for this particular lamp intensity level. These computations can then be repeated for all lamp levels and we can obtain a relationship between wave velocity and crystal conductivity. This relationship is shown below.
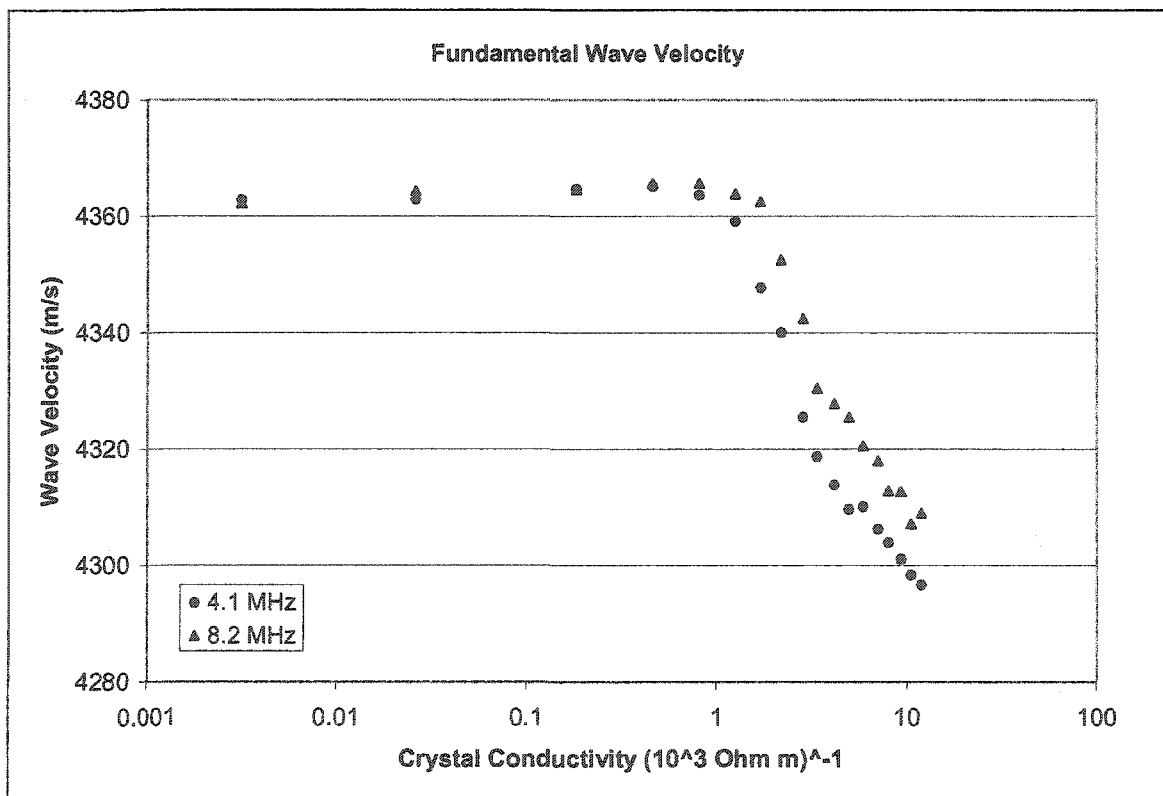
Figure 6.9. Fundamental wave velocity versus conductivity.

119

5. Nonlinear Domain: Experiment

The nonlinear portion of experimentation can be subdivided into two separate investigations: the study of the subsequent echoes of the second harmonic and the examination of the relationship between higher harmonics, namely the 2nd, 3rd, 4th and 5th. The general experimental arrangement for both parts of this portion of the research project was identical, save for the transducer with which the higher harmonics were received. This setup can be seen below in Figure 6.10.
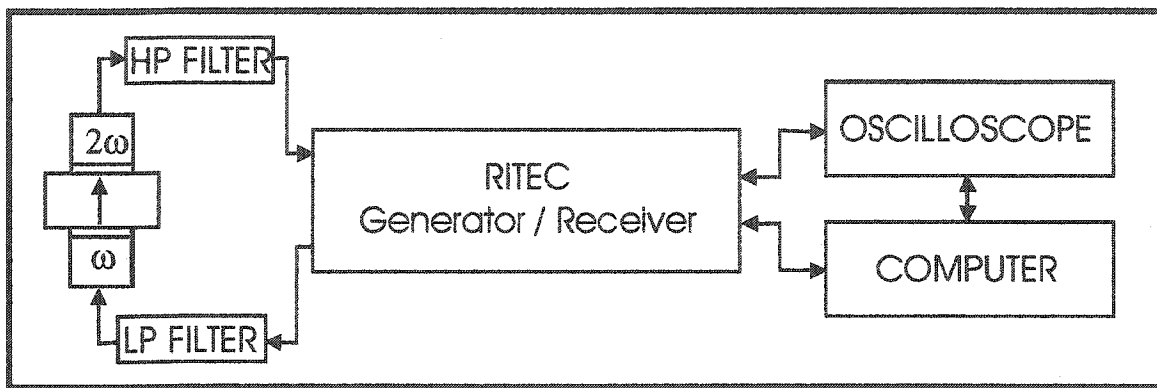
Figure 6.10. Arrangement of acoustic apparatus for nonlinear acoustic experimentation.

As can be seen in comparing Figure 6.10 with Figure 6.2, the basic apparatus utilized for the nonlinear experiments is the same as in this section. The Ritec system was responsible for generating and receiving, as well as processing, the acoustic signal. The LeCroy oscilloscope was used to monitor the signal while the computer both processed the data and controlled the Ritec machine. Throughout this investigation a 4.1 MHz 8-cycle wave pulse was generated. A through transmission technique was made use of in order to allow for the appropriate transducer to receive the signal. A low-pass filter of 5 MHz was employed to assure that no higher harmonics entered the Cadmium Sulfide crystal. Also, a high-pass filter was placed between the second transducer and the Ritec receiver to eliminate the fundamental frequency. For the investigation of just the second

120

harmonic a 7.5 MHz Aerotech transducer was utilized to receive the 8.2 MHz signal. On the other hand, in order to enable the simultaneous study of harmonics as high as the fifth, a Aerotech transducer of 15 MHz was employed. More will be said on the nature of the use of these transducers at a later time.
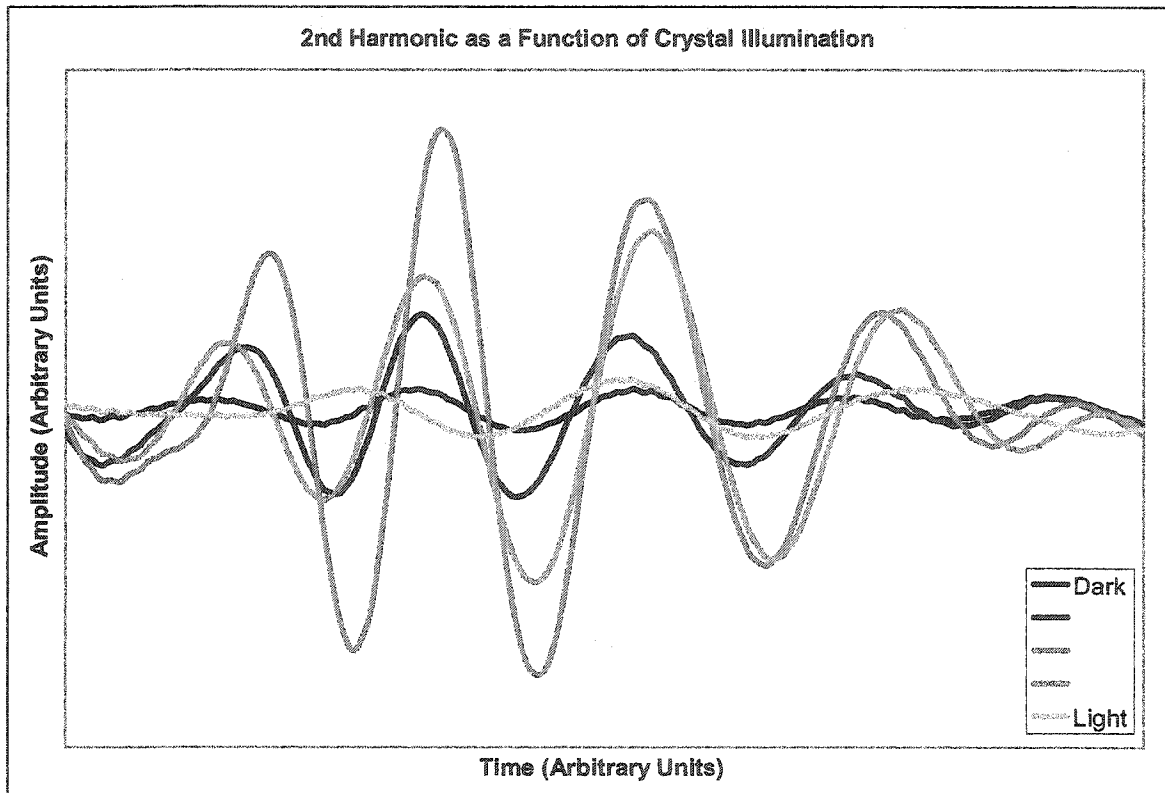
Figure 6.11. Oscilloscope data for 2nd harmonic with illumination level as a parameter. Shown above are five typical waveforms of a single received pulse of the 2nd harmonic of a 4.1 MHz wave for various levels of light intensity. In a manner opposite the fundamental frequency, the amplitude of the 2nd harmonic appears to move through a maximum as a function of increased conductivity.

Again, as with the study of linear phenomena, it is useful to engage in a qualitative description of the acoustic nonlinearity that is of interest. Above, in Figure 6.11, is shown a single pulse of the second harmonic that has come about as a result of the acoustoelectric effect in CdS. This pulse is shown for several different conductivities. As can be seen, this pulse goes through a maximum as light increases to a maximum, at which time its amplitude approaches its dark-crystal value. Thus, we can physically

121

observe a qualitative relationship between harmonic generation and crystal conductivity. It is this relationship that is investigated throughout the remainder of this chapter.

6. Procedure: 2nd Harmonic

The preliminary goal of this portion of research was the examination of the 2nd harmonic. For this reason, as mentioned above, a filter was utilized to remove the fundamental frequency from the received signal. Also, a 7.5 MHz transducer that was employed and a through transmission technique was used. Of primary interest was the relationship between nonlinearity and conductivity, however, this project also concerned itself with the amplitude of this was with respect to distance. That is, not only was it important to physically observe the amplitude of the 2nd harmonic, the amplitude of successive echoes as a function of conductivity was also of interest. Thus, while in the study of linear attenuation and velocity it was necessary only to view the first and second echo, this required the simultaneous surveillance of many echoes. Due to the effect of attenuation, however, this proved somewhat tedious.

At both low and high levels of illumination, as can be seen in Figure 6.10., the amplitudes of higher harmonics are much reduced. For this reason, in order to distinguish many consecutive echoes of the 2nd harmonic, it is necessary to increase the receiver gain. Unfortunately, as light intensity approaches its half-maximum the harmonic amplitudes increase substantially, thus saturating the receiver. Hence it was necessary to subdivide the observation of these echoes. This, however, required some degree of savvy and, further, appropriately sophisticated equipment. Thanks in no small

122

part to the versatility of the software that accompanied the Ritec system, a procedure could be developed with which this difficulty could be avoided.

Indeed, with the superior processing system that controls the Ritec machine, many otherwise difficult tasks can be completed with relative ease. The measurement of harmonic amplitudes is one example of its capacity. Indeed, by merely *gating*, that is, distinguishing a region of particular wave pulse, Ritec's powerful integrators are able to accurately determine the amplitude of each constituent frequency. In fact, two separate can be monitored simultaneously. Further, specific settings of the Ritec software can be saved so that within a few seconds these presets can be activated.

With this being said, then, it is again stated that the goal of this procedure is the simultaneous observation of subsequent echoes of the second harmonic. This, however, is not completely possible through the entire range of light intensities due to both the significant changes in amplitude and receiver saturation concerns. If the receiver gain is increased to the point that the harmonics are detectable at either low or high intensities then the receiver is saturated within the middle ranges. Conversely, if within the mid-ranged light intensities the gain is set so that the receiver is not saturated then the harmonics are not visible at either low or high intensities. One solution to this dilemma is to measure the relative amplitudes of each of these echoes at a range where they are all visible yet the receiver is not saturated. Separate recordings of the amplitudes can then be taken with levels of gain appropriate to each individual echo, thus documenting their individual relationships with respect to conductivity. The magnitude of these echoes can then be scaled in such a way that they are consistent with the results of the trial

which measured their relative amplitudes. With this being said it is appropriate to expound upon the exact details of the experiment.

Within the Ritec software four separate settings were programmed in advance to the beginning of this particular procedure. Two of the presets were designed in such a way to measure the relative amplitudes of all four echoes at identical levels of gain, while the remaining two had as their purpose the measurement of just two echoes throughout the range of conductivities. In order to reduce the complexity of this description these will be referred to as *preset one, preset two, preset three,* and *preset four.* Aside from the differences outlined below, all four presets were identical:

> *Preset One*: Gated echoes one and two with the receiver gain set so that these echoes were visible throughout the range of conductivity, yet at no point was the receiver saturated.

> *Preset Two*: Gated echoes three and four with the receiver gain set so that these echoes were visible throughout the range of conductivity, yet at no point was the receiver saturated.

> *Preset Three*: Gated echoes one and two with the receiver gain set so that all echoes were visible at one of the predetermined mid-level light intensities.

> *Preset Four*: Gate echoes three and four with the receiver gain set so that all echoes were visible at one of the predetermined mid-level light intensities.

Thus, through the use of these particular presets, a procedure could be developed to investigate the relationship between these echoes in a nearly seamless manner.

The specific procedure followed in this particular investigation was as follows: the water bath was, as usual, set to 20°C and all light sources were shut off so that the crystal was in complete darkness. The Ritec machine was turned on and a 4.1 MHz acoustic wave was generated within the Cadmium Sulfide crystal. The crystal was

124

allowed to remain in this state for one half hour. At this time, then, with preset one activated, the Ritec software was utilized to measure the amplitude of the second harmonic for the first and second echo. Upon recording this reading preset two was initiated and the amplitudes of the third and fourth echoes were measured. By oscillating between preset one and two three amplitude measurements were taken for each echo of the second harmonic at this conductivity level. Also, with each pair of reading (i.e. the first and second or the second and third), the corresponding crystal resistance was recorded. After completing these readings, the lamp intensity level was increased to a level of 223. In keeping with the results of Chapter IV, no measurements were made for one half hour at which point the crystal had reached a more stable level of resistance. With a similar method as described above, three amplitude measurements were recorded for each echo. After this reading the crystal was returned to its dark-level for ten minutes. Once this period of time had passed the lamp intensity was again increased, this time to a level of 273 and the above procedure was again repeated. This process continued for lamp intensities of 0, 223, 273, 323,...,923 , 973, and 1023.

The only deviation from this procedure took place at a lamp intensity level of 373, corresponding to a conductivity of $7 \times 10^{-3} \, \Omega^{-1} \, m^{-1}$. At this level, after having recorded the amplitude readings for the first and second as well as the third and fourth echoes, the settings corresponding to preset three were loaded. Under these presets all amplitudes were simultaneously visible. Preset three, then enabled the measurement of the amplitude of the first and second echo. Upon recording these numbers, then, preset four was initiated so that the amplitudes of echoes three and four could be recorded with the same gain. In this way, at this point, we had provided a means by which the separately

125
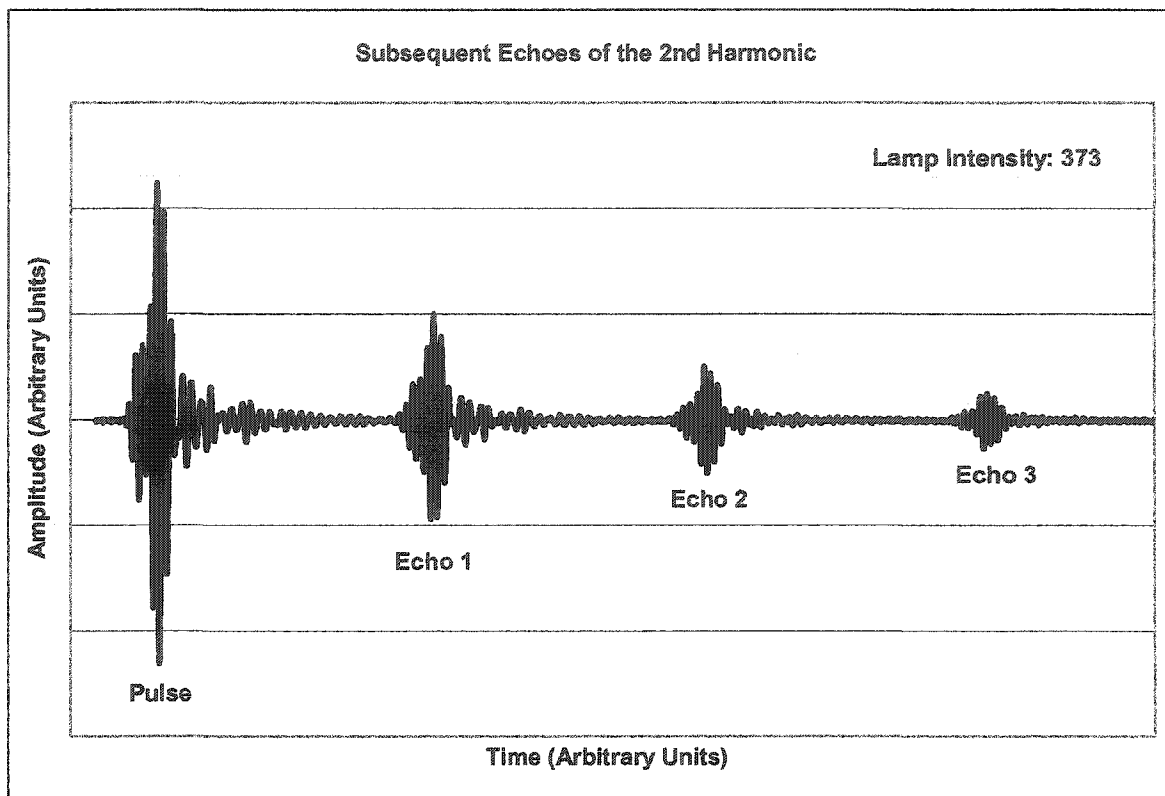
Figure 6.12. Oscilloscope data depicting four subsequent echoes of the 2nd harmonic. The above figure depicts the situation at mid-range illumination levels where all echoes are simultaneously visible for an input voltage that fails to saturate the receiver. Using the relative amplitudes of the four echoes taken from measured values of *preset three* and *preset four* the entire data set can be scaled appropriately. This procedure is described in the results section for the 2nd harmonic.

recorded amplitude measurements of the first, second, third and fourth echoes could be compared. Thus, upon having completed this procedure we had effectively documented the relative amplitudes of the first four echoes of the 2nd harmonic. Sample oscilloscope data depicting the amplitude of the four echoes at this level of illumination is shown above in Figure 6.12.

7. Results: 2nd Harmonic

Due to the relatively stable Cadmium Sulfide resistance, all readings taken at the various lamp intensity levels corresponded to reasonably consistent conductivity levels. It is then reasonable to average the amplitudes from the three trials for each individual

126

echo. Further, as the six corresponding conductivities were also similar, it is possible to average these values. Thus, we are able to effectively compare the relative amplitudes of the four subsequent echoes at a single level of conductivity.

The analysis of the data obtained from the above procedure, however, hinges on the ability to compare the relative amplitudes of the echoes of the 2nd harmonic. In order to scale these amplitudes appropriately, we must analyse the data presented below in Figure 6.13. This graph corresponds to amplitudes that were measured under identical receiver gains.
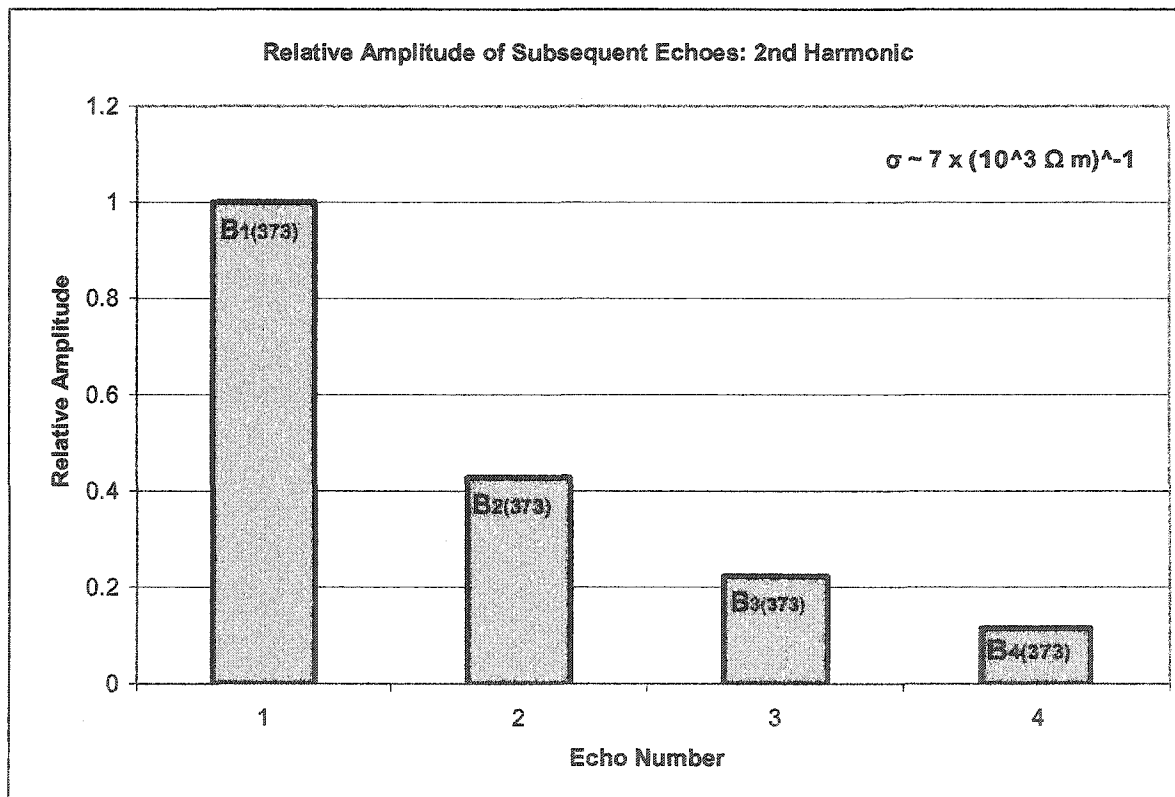
Figure 6.13. Relative amplitude of subsequent echoes of the 2nd harmonic. Using this data all other results from the procedure described above can be scaled.

In order to discuss the procedure by which the amplitudes for each echo were scaled it beneficial to summarize the nature of the data that has been obtained thus far. The amplitudes of the four echoes have essentially been recorded in two groups of two;

127

the first and second and the first and third. For the first two echoes we have a complete record of the amplitude (with receiver gain constant between readings) versus specific conductivity levels. For bookkeeping purposes let us denote the elements of this data set $A_{1\gamma}$ and $A_{2\gamma}$ where the first subscript denotes the echo number and γ denotes the corresponding lamp intensity level at which it was recorded. Likewise, a similar set of measurements has been taken for the third and fourth echo; however, these echoes were measured at a separate level of gain. Again, following the notation above these elements will be labeled $A_{3\gamma}$ and $A_{4\gamma}$. In order to compare the relative amplitudes for all conductivity levels we also have a second data set containing four amplitude elements which we will label $B_{1(373)}$, $B_{2(373)}$, $B_{3(373)}$, and $B_{4(373)}$. These amplitudes correspond to the amplitudes of the four echoes shown in Figure 6.12. As each of these measurements was taken with identical receiver gain settings, we can use them to scale the rest of the amplitudes this can be done with the following equation:

$$B_{x\gamma} = A_{x\gamma} \cdot \frac{B_{x(373)}}{A_{x(373)}}, \qquad (6.4)$$

where,

$$x \in 1, 2, 3, \, or \, 4, \qquad (6.5)$$

and,

$$\gamma = 0, 223, 273,..., 973, 1023. \qquad (6.6)$$

In this way, then, we have a four new arrays of data, $B_{1\gamma}$, $B_{2\gamma}$, $B_{3\gamma}$, and $B_{4\gamma}$, corresponding to the amplitudes of each individual echo at specific levels of light intensity. Each of these amplitudes has been scale appropriately, and thus their amplitudes can be compared directly. Further, these light intensity levels in turn

128

correspond to the averaged conductivity levels as described earlier; hence, we have a means of describing the relationship between the relative amplitude of consecutive echoes with respect to crystal conductivity. This relationship is plotted below.
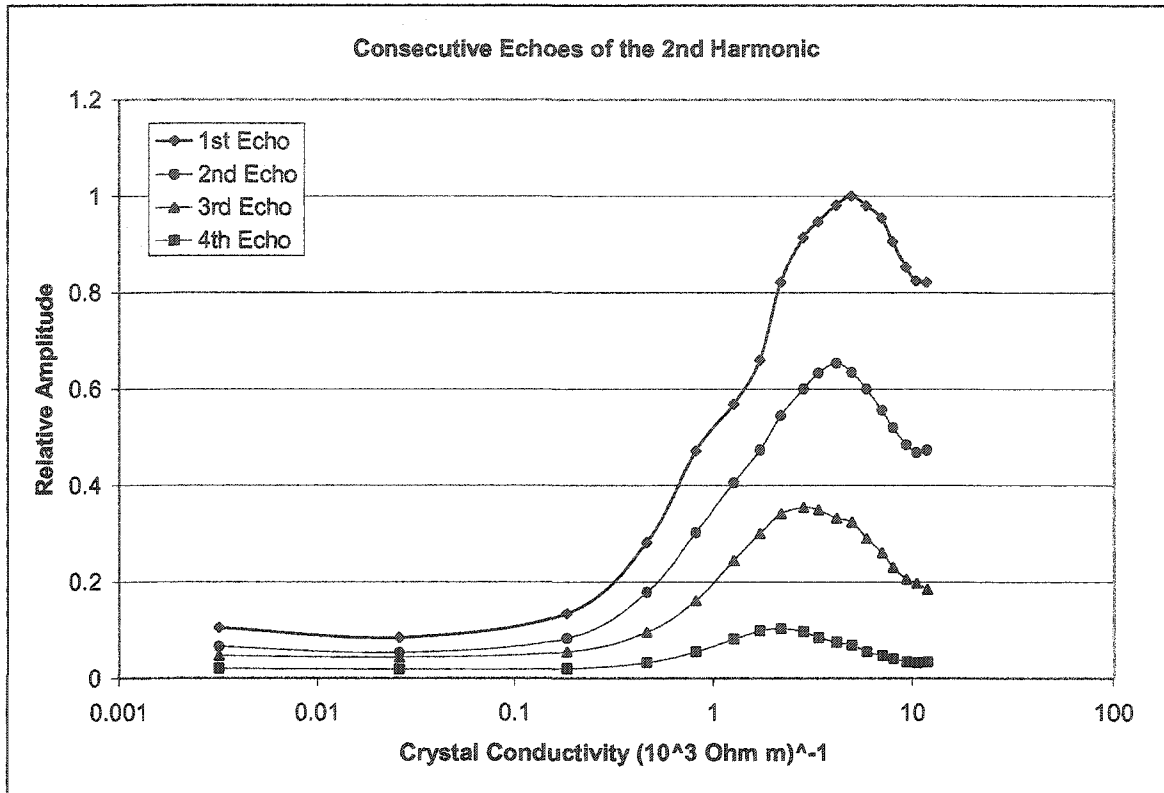
Figure 6.14. Relative amplitudes of consecutive echoes of the 2nd harmonic with respect to conductivity. All amplitudes are relative to the first echo which has been normalized.

In the above graph we can easily see the relationship between the amplitude of the 2nd harmonic and conductivity. Clearly, the amplitude of the first echo can be seen to pass through a maximum around 10^{-3} Ω^{-1} m^{-1}. A trend can also be seen in that the amplitudes of each echo of this pulse peak at different conductivities. This relationship is shown quantitatively in Table 6.2. Indeed, there appears to be an inverse relationship between the distance each echo travels increases, and the level of conductivity at which its amplitude peaks.

Echo Number	1	2	3	4
Pathlength (cm)	0.72	1.44	2.16	2.88
Relavite Peak Amplitudes	1.00	0.22	0.06	0.03
Conductivity Corresponding to Peak Amplitude $(10^3 \text{ Ohm m})^{-1}$	4.96	4.15	2.84	2.18

Table 6.2. The above table demonstrates the inverse relationship between the peak amplitudes of consecutive echoes and the distance that echo has traveled.

8. Procedure: Higher Harmonics

In order to more fully understand the consequences of the acoustoelectric effect, it is valuable to further explore the fundamental nature of harmonic generation. Although in the previous section the 2nd harmonic was investigated, nothing has yet been learned of its relationship to higher harmonics. A procedure was developed, then, specifically for this purpose.

One of the fundamental difficulties with working with Cadmium Sulfide, as discussed at length in the previous sections and chapters of this thesis project, is the metastability of conductivity. During long periods of time, the level of excitation within a particular crystal can drift in one direction or another. For this reason it can be difficult to duplicate exact levels of conductivity. It is necessary, then, in investigations whose purpose is the comparison of aspects such as wave amplitude, to develop procedures in which the elements are measured simultaneously; or at least to the extent that it is possible within a given experiment. The degree to which results can be compared is in this way directly related to the synchronization of measurement. This issue is of considerable concern in this portion of the experiment. In fact, it is the goal of this procedure to determine the relationship between the fundamental frequency and the, 2nd,

130

3rd, 4th and 5th harmonic with respect to conductivity—a daunting task with regard to the metastable photoconductivity properties of CdS.

This investigation, then, required the measurement of the relative amplitudes of 2nd through 5th harmonic for specific levels of light intensity. In order to measure the amplitude of each harmonic a single transducer of 15 MHz was employed. The frequency response of this particular transducer was then utilized to scale the relative amplitudes accordingly. In order to determine this frequency response, however, a separate procedure was required.

The 15 MHz Aerotech transducer was used with a pulse-echo method to determine the amplitude of reflected waves from a parallel-surfaced, 2.2 cm thick, aluminum block. The ultrasonic waves were generated and received with the Ritec machine. Specifically, a 12-cycle wave pulse was generated at 4.1 MHz—corresponding to the fundamental frequency—and the Ritec software was set in such a way as to measure the amplitude of the received pulse at this same frequency. This amplitude was measured three times and the average value was recorded. This process was repeated, without moving the transducer, for frequencies of 8.2 MHz, 12.3 MHz, 16.4 MHz, and 20.5 MHz. Naturally, these frequencies were chosen to match the harmonics of the 4.1 MHz wave. Once the average amplitudes of the received pulses at each frequency had been obtained, the magnitude of the largest amplitude was normalized and the relative amplitudes of the other amplitudes were scaled to this value. These figures appear in Table 6.3. This method, then, determined the spectral response of the 15 MHz transducer and, in turn, the measured amplitudes of the higher harmonics could be scaled appropriately.

131

Transducer Frequency Response (Relative Scale)				
Fundamental	Harmonics			
4.1 MHz	8.2 MHz	12.3 MHz	16.4 MHz	20.5 MHz
0.354	0.771	1.000	0.512	0.131

Table 6.3. The above table reports the frequency response of the 15 MHz Aerotech transducer. Using these values, the harmonic amplitudes measured by the transducer could be appropriately scaled.

Having laid the groundwork for this portion of experimentation, then, it is appropriate at this point to describe the primary procedure. The principal elements of this investigation remained unchanged from that described for the 2nd harmonic. The water bath was utilized to regulate the temperature of the crystal and the DC 1100 light source stimulated crystal conductivity. The Ritec system generated, received and processed the ultrasonic signal and the LeCroy digital oscilloscope allowed for the wave to be visually monitored. To transmit the ultrasonic wave, an Xactex 4.1 MHz transducer was employed. The only alteration, besides the procedure itself, was the replacement of the 7.5 MHz receiver transducer with the Aerotech 15 MHz transducer as described above. These transducers were exchanged in order to allow for greater sensitivity when measuring the higher harmonics.

Just as in the last procedure, the versatility of the Ritec system facilitated what could otherwise have been an extremely difficult task. Several new presets were saved into the memory of the computer to expedite the measurements. All of these settings were aimed at the measurement of the first received pulse from CdS crystal; however, with the aid of Ritec's advanced integrators, the magnitude of various frequencies could be extrapolated from these signals. The prominent differences between the presets can be outlined in the following fashion:

132

Preset One: Measured the 2nd and 3rd harmonic amplitudes.

Preset Two: Measured the 3nd and 4th harmonic amplitudes.

Preset Three: Measured the 4th and 5th harmonic amplitudes.

Preset Four: Measured the 2nd and 5th harmonic amplitudes.

With these settings stored into memory, then, they took but a few seconds to load and, consequently, greatly decreased the time between measurements. In this way, as previously discussed, the slight changes in conductivity between readings were relatively insignificant.

Prior to the beginning of the experimental procedure, all light sources were shut off and the water bath was set to 20°C. One half hour was allowed before any measurements were made. At this time, prior to measuring the harmonics, the high pass filter was removed from between the 15 MHz transducer and the receiver, thus allowing for the measurement of the fundamental frequency. As the amplitude of the first harmonic had been documented through the first investigation of this chapter, this initial measurement would provide a means to relate the two sets of results. After recording the relative amplitudes of the 1st and 2nd harmonic the filter was again placed in line. At this time *preset one* was activated and the amplitudes of the 2nd and 3rd harmonic were measured. By changing to *preset two* the amplitudes 3rd and 4th harmonic could be recorded in a similar fashion. In fact, by cycling through the four presets, there then existed two amplitude readings for each harmonic. To accompany these measurements, the resistance of the CdS crystal was recorded with each preset.

Once this series of data was recorded the light intensity was set to a value corresponding to lamp level 223. Again, one half hour was allowed for the conductivity

133

to reach relative stability. By quickly cycling through these four Ritec settings, these same measurements could then be taken for this level of excitation. Upon making the final reading, the lamp level was once again returned to 0. With the passing of ten minutes the lamp was set to 273 and the process could be repeated. Amplitude measurements of the 2nd, 3rd, 4th and 5th harmonic were made, then, for lamp levels of 0, 223, 273, 323,..., 973, and 1023. Also, for each of these light intensities, the crystal resistance was recorded; thus, these lamp levels could in turn be replaced with specific crystal conductivity values. The completion of this procedure, then, the amplitudes of the harmonics could be compared, both with respect to each other, and to conductivity.

9. Results: Higher Harmonics

Before the results of this last procedure could be properly scrutinized, several initial adjustments were required. As mentioned above, there existed, for each lamp intensity level, four crystal resistance readings and eight amplitude readings. In order to facilitate the comparison of the relative amplitudes of the harmonics, the four crystal resistance readings were averaged to produce a single, shared value. This resistance was then converted to conductivity as discussed in Chapter III. To further simplify the results, the two amplitude measurements for each harmonic were also averaged. Thus, there existed an array for each harmonic in the resultant data set which in turn contained a single amplitude reading with respect to a specific conductivity. These conductivity values were common across each array.

Now, recall that each of these amplitude measurements was made with the same 15 MHz transducer. In this way, then, the above amplitudes strongly reflect the

134

frequency response of this transducer and for this reason require some adjustment. In order to correct for this, each array must be multiplied by

$$\frac{1}{A_h},\qquad\qquad(6.7)$$

where the A_h are the relative amplitudes of particular harmonics, h, (where $h = 1^{st}$, 2nd, 3rd, 4th, or 5th) with respect to the frequency response procedure. These values are given in Table 6.3.

By employing this multiplicative factor to each array containing the amplitudes of the four harmonics, then, a new data set is created showing the relative harmonic amplitudes for a 4.1 MHz wave in Cadmium Sulfide with respect to conductivity. This data is plotted in Figure 6.15. The amplitude of the 5th harmonic with respect to conductivity was plotted on a separate axis in order to reveal the details of its shape.
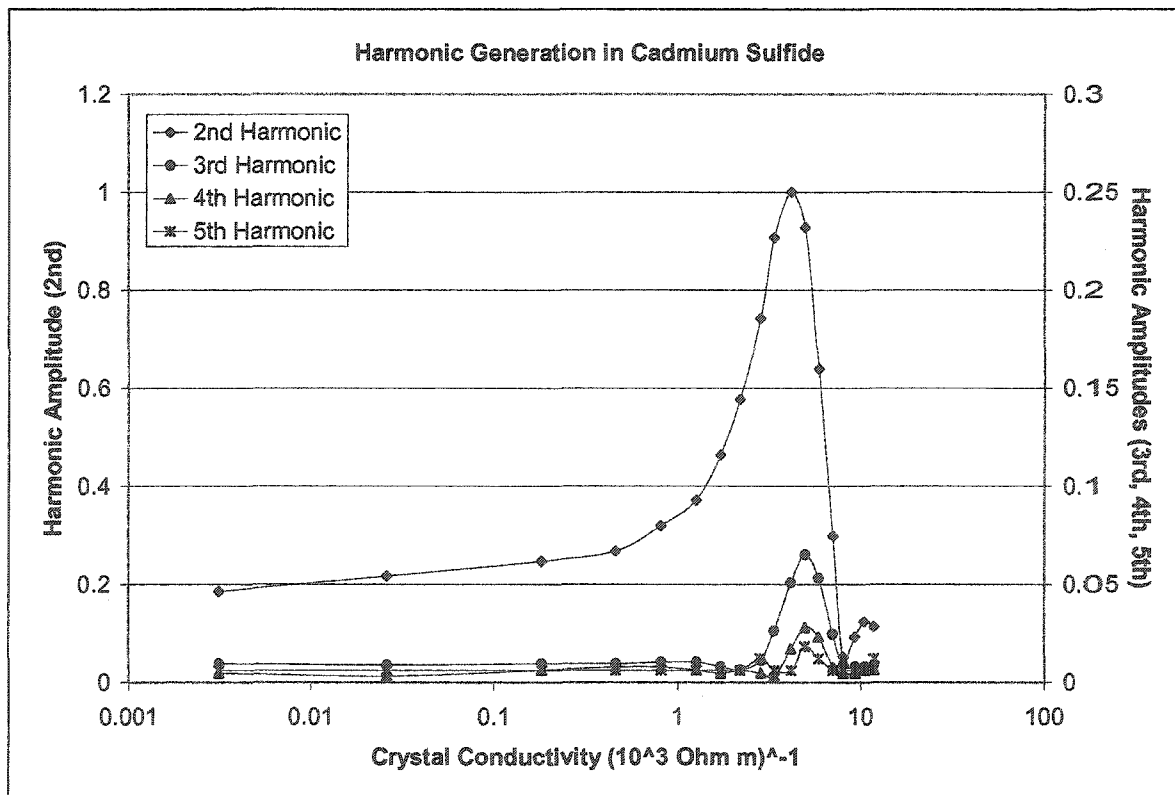

Figure 6.15 Harmonic generation as a function of conductivity. The 3rd 4th and 5th harmonics are shown on a separate axis to reveal their shape.

135

10. Discussion of Results

Having obtained figures which qualitatively match what one might expect from the basic principles of the acoustoelectric effect, it is necessary at this point to further analyse the data. In this section, then, the results are tested to determine their validity.

As a first step in this procedure, having a significantly developed linear theory, we can check the accuracy of the results pertaining to wave attenuation and linear dispersion in a rather direct manner. Although many of the specific details of this curve fitting process are left to Appendix C, a few remarks will be made at this time. The basic equations which describe the dispersion and attenuation effects are Equation (5.39) and Equation (5.40). Within the linear experiments described above, the frequency that was used was either 4.1 MHz or 8.2 MHz. For this reason both attenuation and velocity are, for our purposes, functions of conductivity alone. Conductivity, however, was calculated using the current cross section, A_{cross}, (see Equation 3.2) which, in turn was based on the estimation of the depth of penetration, d_p, of radiation energy. For this reason, it is reasonable to suggest that this number can be adjusted to some degree. Also, it is common through experimental literature to vary both the piezoelectric stress modulus, e, and the strain modulus, c [46]. For this reason they were also used as parameters with which to fit the experimental data to a theoretical curve. Along with these adjustments, an additional constant was added to the attenuation coefficient in order to account wave attenuation that was not a result of the acoustoelectric effect.

Having generated the attenuation and dispersion plots from the same waveform, the process of comparing experimental results to theory needed only to be completed once. The attenuation and dispersion equations, in fact contain the same set of constants

136

and variables. For this reason, then, the process of determining the appropriate values of the current cross section, as well as both the stress and strain modulus for one plot necessarily determined the fit of the other. Hence, this provided a powerful means by which the validity of the linear results could be compared. Further, having performed this experiment for both 4.1 and 8.2 MHz waves, meant that there existed an even more powerful means of evaluating the results. In fact, not only was the velocity and attenuation data being compared with respect to conductivity, but also to frequency. In this case, the velocity curves for the 4.1 MHz and 8.2 MHz waves were matched with theory. From these adjusted parameters, the corresponding attenuation curves could also be generated. The results are shown below in Figure 6.16 and Figure 6.17.
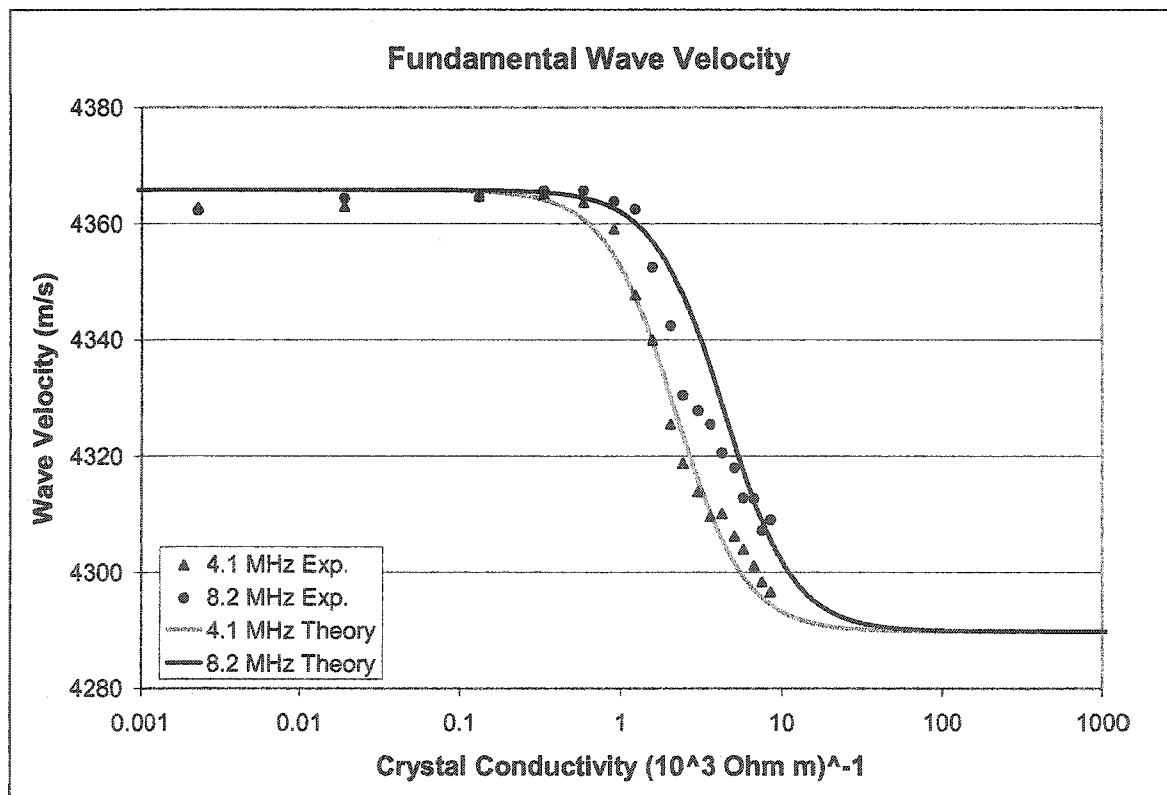
Figure 6.16. Theoretical and experimental curves of fundamental velocity as a function of conductivity. Curve fitting techniques are described in Appendix C.

137
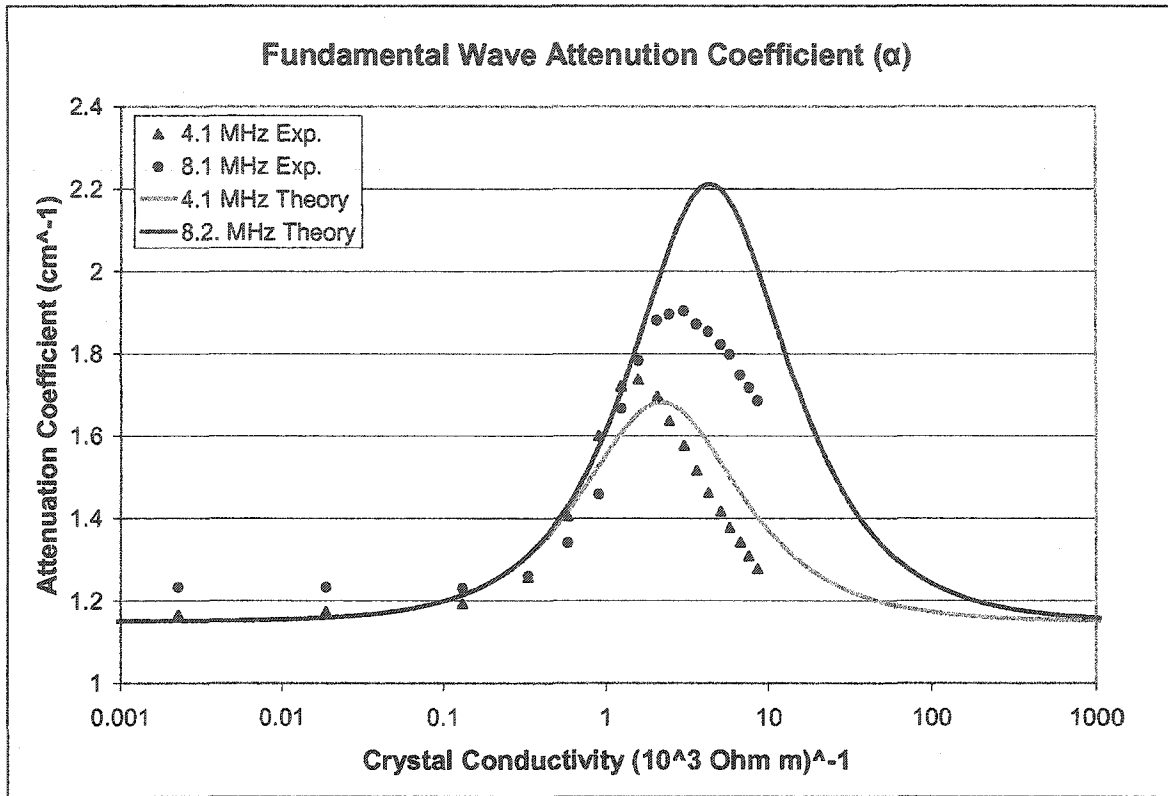
Figure 6.17. The Theoretical and experimental curves of fundamental amplitude as a function of conductivity. These curves come as a result of the parameters used to plot Figure 6.15.

Having satisfied ourselves that, at the very least, the experimental results are on the right track, it is interesting to try to correlate the linear and nonlinear results. Consider as an example, the relationship between the amplitude of the fundamental wave and that of the harmonics. According to theory, acoustic attenuation is a direct consequence of the nonlinear effect [24]. For this reason, we present a plot correlating the attenuation coefficient of the 4.1 MHz wave in the linear portion of experimentation, with the sum amplitude of the harmonics from Figure 6.14. This graph is shown below in Figure 6.17. As we are looking for a qualitative observation of the coincidence of their peaks, the two curves are normalized and plotted against separate vertical axes.

138

Attenuation Due to Harmonic Generation
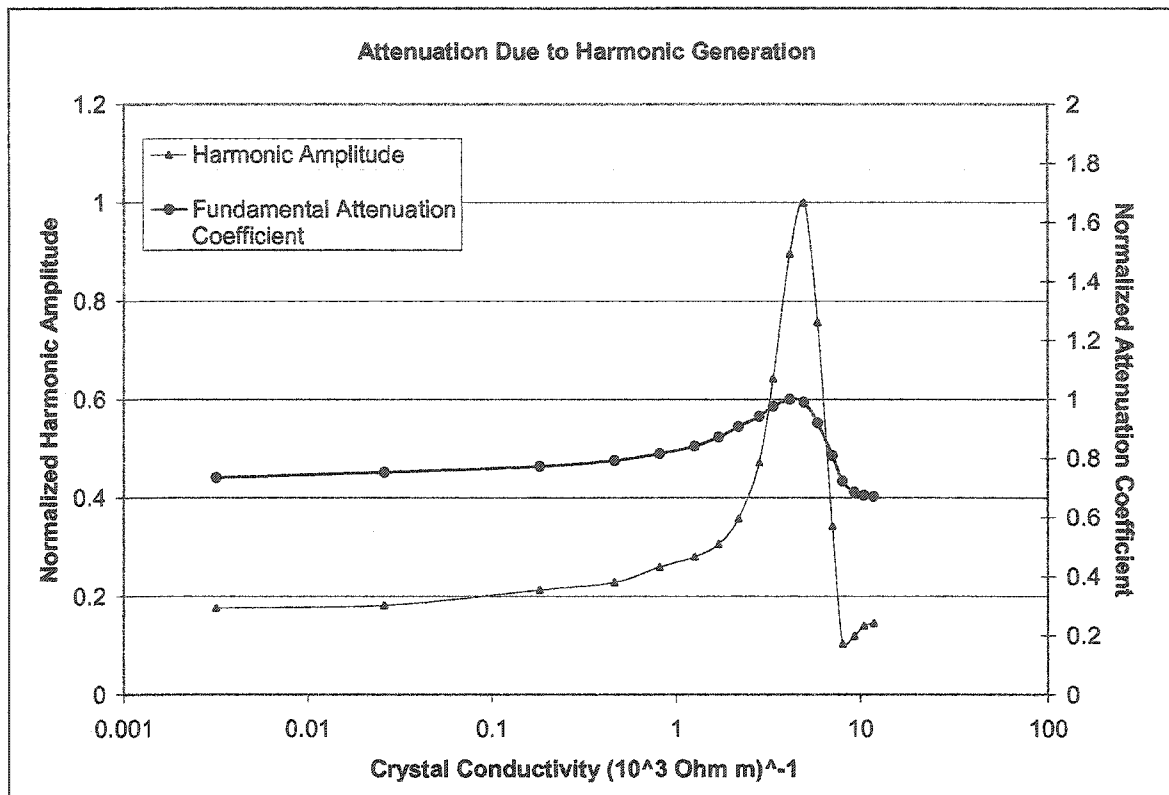
Figure 6.18.   Fundamental attenuation compared with harmonic amplitude.   This graph qualitatively demonstrates the coincidence of peak attenuation of the first harmonic with peak amplitude of the 2nd.

It can, therefore, be qualitatively verified that there is a correlation between the amplitude of the fundamental wave and those of the higher harmonics.   Indeed, these results seem to verify theory.   It seems that at least a portion of the energy lost by an acoustic wave in the presence of many free charge carriers can be attributed nonlinear effects.

To quantitatively compare the amplitudes of the first and second harmonic wave is a somewhat more tedious task.   We do, however, have some of the tools in place to make an initial estimate of this ratio.   Recall that during the course of the experiment involving the higher harmonics, a handful of measurements were made with regard to the

139

amplitude of the first and second harmonic. Upon compiling these data, we can create an algorithm with which to compare the linear data with the nonlinear. Each of the measurements recorded for the higher harmonics were performed with the 15 MHz transducer. Further, a filter was utilized to dampen the fundamental frequency. Also, at the beginning of this experiment we recorded the following ratios:

$$\frac{A_{2\omega}(without\ filter)}{A_{2\omega}(with\ filter)},$$ (6.8)

and

$$\frac{A_{2\omega}(without\ filter)}{A_{\omega}(without\ filter)}.$$ (6.9)

Thus, by multiply the second harmonic data by Equation (6.8), the amplitudes are increased to where they would have been measured in the absence of a filter. This situation is then comparable to that of the linear experiment. The effects of the transducer's frequency response can be removed from Equation (6.9) by utilizing the Equation (6.7) and also the data listed in Table 6.3. This process has then created an effective ratio between the amplitudes of the first and second harmonics for the dark-crystal conductivity level. Hence, the data series which corresponds to the amplitude of the 1st harmonic and that which contains information about the amplitude of the 2nd harmonic can be scaled appropriately for direct comparison. The dB plot of these two data sets can be seen in Figure 6.19.
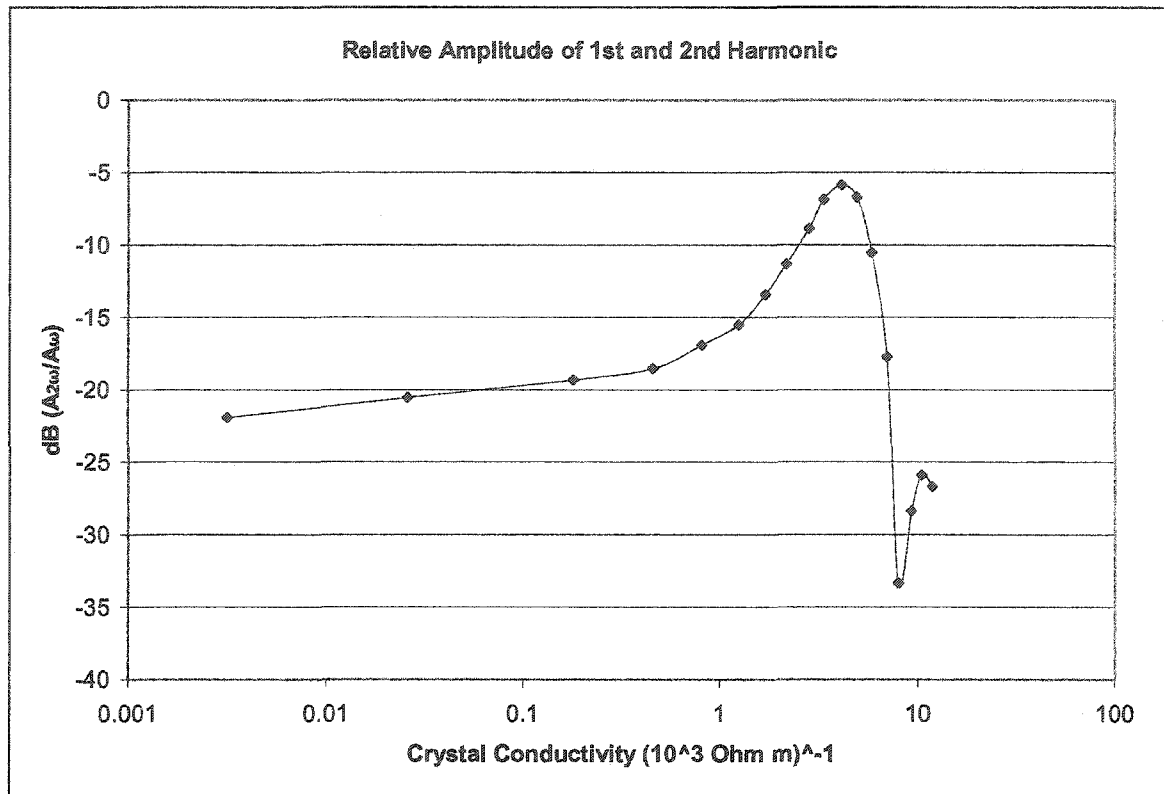
Figure 6.19. The relative amplitude of the 2nd harmonic is compared to that of the fundamental. The amplitude data was taken from two separate experiments and they were related using the procedure discussed in the preceding paragraph.

Although within this thesis project no extensive nonlinear theory has been presented, some of the qualities seen with in this graph can also be also be distinguished in one of the pioneering papers by Tell [43].

Concluding Remarks

Within this portion of the research, an introductory investigation of acousto-electric phenomenon was undertaken. Through the use of the results from Chapter IV and also taking into account earlier studies in this area, methods and procedures were developed to properly scrutinize this phenomenon. In an effort to properly understand the major components of this field of research, focus was initially placed on addressing some of the fundamental principles of the acoustoelectric effect. In this regard, then, the

141

experiment was further subdivided into linear and nonlinear segment. Each of these fields, however, afforded interesting and, in some cases novel results.

The linear section of experimentation provided a means to develop a familiarity with the principles and foundations the acoustoelectric effect. Further, it was necessary to begin with more primitive observations before moving onto more complicated endeavours. Firstly, the dispersive nature of CdS was quantitatively characterized. In a similar manner, the attenuation of both a 4.1 and 8.2 MHz wave was documented. In turn, then, an effort was made to plot these four curves together using the same parameters. This was met with reasonable success. Indeed, this portion of experimentation served as a basis for the nonlinear portion of this research project.

The examination of nonlinear phenomenon contained two principal experimental procedures: the first procedure concerned itself with the investigation of the relative amplitudes of successive echoes in the 2nd harmonic. It was repeatedly detected that the 2nd harmonic indeed reaches its maximum amplitude at different conductivity levels for different wave-path lengths. The second experiment had as its objective, the measurement of the amplitudes of higher harmonics, specifically the 2nd, 3rd, 4th and 5th. This portion of research appears have been uncharted, however, mostly due to the technological advances it has become accessible.

Finally, attempts were made to correlate data between the linear and nonlinear experiments. A procedure was utilized which allowed for the two sets of data to be both qualitatively and semi-quantitatively compared. Further, the relative amplitude of the first and second harmonic was examined.

In this way, then, the results presented in this portion of the research project are quite promising. The experimental data compiled to this point are quite interesting, and further, seem to be in reasonable agreement with theory. There are, however, several questions that have yet to be answered. One of the major variables, it seems, is the level of gain that experiments were performed at. Indeed, these changes seen to have an affect on results. For this reason this data should be clarified. This initial set of investigations, in this regard, has provided a strong foundation for considerably more investigations within this intriguing field. In this way, then, the results of this examination are quite satisfying.

143

CHAPTER VII

Discussions, Conclusions and Future Work

The main objective of this research project was the investigation of the acoustic wave interactions with free charge carriers in a piezoelectric semiconductor, namely Cadmium Sulfide. The preliminary examination of photoconductivity provided a fundamental understanding of Cadmium Sulfide with which to approach this study. In this way, although much of this manuscript was devoted to the description and explanation of experimental procedures distinct from acoustics, this work served more as a preamble to the study of the acoustoelectric effect. It is this exploration which was motivation for all experimentation within this project.

With this being said, however, the study of photoconductive Cadmium Sulfide was not without merit. In fact, this investigation laid much of the groundwork for the procedures implemented for the acousto-electronic investigations. In the first significant procedure of this project, a long-term examination of photoconductivity was undertaken. Although, in this initial experiment, the water bath that was employed was successful in limiting the change in temperature of the CdS crystal, it could not completely eliminate it. The main goal of this procedure, however, was realized. Indeed, the conductivity was documented for the course of an hour under constant illumination. Upon completing this procedure for several levels of light intensity, and comparing the results, a long-term metastability was detected. Further, it was determined that, although still present, this instability settled considerably after the first 20 minutes of photo-stimulation.

144

In order to further characterize the effect of crystal heating on conductivity, a second inquiry was carried out. Taking into account the results of the first experiment, this investigation compared temperature effects only after allowing the conductivity to stabilize. The results of this experiment concluded that within the range of this experiment, namely 20° to 80°C, temperature changes in Cadmium Sulfide had negligible influence on conductivity. Upon making this determination, then, several conclusions were drawn. Specifically, CdS was found to demonstrate slightly irregular conductivities, even when subject to illumination levels that were both consistent and repeatable.

Although this study of photoconductivity facilitated the basic experimental techniques utilized throughout this research project, the most intriguing results were those associated with the study of acoustic interactions with charge carriers in CdS. In the linear portion of this investigation, the fundamental phenomena that arose as a consequence of this interaction were explored; specifically, this study documented wave attenuation and velocity dispersion. These aspects were explored in two investigations; the first was at 4.1 MHz, while the second was at 8.2 MHz. Data from these experiments were plotted together, and, in turn, against theoretical curves to satisfactory agreement.

The nonlinear explorations also yielded reasonable results. In the first procedure, the relative amplitudes of four successive pulses were recorded. It was determined that there was a dependence of their relative peak amplitude on propagation distance. Further, the relative amplitudes of the 2nd, 3rd, 4th and 5th harmonics were compared through a range of conductivity levels. These results, having been strongly dependent on the advancement of modern technology, appear to be rather novel.

Finally, a couple interesting procedures were developed with which to compare linear and nonlinear results. First, a coincidence between the wave amplitude attenuation of the 2nd harmonic was qualitatively demonstrated. And finally, the relative wave amplitudes of the 1st and 2nd harmonic were compared between two separate experiments.

Surely, there are several aspects of this investigation which require further scrutiny. Much of this work, although encouraging, has merely begun to uncover the phenomenon of acousto-electron interactions. To fully evaluate the results of this experiment, particularly with respect to the nonlinear domain, a theoretical model specific to this experimental setup should be developed. Indeed, from initial work within this field, it can be seen that these effects should be characterized in order to make further progress.

146

References

[1] W. Voigt. *Lehrbuch der Kristallphysik*. New York : Johnson Reprint Corp., (1966).

[2] A. Ballato. *Piezoelectricity: Old Effect, New Trusts*. IEEE Transactions on Ultrasonics, Ferroelectrics, and Frequency Control. 42 (1995) 916-926.

[3] W.G. Cady. Piezoelectricity. Dover, New York, (1964).

[4] T. Ikeda. *Chapter 4 – Sound Propagation and the depolarizing-field effect in piezoelectric media*. Fundamentals of Piezoelectricity. Oxford University Press, New York, (1996). Pages 54-82.

[5] B.A. Auld. Acoustic Fields and Waves in Solids. Krieger Publishing Company, Florida, (1990).

[6] B. Gudden. *Lichtelektrische Erscheinungen*. Braunschweig, F. Vieweg, (1914).

[7] R.H. Bube. Photoconductivity of Solids. John Wiley & Sons, Inc., New York, (1960).

[8] A. Rose. Concepts in Photoconductivity and Allied Problems. (Ed. by R.E. Marshak), Interscience Publishers, New York, (1963).

[9] J. Mort, D.M. Pai. Photoconductivity and Related Phenomena. Elsevier Scientific Publishing Company, New York, (1976).

[10] J.J. Kyame. *Conductivity and Viscosity Effects on Wave Propagation in Piezoelectric Crystals*. The Journal of the Acoustical Society of America. 26 (1954) 990-993.

[11] V. Pustovoit. *Ultrasonic Waves Interaction with Electrons in Semiconductor Materials*. Review Physics-Uspekki. 97 (1969) 257-306.

[12] K.W. Boer. Survey of Semiconductor Physics. Van Nostrand Reinhold, New York, (1990).

[13] R.H. Bube. Photoelectronic Properties of Semiconductors. Cambridge University Press, Great Britain, (1992).

[14] D. Redfield, R.H. Bube. *Chapter 1 – Introduction: Metastable Defects*. Photoinduced Defects in Semiconductors. (Ed. by H. Ahmed, M. Pepper, and A. Broers), Cambridge University Press, USA, (1996). Pages 1-23.

[15] J.J. Kyame. *Wave Propagation in Piezoelectric Crystals*. The Journal of the Acoustical Society of America. 21 (1949) 159-167.

[16] H.N. Spector. *Amplification of Acoustic Waves through Interaction with Conduction Electrons*. Physical Review. 127 (1962) 1084-1090.

[17] R.H. Parmenter. *The Acousto-Electric Effect*. Physical Review. 89 (1953) 990-998.

[18] W.P. Mason. *Ultrasonic Attenuation due to Lattice-Electron Interaction in Normal Conducting Metals*. Physical Review. 97 (1955) 557-558.

[19] R.W. Morse. *Ultrasonic Attenuation in Metals by Electron Relaxation*. Physical Review. 97 (1955) 1716-1717.

[20] C. Kittel. Introduction to Solid State Physics. John Wiley & Sons, Inc., Canada, (1996).

[21] J.R.A. Beale. *Acoustoelectric Effects with Hypersonic Waves of Large Amplitude*. Physical Review. 135 (1964) 1761-1766.

[22] G. Weinreich. *Acoustodynamic Effects in Semiconductors*. Physical Review. 104 (1956) 321-324.

[23] N. Mikoshiba. *Interaction of Conduction Electrons with Acoustic Phonons*. Journal of the Physical Society of Japan. 14 (1959) 22-30.

[24] G. Weinreich, T.M. Sanders, Jr., H.G. White. *Acoustoelectric Effect in n-Type Germanium*. Physical Review. 114 (1959) 33-44.

[25] H.D. Nine. *Photosensitive Ultrasonic Attenuation in CdS*. Physical Review Letters. 4 (1960) 359-361.

[26] A.R. Hutson. *Piezoelectricity and Conductivity in ZnO and CdS*. Physical Review Letters. 4 (1960) 505-507.

[27] H.D. Nine, R. Truell. *Photosensitive-Ultrasonic Properties of Cadmium Sulfide*. Physical Review. 127 (1961) 799-803.

[28] A.R. Hutson, J.H. McFee, D.L.White, *Ultrasonic Amplification in CdS*. Physical Review Letters. 7 (1961) 237-238.

[29] A.R. Hutson. *Piezoelectric Scattering and Phonon Drag in ZnO and CdS*. Journal of Applied Physics. 32 (1961). 2287-2292.

[30] W.C. Wang. *Strong Acoustoelectric Effect in CdS*. Physical Review Letters. 9 (1962) 443-445.

[31] D.L. White. *Amplification of Ultrasonic Waves in Piezoeletric Semiconductors*. Journal of Applied Physics. 33 (1962) 2547-2554.

[32] A.R. Hutson, D.L. White. *Elastic Wave Propagation in Piezoelectric Semiconductors*. Journal of Applied Physics. 33 (1962) 40-47.

[33] R.W. Smith. *Current Saturation in Peizoelectric Semiconductors*. Physical Review Letters. 9 (1962) 87-90.

[34] J.H. McFee. *Ultrasonic Amplification and Non-Ohmic Behavior in CdS and ZnO*. Journal of Applied Physics. 34 (1962) 1548-1553.

[35] A.R. Hutson. *Acousto-Electric Explanation of Non-Ohmic Behavior in Piezoelectric Semiconductors and Bismuth*. Physical Review Letters. 9 (1962) 296-298.

[36] H. Kroger, E.W. Prohofsky, & H.R. Carleton. *Current Oscillations and Collective Waves in CdS*. Physical Review Letters. 12 (1964) 555-558.

[37] A.R. Moore. *Current and Voltage Saturation in Semiconducting CdS*. Physical Review Letters. 12 (1964) 47-50.

[38] K. Nakamura. *Current Fluctuations Associated with the Acoustoelectric Instability*. Journal of the Physical Society of Japan. 4 (1975) 860-867.

[39] E.W. Prohofsky. *Collective Phonon-Electron Waves and Oscillations in Piezoelectric Materials*. Physical Review. 136 (1964) 1731-1740.

[40] A.R. Moore. *Acoustoelectric Current Saturation in CdS as a Fluctuation Process*. Journal of Applied Physics. 38 (1967) 2327-2339.

[41] C. Elbaum, R. Truell. *Dependence of Ultrasonic Anharmonic Effects and Stress Wave Propagation on Density of Charge Carriers in Cadmium Sulphide*. Applied Physics Letters. 4 (1964) 212-213.

[42] H. Kroger. *Electron-Stimulated Piezoelectric Nonlinear Acoustic Effect in CdS*. Applied Physics Letters. 4 (1964) 190-192.

[43] B. Tell. *Piezoelectric Ultrasonic Harmonic Generation in Cadmium Sulfide*. Physical Review. 136 (1964) 772-775.

[44] P.K. Tien. *Nonlinear Theory of Ultrasonic Wave Amplification and Current Saturation in Piezoelectric Semiconductors*. Physical Review. 171 (1968) 970-986.

148

[45] R. Mauro, W.C. Wang. *Acoustoelectric Interactions in Piezoelectric Semiconductors*. Physical Review B. 1 (1970) 683-687.

[46] V.E. Henrich, G. Weinreich. *Pulsed Ultrasonic Studies of the Acoustoelectric Effect, Ultrasonic Attenuation, and Trapping in CdS*. Physical Review. 178 (1969). 1204-1217.

[47] V.V. Lemanov, YU.V. Ilisavsky. *Piezoelectricity and Acoustoelectronics*. Ferroelectronics. 42 (1982). 77-101.

[48] P. Gorlich. Photoconductivity in Solids. (Ed. by L. Jacob), Dover Publications Inc., New York, (1967).

[49] C. Kittel. Introduction to Solid State Physics. John Wiley & Sons, Inc., Canada, (1996).

[50] K.W. Boer. Survey of Semiconductor Physics Volume II. Van Nostrand Reinhold, New York, (1992).

[51] V.E. Henrich, G. Weinreich. *Pulsed Ultrasonic Studies of the Acoustoelectric Effect, Ultrasonic Attenuation, and Trapping in CdS*. Physical Review. 178 (1969). 1204-1217.

[52] W. Smith. *Effect of Light on Selenium during the Passage of an Electric Current*. Nature. 7 (1873) 303.

[53] M. Ali Omar. *Elementary Solid State Physics*. Addison-Wesley Publishing Company, (1993).

[54] W. Borchardt-Ott. *Crystallography*. Springer-Verlag Berlin Heidelberg, (1995)

Appendix A

Properties of Cadmium Sulfide

Within the scope of this thesis, all acoustic waves are longitudinal and along the hex-axis. For this reason, only properties necessary for making calculations regarding waves propagating along this axis are provided.

Symmetry Class	Hexagonal		[54]
Space Group	6mm		[54]
Density, p	3009	kg m^{-3}	[5]
Stiffness, c_{33}	9.38×10^{10}	N m^{-3}	[5]
Piezoelectric Stress Constant, e_{z3}	0.092	C m^{-2}	[5]
Lattice Constant, a	5.82	Å	[53]
Band Gap, E_g (at 300°C)	2.42	eV	[49]
Electron Mobility, μ_e	340	cm^2 V^{-1} s^{-1}	[53]
Hole Mobility, μ_p	18	cm^2 V^{-1} s^{-1}	[53]
Electron Effective Mass, m_e^*	0.21	m_e^*/m_0	[53]
Hole Effective Mass, m_p^*	0.8	m_p^*/m_0	[53]

150

Appendix B

Discussion of Experimental Temperature Fluctuations in CdS

This appendix provides a preliminary explanation for the variations of temperature seen CdS for Experiment A of Chapter IV. It should be noted at the outset that, generally speaking, to fully characterize the thermodynamic properties of the experimental apparatus would be a complicated task. For this reason, this discussion is meant to be primarily of a qualitative, and perhaps even conversational, nature.

It is perhaps beneficial to include Figure 4.12 directly within this appendix to facilitate discussion:
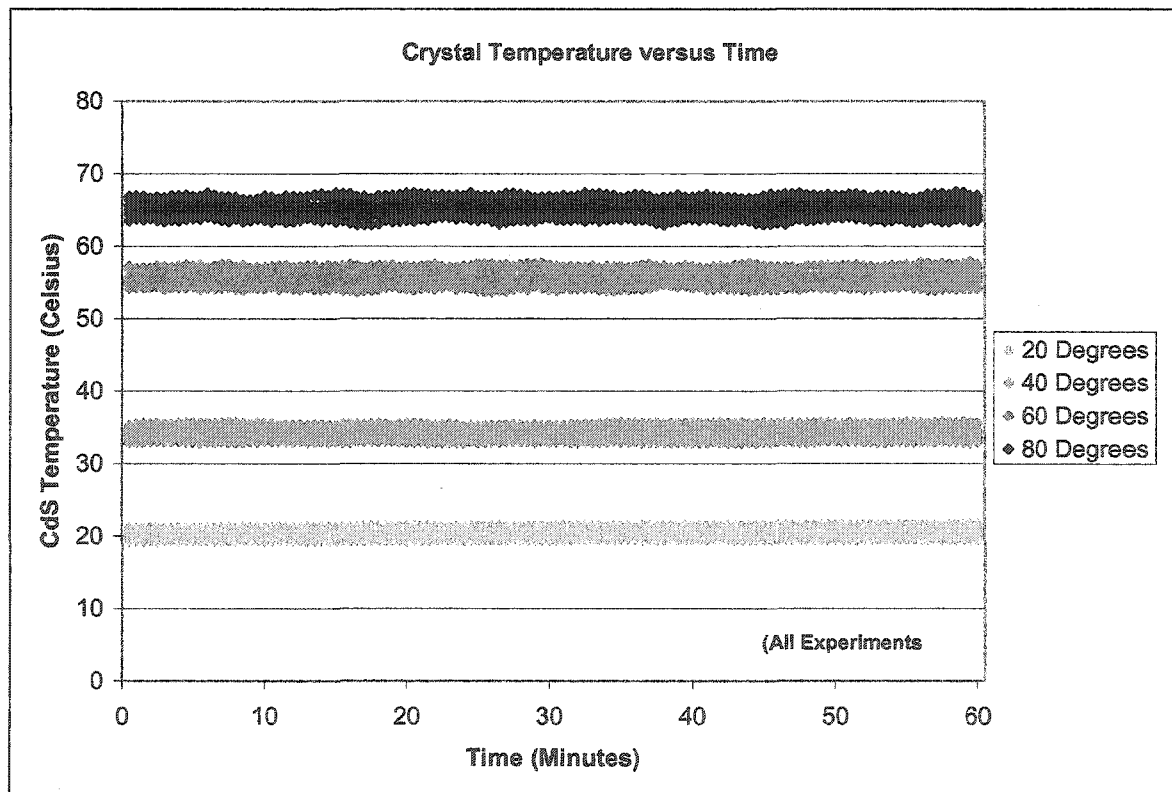

Figure B.1. Crystal temperature versus time: all bath temperatures. Formerly Figure 4.12 from Chapter IV, the graph contains all crystal temperature information from Experiment A.

151

As discussed briefly in Chapter IV, despite the inclusion of both a moderating water bath and a (light guide to reduce thermal radiation) in the general experimental setup, temperature effects can still be discerned from the data. Above, in Figure B.1, it can be seen that as bath temperature increases, there seems to be a variance in the thickness of each composite curve, or curve 'bundles'. The explanation for this, it seems, stems from the fact that within each one of these bundles is hidden the details of the particular experiments. The bottom curve in each of these bundles is affiliated with a light output intensity value of 223 whereas the top curve represents that of 1023. Herein lays a possible explanation: at the highest lamp intensities, there is a greater temperature gradient between the crystal and the water than at lower bath temperatures. For this reason, lower water bath temperatures are more effective at moderating the temperature of the crystal. Hence, as the water bath temperatures increase, so do the discrepancies in the temperature of the CdS crystal at low and high lamp intensities.

There is also, a second observation that can be made which is perhaps a little more subtle. Although not necessarily visible to the naked eye, the slope of the curves in Figure B.1 slowly decreases as the temperature of the water bath increases. This relationship can be seen more clearly in the graphs for the individual experiments shown below. Also, the slopes of the lines are shown quantitatively in Table B.1. As the slope of these curves is essentially a measure of the difference between the final temperature of the Cadmium Sulfide crystal (at t = 60 minutes) with respect to the initial Cadmium Sulfide crystal (at t = 0 minutes), this seems to imply that, contrary to the argument made above, the higher bath temperatures are better able to control the thermal effects of the lamp. This, unfortunately, is a little deceiving, and is more a consequence of the

152

moderating bath itself. The mechanism by which the water bath regulates its temperature is through circulating the water and heating it with a heating element. For this reason it has only the ability to heat the water and not to cool it. A water bath temperature of 20°C, then, is in near thermal equilibrium with the surrounding environment. When the lamp is set to a high intensity, then, through the course of the hour-long experiment, the water bath absorbs significant thermal energy and, subsequently, the crystal temperature is slowly increases. At 80°C, on the other hand, the thermal energy absorbed by the water bath is easily expelled due to the higher temperature gradient it has with the external environment. Hence, as is shown quantitatively in Table B.1, the temperature of the crystal during the course of a single experiment remains rather constant. In this way, then, lower bath temperatures are more effective at maintaining consistent crystal temperatures between experiments performed at different lamp intensities, while higher bath temperatures have more effect when attempting to maintain the consistency of the crystal temperature during the course of a long experimentation process.

Comparison of Curve Slopes in Figure B.1.	
Water Bath Temperature (°C)	Average Slope of Curves (°C/min)
20	0.0059
40	0.0016
60	0.0015
80	0.0012

Table B.1. This table indicates the ability of the water bath to regulate the temperature of the CdS crystal. The slopes of subsequent curves in Figure B.1 can be seen to decrease with the water bath temperature.

Now that some preliminary analysis has been attempted with regard to general trends amongst the four separate experiments, focus can be shifted to the individual trials. These four trials are shown below in Figure B.2, Figure B.3, Figure B.4 and Figure B.5.

153

Care was taken to ensure that the scales on the y-axis were consistent between the charts so that accurate comparisons could be made between them with relative ease.
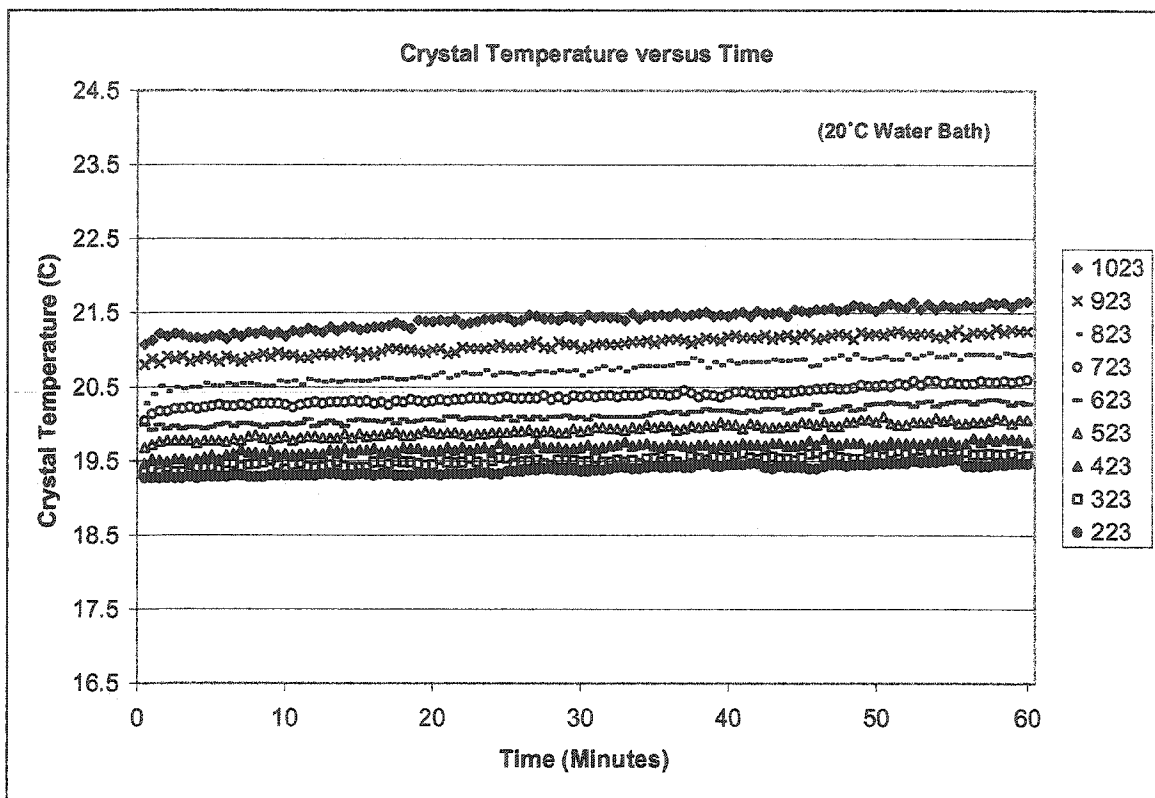

Figure B.2. Crystal temperature versus time: 20°C bath temperature.

The results from the experiment performed with the 20°C water bath (see Figure B.1 above) satisfactorily demonstrates the effect that increasing the lamp intensity has on the crystal temperature. Without the effectiveness of a higher water bath temperature to combat the effects of the lamp's heat energy, as the light intensity increases, the crystal's temperature also rises. It is interesting to note not only the spread between the 223 and 1023 light intensity curves, but also the gradual increase in the spacing between subsequent curves with each increase in lamp intensity. This seems to correspond with the exponential increase in light intensity that accompanies these particular lamp levels.

154

Unsurprisingly, the significant increase in heat energy at the higher lamp output values contributes to a more dramatic increase in the temperature of the CdS crystal during the course of each 1 hour experiment. This is consistent with the above discussion of the thermal effects of the lamp; indeed, higher lamp intensities contributed to a heating of the water bath and, consequently, the CdS crystal. The numerical representation of these observations can be seen in Table B.2. Also, similar tables, corresponding to Figures C3, C4, and C5, are placed below for convenience of comparison.

Comparison of Curve Slopes in 20°C Water	
Average slope of curves 223, 323, 423	0.0038
Average slope of curves 523, 623, 723	0.0060
Average slope of curves 823, 923, 1023	0.0079

Table B.2. The above table demonstrates the increase in curve slope corresponding to the greater heating of the water bath at high lamp intensities. Units: °C / min.

Comparison of Curve Slopes in 40°C Water	
Average slope of curves 223, 323, 423	0.0001
Average slope of curves 523, 623, 723	0.0018
Average slope of curves 823, 923, 1023	0.0030

Table. B.3. This table demonstrates the average slopes of the curves in Figure B.3. Units: °C / min

Comparison of Curve Slopes in 60°C Water	
Average slope of curves 223, 323, 423	0.0005
Average slope of curves 523, 623, 723	0.0015
Average slope of curves 823, 923, 1023	0.0024

Table B.4. This table demonstrates the average slopes of the curves in Figure B.4. Units: °C / min

Comparison of Curve Slopes in 80°C Water	
Average slope of curves 223, 323, 423	-0.0001
Average slope of curves 523, 623, 723	0.0013
Average slope of curves 823, 923, 1023	0.0022

Table B.5. This table demonstrates the average slopes of the curves in Figure B.5. Units: °C / min
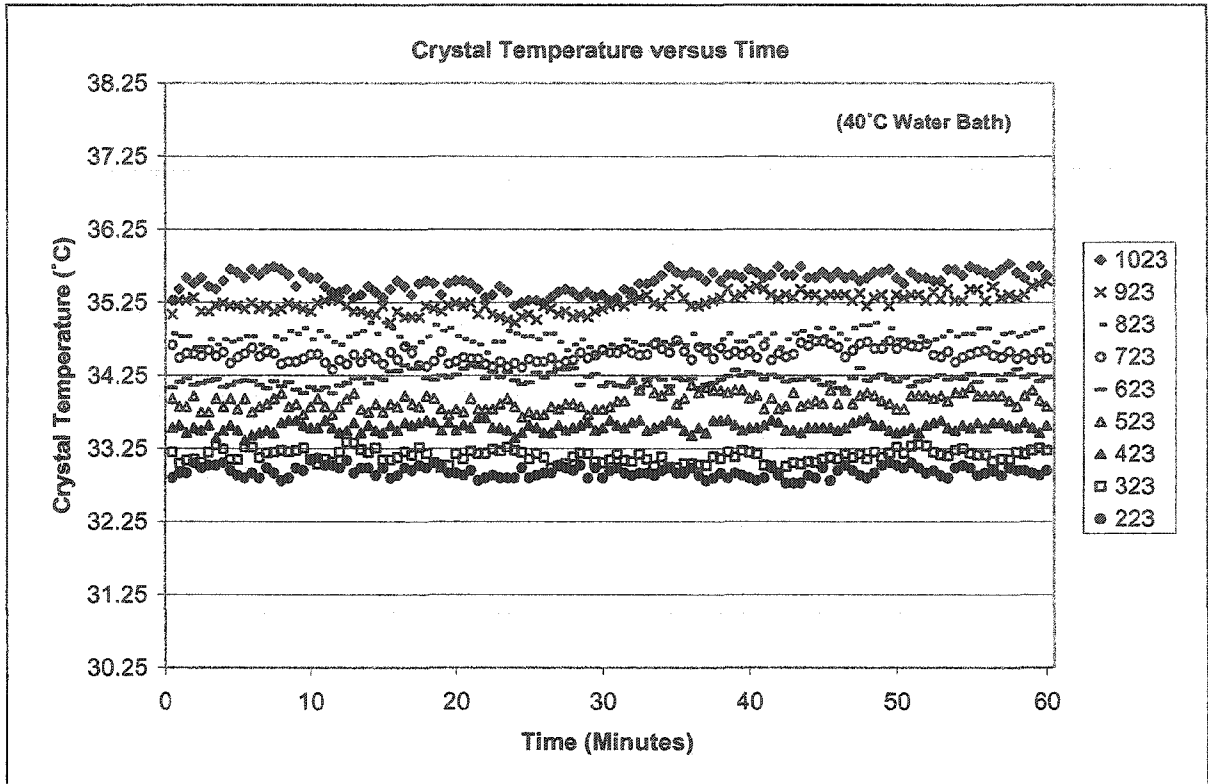
155

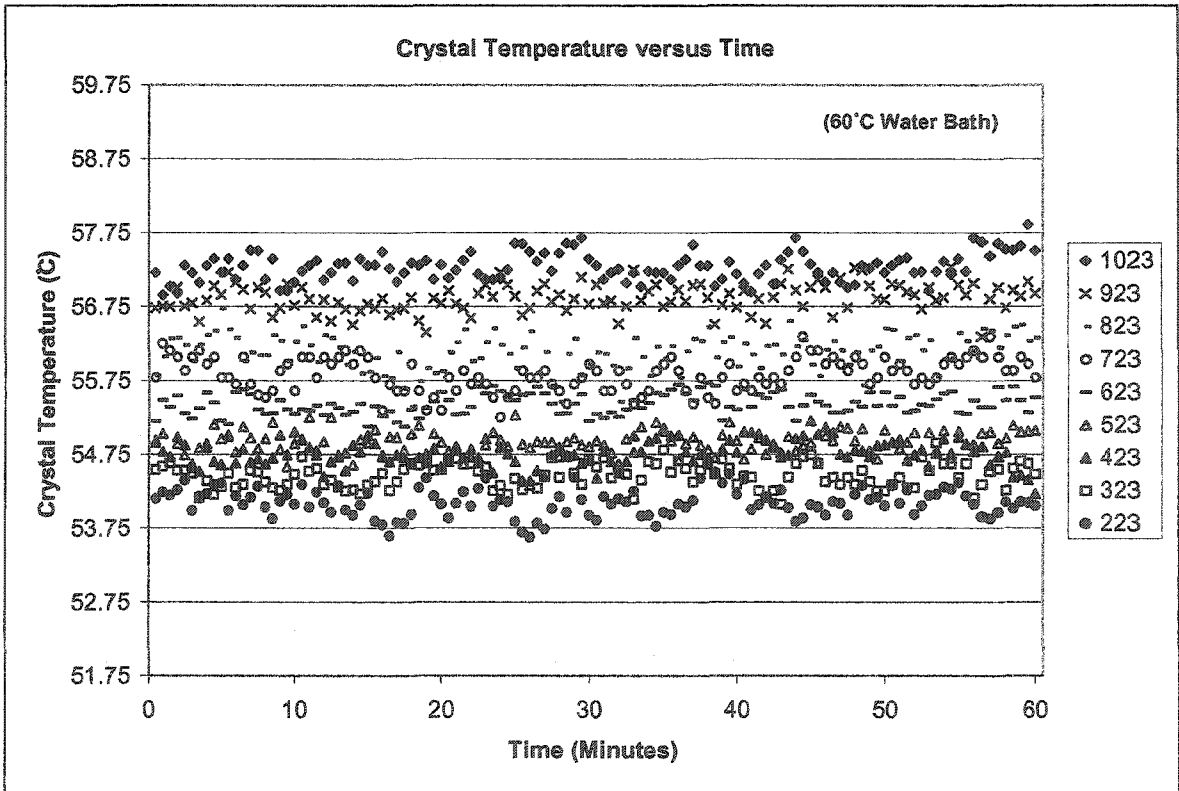Figure B.3. Crystal temperature versus time for 40°C bath water.

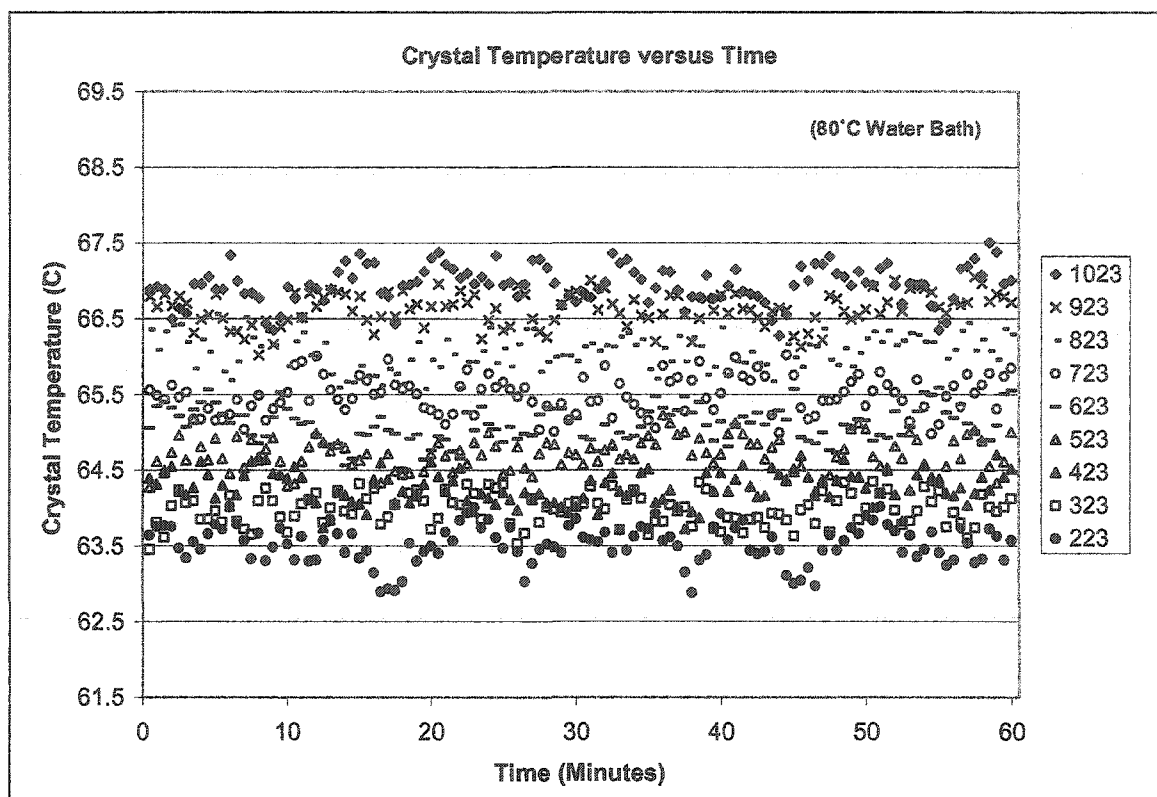Figure B.4. Crystal temperature versus time for 60°C bath water.

156

Figure B.5 Crystal temperature versus time for 80°C bath water.

Although the general trends of these graphs are the same, there is a major discrepancy which does require at least a quantitative explanation. For the experiments performed in the 20°C water bath, we see that the temperature of the crystal rises in a consistent manner with 'smooth' curves. On the other hand, the points which comprise the curves become considerably more unpredictable as the water bath temperature increases. Indeed the crystal temperature seems to 'jump around' rather sporadically at high water bath temperatures.

The origin of this temperature instability is most likely do to the interplay between the dissimilar thermal properties of the experimental components. It is, however, difficult to quantitatively describe the exact nature of this thermal interaction. In fact, there are many aspects that must be accounted for. With high light intensities,

157

there is a great deal of thermal energy transferred to the CdS crystal. Also, the thermal absorption decays exponentially below the surface of the crystal. There is then a dissimilar temperature gradient throughout the crystal. As the thermister is coupled to the upper side of the CdS crystal, its resistance is influenced by both the temperature of the crystal and also, by the light source, both directly and indirectly. Further, the atmosphere surrounding the entire experiment is constantly in motion. As the water bath temperature increases, it indirectly increases the temperature gradient between the thermister and the surrounding environment; thus, the heat exchange that take place directly between the air and the thermister increases.

With this being said, a quantitative explanation of this occurrence is at the very least a tedious undertaking. For the most the thermodynamic principles which govern this interaction lie outside the scope of this thesis project. For this reason only the following qualitative explanation is offered: simply stated, as the temperatures of the constituent components of the experiment begin to deviate from one another, the corresponding temperature gradients give rise to intrinsic temperature instabilities (for instance, at either high lamp intensities or water bath temperatures). In order resolve, or at least fully understand this volatility, the specific thermodynamic properties of this system must be scrutinized.

Appendix C

Curve Fitting: Equation (5.39) and Equation (5.40)

In order to begin the curve fitting process for this particular set of equations, all the parameters must be appropriately defined. The equations are

$$v = v_0 \left[1 + \frac{\kappa^2}{2} \cdot \frac{1 + \frac{\omega}{\omega_D}\left(\frac{\omega_C}{\omega} + \frac{\omega}{\omega_D} \right)}{1 + \left(\frac{\omega_C}{\omega} + \frac{\omega}{\omega_D} \right)^2} \right], \qquad (5.39)$$

and

$$\alpha = \frac{\omega}{v_0} \left[\frac{\kappa^2}{2} \cdot \frac{\frac{\omega}{\omega_C}}{1 + \left(\frac{\omega_C}{\omega} + \frac{\omega}{\omega_D} \right)^2} \right], \qquad (5.40)$$

where the Equation (5.39) is the velocity dispersion equation and, Equation (5.40) is the attenuation equation as given by McFee [24]. Here v_0 is the unstiffened velocity; in our case it is the longitudinal velocity. The other parameters are

$$\omega_C \equiv \frac{n_0 q \mu}{\varepsilon}, \qquad \text{(conductivity relaxation frequency)} \qquad (C.1)$$

$$\omega_D \equiv \frac{v_0^2}{\vartheta}. \qquad \text{(electron "diffusion" frequency)} \qquad (C.2)$$

and,

$$\kappa^2 \equiv \frac{e^2}{c\varepsilon}. \qquad \text{(electromechanical coupling constant)} \qquad (C.3)$$

158

First we consider Equation (C.1), the conductivity relaxation frequency. This can be further written as

$$\omega_c \equiv \frac{\sigma}{\varepsilon}, \qquad (C.4)$$

where σ is the CdS conductivity and ε is the electric permittivity constant. Also, as an aside,

$$\sigma = n_0\, q\mu, \qquad (C.5)$$

where n_0 is the density of free electrons, q is the charge per electron, and μ is the electron mobility. Now, the *electron diffusion frequency*, Equation (C.2), is a function of the square of the unstiffened velocity and also

$$\wp = \frac{\mu\, kT}{q}, \qquad \text{('Einstein Relation')} \qquad (C.6)$$

where $\wp$ is the electron diffusion coefficient, k is the Boltzmann constant, and T is the temperature in Kelvin. Finally, the electromechanical coupling constant is a function is a function of the electric permittivity constant as well as of c, the elastic stiffness, e, the piezoelectric constant.

Now, in order to fit a theoretical curve to experimental data, as is common practice in most experimental papers regarding the acoustoelectric effect, elastic stiffness, c, and the piezoelectric constant, e, are varied to adjust the theoretical curve [46]. As can be seen, these parameters appear only in the Equation (C.3). All other variables in Equation (5.39) are taken to be constant, save for ω_c which is taken to be linearly proportional to conductivity. Also, as can be seen by equation (C.6), that $\wp$ is also a function of temperature. However, as $\omega_c \gg \omega_d$ it can too be considered a constant.

For very high conductivities, Equation (5.30) reduces to, simply $v = v_0$, where

159

$$v_0 = \left(\frac{c}{\rho} \right)^{1/2},$$ (C.6)

in which ρ is the density of CdS, which we assume to be constant. As it turns out, v_0, is the lower bound of wave velocity in a piezoelectric semiconductor. Thus, if adjustments are to be made with respect to the lower bound, they are controlled (within this curve-fitting procedure) exclusively the value used for the elastic stiffness. In the other limit, at low illumination levels we have

$$v = v_0 \left[1 + \frac{\kappa^2}{2} \right].$$ (C.5)

This is referred to as the *stiffened* velocity—the upper bound for wave dispersion. Hence, after c is set to fit the asymptotic limit of the velocity at high conductivity, then e and ε can be varied to fit the asymptotic limit at low conductivity. In this way, then, given a set of numerical data, the upper and lower bound of the theoretical curve can be adjusted for goodness-of-fit.

Aside from acoustic wave frequency adjustments, there is no means for adjusting the horizontal displacement of the theoretical data. For our particular experimental data, however, this remains constant, and thus another means is required for curve-fitting. In this experiment, experimental conductivity values were calculated by

$$\sigma_{CdS} = \frac{l}{R_{CdS} \cdot A_{cross}} = \frac{l}{R_{CdS} \cdot d_p \cdot d} \quad (\Omega \cdot \text{m})^{-1},$$ (3.3)

where R_{CdS} was the measured crystal resistance, l is the distance between the contact leads, d is the width of the crystal and d_p is the depth of penetration of radiation. In this way, these last two terms combine to form the current cross section, A_{cross}. Thus the only reasonable adjustments that could be made were in the ratio $l / (d_p \cdot d)$. In other words, this

160

manipulation effectively adjusted the volume corresponding to the measured crystal resistance. Due, for the most part, to the depth of penetration of radiation energy, this ratio differed from the volume of the crystal itself. Hence, by adjustment of this volume, a theoretical curve could be fit to the experimental data.

As can be seen above, the equations for attenuation (Equation 5.39) and dispersion (Equation 5.40) contain identical variables. For this reason, upon completing the curve fitting procedure for the first, no adjustable parameters remain for the latter.

Within the case of our experiment, the final parameters were chosen to be

e	88.7	GPa
c	0.515	$C\,m^{-2}$
$\dfrac{l}{d_p \cdot d}$	1.44e-4	cm^{-1}

Table C.1. The actual number used in the curve fitting process.

These numbers appear to be quite reasonable. In fact, if we calculate the electromechanical coupling constant, it is within the range of tolerance given by Hutson and White [32]. Further, using the experimental values of l and d it can be found that d_p also is consistent with the value suggested by Bube [13]. For this reason, the experimental fitting procedures used to create Figure 6.15 and Figure 6.16 are quite reasonable in our estimation.

Appendix D

Lamp Spectrum Considerations

Conductivity within a particular photo-semiconductor is dependent not only on the intensity of the light source, but also on its frequency. This reason for this dependence can be seen more clearly below in Figure D.1.
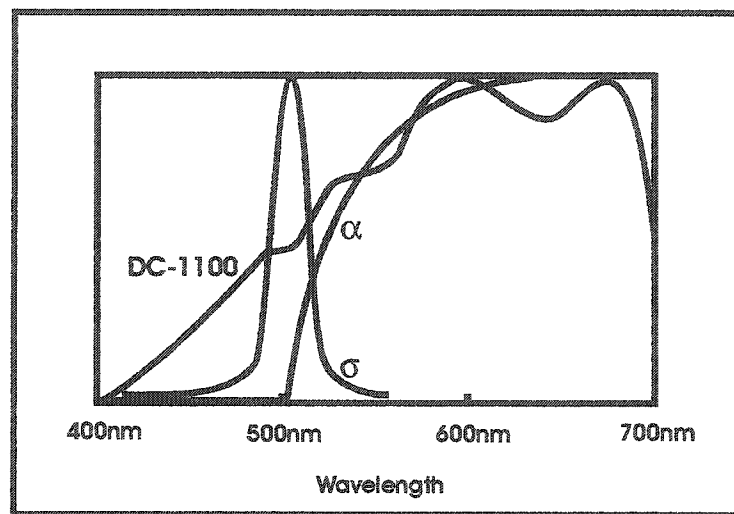

Figure D.1. Spectrum comparison: Light source, CdS Conductivity and Absorption. Note: conductivity, σ, and absorption, α [50].

Although the conductivity and absorption curves shown in Figure D.1 correspond to a thin sample of CdS [50], they can be useful in understanding how light intensity and wavelength affect our experiment. As can be seen, the light source spans the entire visible light spectrum. Crystal conductivity, however, only begins to increase at around 500nm, at which point the photon energies become greater than the band gap. For this reason, then, the portion of the lamps spectrum which is above this wavelength cannot stimulate crystal conductivity. In this way, then, long wavelengths of light are able to pass through the crystal, whereas short wavelengths are completely absorbed upon

162

penetrating only a short distance into the crystal. It is for this reason that the conductivity of the crystal once again decreases after reaching its peak. Given the light spectrum of our experiment, then, we can deduce that although the DC 1100 spans the entire visible spectrum, the portion of its total intensity responsible for crystal conductivity is only that which lies within a few nanometers on either side of 500 nm.

Vita Auctoris

Name: Wesley Arthur

Place of Birth: Meaford, Ontario, Canada

Date of Birth: October 21, 1976

Education: BA in Mathematics and Physics (2000), Anderson University,

Anderson, Indiana, USA.

Articles
- W. Arthur, B. O'Neill, R. Maev, and I. Solodov. *Acoustic Wave Interaction with Electrons in Piezoelectric Semiconductors*. 16th International Symposium on Nonlinear Acoustics, Volume 2 (2002) 625.